National Library of Canada
Acquisitions and Bibliographic Services Branch
395 Wellington Street
Ottawa, Ontario
K1A 0N4

Bibliothèque nationale du Canada
Direction des acquisitions et des services bibliographiques
395, rue Wellington
Ottawa (Ontario)
K1A 0N4

Your file Votre référence

Our file Notre référence

NOTICE

The quality of this microform is heavily dependent upon the quality of the original thesis submitted for microfilming. Every effort has been made to ensure the highest quality of reproduction possible.

If pages are missing, contact the university which granted the degree.

Some pages may have indistinct print especially if the original pages were typed with a poor typewriter ribbon or if the university sent us an inferior photocopy.

Reproduction in full or in part of this microform is governed by the Canadian Copyright Act, R.S.C. 1970, c. C-30, and subsequent amendments.

AVIS

La qualité de cette microforme dépend grandement de la qualité de la thèse soumise au microfilmage. Nous avons tout fait pour assurer une qualité supérieure de reproduction.

S'il manque des pages, veuillez communiquer avec l'université qui a conféré le grade.

La qualité d'impression de certaines pages peut laisser à désirer, surtout si les pages originales ont été dactylographiées à l'aide d'un ruban usé ou si l'université nous a fait parvenir une photocopie de qualité inférieure.

La reproduction, même partielle, de cette microforme est soumise à la Loi canadienne sur le droit d'auteur, SRC 1970, c. C-30, et ses amendements subséquents.

Canada

University of Alberta

Passive Ventilation for Combustion Air Supply

by

Patrick Fleming

©

A thesis
submitted to the Faculty of Graduate Studies and Research
in partial fulfilment of the requirements for the degree of
Master of Science

Department of Mechanical Engineering

Edmonton, Alberta

Spring, 1996

National Library
of Canada

Acquisitions and
Bibliographic Services Branch

395 Wellington Street
Ottawa, Ontario
K1A 0N4

Bibliothèque nationale
du Canada

Direction des acquisitions et
des services bibliographiques

395, rue Wellington
Ottawa (Ontario)
K1A 0N4

Your file Votre référence

Our file Notre référence

The author has granted an irrevocable non-exclusive licence allowing the National Library of Canada to reproduce, loan, distribute or sell copies of his/her thesis by any means and in any form or format, making this thesis available to interested persons.

L'auteur a accordé une licence irrévocable et non exclusive permettant à la Bibliothèque nationale du Canada de reproduire, prêter, distribuer ou vendre des copies de sa thèse de quelque manière et sous quelque forme que ce soit pour mettre des exemplaires de cette thèse à la disposition des personnes intéressées.

The author retains ownership of the copyright in his/her thesis. Neither the thesis nor substantial extracts from it may be printed or otherwise reproduced without his/her permission.

L'auteur conserve la propriété du droit d'auteur qui protège sa thèse. Ni la thèse ni des extraits substantiels de celle-ci ne doivent être imprimés ou autrement reproduits sans son autorisation.

ISBN 0-612-10708-6

Canada

UNIVERSITY OF ALBERTA

Library Release Form

Name of Author: Patrick Norman Fleming

Title of Thesis: Passive Ventilation for Combustion Air Supply

Degree: Master of Science

Year This Degree Granted: 1996

Permission is hereby granted to The University of Alberta Library to reproduce single copies for private, scholarly or scientific purposes only. The author reserves other publication rights, and neither the thesis nor extensive extracts from it may be printed or otherwise reproduced without the authors written permission.

P Fleming

#206 10707 81 Ave.

Edmonton, AB

T6E 1Y2

Date: Jan 30/96

UNIVERSITY OF ALBERTA
FACULTY OF GRADUATE STUDIES AND RESEARCH

The undersigned certify that they have read, and recommend to the Faculty of Graduate Studies and Research, for acceptance, a thesis entitled *Passive Ventilation for Combustion Air Supply* submitted by Patrick Norman Fleming in partial fulfillment of the requirements for the degree of Master of Science.

D.J. Wilson

J.D. Dale

L.W. Kostiuk

F.E. Hicks

Date: Jan 25/96

Abstract

Passive vents are commonly used for the supply of air to combustion appliances in houses and buildings. The variability in weather conditions result in variability in the ventilation rate of mechanical spaces. This is especially true in cold climates where extreme winter weather can cause large over–ventilation of mechanical spaces resulting in freezing damage to water lines. Variability in the two driving forces, wind and indoor–outdoor temperature difference, make prediction of ventilation rates difficult, necessitating computer modelling of the passive ventilation.

An existing passive ventilation model, LOCALEAKS–2 was modified for prediction passive ventilation with large local leakage sites, resulting in an improved model, LOCALEAKS–3. This model was validated using measurements made in unoccupied bungalows equipped with passive combustion air vents. The model was then used in a parametric study of a typical mechanical room equipped with combustion air vents as specified by the Uniform Mechanical Code.

Wall averaged wind pressure coefficients are useful in predicting passive ventilation through distributed leakage, but can lead to large errors in predictions if applied to large passive vents. Small differences in wind pressure coefficient between two or more large local leakage sites can result in large ventilation forces that may be ignored in passive ventilation models using only wall averaged wind pressure coefficients. The LOCALEAKS–3 model estimates local wind pressure coefficients on passive vents. The new model resulted in improved ventilation predictions for bungalows equipped with two passive combustion air vents on the same wall.

Acknowledgements

The author would like to thank D.J Wilson and J.D Dale for their guidance and support throughout this project. I would also like to thank Mark Ackerman, Wayne Pittman, John Foy and Terry Nord for their knowledgable technical support, as well as the Department of Mechanical Engineering machine shop staff for their quality workmanship.

Financial support was provided by the American Society of Heating, Refrigeration and Air-Conditioning Engineers, in the form of an ASHRAE Grant-in-Aid, without which this work would not have been possible.

Contents

Abstract iv

Nomenclature xvi

1 Introduction 1
- 1.1 Combustion Air Supply . . . 2
- 1.2 Previous Studies in Passive Ventilation . . . 4
- 1.3 The scope of this study . . . 4

2 Passive Ventilation and LOCALEAKS-3 6
- 2.1 Passive Ventilation . . . 6
  - 2.1.1 Flow Characteristics of Building Leakage . . . 6
  - 2.1.2 Driving Forces of Passive Ventilation . . . 7
  - 2.1.3 Passive Ventilation Through Large Openings . . . 10
  - 2.1.4 Wind Pressure Coefficients and ΔC_p . . . 13
  - 2.1.5 The LOCALEAKS-2 Passive Infiltration Model . . . 17
  - 2.1.6 LOCALEAKS-3 . . . 23

3 Infiltration Model Validation 25
- 3.1 Test Facility . . . 25
- 3.2 Combustion Air Vents . . . 29
  - 3.2.1 Detail and Calibration of the Passive Combustion Air Vents . . . 29
  - 3.2.2 Installation of the Passive Combustion Air Vents . . . 31
  - 3.2.3 Fan Depressurization Testing . . . 33
  - 3.2.4 Infiltration and Vent Pressure Data . . . 33
- 3.3 Measurement of Wall Averaged Wind Pressure Coefficients . . . 38
  - 3.3.1 Experimental Method for Pressure Coefficient Measurements . . . 42
  - 3.3.2 The Wall Averaged Pressure Coefficient Data . . . 44

4 The Local Wind Pressure Model **49**
4.1 Flow Measurements in Combustion Air Vents 49
4.2 LOCALEAKS–2 Predictions of Measured Infiltration 54
4.3 Development of the Local ΔCp Model 59

5 Pressure Coefficient Measurements **72**
5.1 Comparison of Effective Wind Pressure Coefficients of LOCALEAKS-2 with Measured Coefficients 72
5.2 Discussion 74

6 Parametric Study of Mechanical Room Ventilation **78**

7 Conclusions and Recommendations **89**
7.1 Conclusions and Summary of Results 89
7.2 Recommendations for Future Study 90

A Derivations **92**
A.1 Derivation of Equation 2.4 92
A.2 Derivation of Equations 2.10 and 2.11 93

List of Tables

3.1 Relevant construction Dimensions of Alberta Home Heating Research Facility Test Houses. 26
3.2 Depressurization Test Results for Houses 3 and 4. 37
3.3 Infiltration and Ventilation Characteristics of Test Houses. . . 39

List of Figures

1.1 A Typical Installation of Passive Combustion Air Vents in a Mechanical Equipment Room. 3

2.1 The total pressure across a building envelope is the sum of the stack pressure, ΔP_h, the wind pressure, ΔP_l, and the Internal mass–flow balancing pressure difference, ΔP_I. Shown for a stagnation wall (ΔP_l positive). 11

2.2 Passive ventilation in a simple structure with two large openings. Ventilation is driven by indoor–outdoor temperature difference and wind pressure. T_i and T_o are the air temperatures of the interior and exterior air, respectively. H is the vertical distance between the centre of the holes and C_{p1} and C_{p2} are the wind pressure coefficients on holes 1 and 2 respectively. Arrows indicate stack driven flow for $T_i > T_o$. 11

2.3 Calculated ventilation rates in a two–vent house. The indoor–outdoor temperature difference is 40°C and the flow coefficient in each vent is 0.041 $m^3/s \cdot Pa^n$. Ventilation is in m^3/h of indoor temperature air. 14

2.4 Calculated ventilation rates in a two–vent house. The indoor–outdoor temperature difference is 20°C and the flow coefficient in each vent is 0.041 $m^3/s \cdot Pa^n$. Ventilation is in m^3/h of indoor temperature air. 14

2.5 Calculated ventilation rates in a two–vent house. The indoor–outdoor temperature difference is 10°C and the flow coefficient in each vent is 0.041 $m^3/s \cdot Pa^n$. Ventilation is in m^3/h of indoor temperature air. 15

2.6 Calculated ventilation rates in a two–vent house. The indoor–outdoor temperature difference is 0°C and the flow coefficient in each vent is 0.041 $m^3/s \cdot Pa^n$. Ventilation is in m^3/h of indoor temperature air. 15

2.7 Pressure coefficients on a unsheltered bungalow taken from figures in Wiren (1985). Wiren's data was splined with data points every 15°. Wind directions are shown for a north facing wall. 17
2.8 Pressure coefficients used in LOCALEAKS-2 for a north (0°) facing wall on an isolated house and a house in an east-west row. The east-west row C_p is less negative when wind is blowing along the row (90° or 270°) because separation is reduced by the upwind houses. 21
2.9 Pressure and shelter coefficients used for modelling wind on the north (0°) wall of the test houses. As the test houses are in an east-west row, the north wall uses the row sheltered C_p. South wall is similar with 180° shift. 22
2.10 Pressure and shelter coefficients used for modelling the west (270°) wall of the test houses. The west wall does not experience reduced sidewall flow separation from the east-west row of houses, so the C_p is same as an unsheltered house. The effect of the row of houses is accounted for in S_w. The east wall is similar with 180° shift. 23

3.1 The Alberta Home Heating Research Facility viewed from the south. The houses are numbered one through six, from left to right. 27
3.2 Plan view of the Alberta Home Heating Research Facility, showing the row of test houses and adjacent farm buildings. . 28
3.3 Passive vent installed in Houses 3 and 4. NTS 30
3.4 Calibration apparatus for air vent flow characteristics. 30
3.5 Calibration of a 356x254 *mm* (14x10 in.) combustion air vent as fitted to Houses 3 and 4. Solid line is the curve derived from house depressurization tests conducted by M.Y. Ackerman (private communication). 32
3.6 Calibration of a reduced area 356x127 *mm* (14x5 in.) combustion air vent as fitted to Houses 3 and 4. Solid line is the curve derived from house depressurization tests conducted by M.Y. Ackerman (private communication). 32
3.7 Unsheltered combustion air vents on north wall of House 3 . . 34
3.8 Sheltered combustion air vents on west wall of House 4 35
3.9 Indoor view of combustion air vents in House 4 showing the motorized damper control and pressure transducers. 36
3.10 Schematic diagram of house depressurization equipment. . . . 37

3.11 Indoor air infiltration rate in House 4 with large 356x254 *mm* (14x10 in), sheltered combustion air vents, vents open. 40
3.12 Indoor air infiltration rate in House 4 with large 356x254 *mm* (14x10 in), sheltered combustion air vents, vents closed 40
3.13 Pressure across upper vent of House 4 (sheltered vents). Vents are large, 356x254 *mm* (14x10 in). Positive pressure is inflow. 41
3.14 Pressure across lower vent of House 4 (sheltered vents). Vents are large, 356x254 *mm* (14x10 in). Positive pressure is inflow. 41
3.15 Schematic diagram of the pressure measurements made on the exterior walls of House 2 for the measurement of wall averaged wind pressure coefficients. 42
3.16 Wall averaged pressure coefficients, measured on the unsheltered south wall ($\theta = 180°$) of House 2. The 6236 data points have wind speeds greater than 1 m/s. 46
3.17 Wall averaged pressure coefficients measured on the sheltered west wall ($\theta = 270°$) of House 2. The 6236 data points have wind speeds greater than 1 m/s. 46
3.18 Wall averaged pressure coefficients measured on the unsheltered south wall ($\theta = 180°$) of House 2. The 1220 data points have wind speeds greater than 4 m/s. 47
3.19 Wall averaged pressure coefficients measured on the sheltered west wall ($\theta = 270°$) of House 2. The 1220 data points have wind speeds greater than 4 m/s. 47
3.20 Binned wall averaged pressure coefficients measured on the unsheltered south wall ($\theta = 180°$) of House 2. The 1220 data points have wind speeds greater than 4 m/s. Bars show plus or minus one standard deviation. 48
3.21 Binned wall averaged pressure coefficients measured on the sheltered west wall ($\theta = 270°$) of House 2. The 1220 points have wind speeds greater than 4 m/s. Bars show plus or minus one standard deviation. 48

4.1 Unsheltered combustion air vents on north wall of House 3 (no flue). Measured mass flow rate of air through the upper vent, normalized with total infiltration rate versus wind direction. All wind speeds. The wind is normal to unsheltered vents at 0°. In–flow is positive 51

4.2 Unsheltered combustion air vents on north wall of House 3 (no flue). Measured mass flow rate of air through the lower vent, normalized with total infiltration rate versus wind direction. All wind speeds. The wind is normal to unsheltered vents at 0°. In–flow is positive. 52
4.3 Unsheltered combustion air vents on north wall of House 3 (no flue). Measured mass flow rate of air through the upper and lower vents, normalized with total building infiltration rate versus total infiltration rate. In–flow is positive. 53
4.4 Unsheltered combustion air vents on north wall of House 3 (no flue). Measured mass flow rate of air through the upper vent versus that of the lower vent. Both flow rates are normalized with the total infiltration rate of the house. In–flow is positive 55
4.5 Predicted Infiltration versus measured infiltration for House 4, with an open, unheated flue and combustion air vents closed. 56
4.6 Predicted infiltration divided by measured infiltration versus wind direction for House 4 with an unheated, open flue and no combustion air vents. The largest wind direction bin has 170 data points, the smallest has 24. 57
4.7 Predicted divided by measured infiltration for House 3 with sheltered 356x127 mm (14x5 in.) combustion air vents open. Data is binned every 22.5° and error bars are ± one standard deviation. Wind is normal to unsheltered vents at 0°. The largest bin has 178 data points, the smallest has 23 data points. 58
4.8 Predicted divided by measured infiltration for house 4 with sheltered 356x127 mm (14x5 in.) combustion air vents open and an unheated flue. Data is binned every 22.5° and error bars are ± one standard deviation. Wind is normal to sheltered vents at 270°. The largest bin has 169 data points, the smallest has 25 data points. 59
4.9 Predicted divided by measured infiltration for house 3 with unsheltered 356x127 mm (14x5 in.) combustion air vents open. Binned ΔC_p correction. Data is binned every 22.5° and error bars are ± one standard deviation. Wind is normal to unsheltered vents at 0°. The largest bin has 178 data points, the smallest has 23 data points. 61

4.10 Predicted divided by measured infiltration for house 4 with sheltered 356x127 mm (14x5 in.) combustion air vents open. Binned ΔC_p correction. Data is binned every 22.5° and error bars are ± one standard deviation. Wind is normal to sheltered vents at 270°. The largest bin has 169 data points, the smallest has 25 data points. 62
4.11 Modelled ΔC_p and wind shelter factor, S_w, used in LOCALEAKS-3 for the north (0°) wall. 64
4.12 Modelled $\Delta C_p S_w^2$ factor used in LOCALEAKS-3 for the north (0°) wall, with binned $\Delta C_p S_w$ values, that produce minimum bias in the model. 65
4.13 Modelled ΔC_p and wind shelter factor, S_w, used in LOCALEAKS-3 for the west (270°) wall. 66
4.14 Modelled $\Delta C_p S_w^2$ factor used in LOCALEAKS-3 for the west (270°) wall, binned $\Delta C_p S_w$ values, that produce minimum bias in the model. 67
4.15 Predicted to measured infiltration ratio plotted against wind direction for House 3. Unsheltered 356x127 mm (14x5 in.) combustion air vents on the north wall. Modelled ΔC_p. Data is binned every 22.5°, with error bars of ± one standard deviation. Wind is normal to unsheltered vents at 0°. The largest bin has 178 data points, the smallest has 23 data points. . . . 68
4.16 Predicted to measured infiltration ratio plotted against wind direction for House 4. Sheltered 356x127 mm (14x5 in.) combustion air vents on west wall. Modelled ΔC_p. Data is binned every 22.5°, with error bars of ± one standard deviation. Wind is normal to sheltered vents at 270°. The largest bin has 169 data points, the smallest has 25 data points. 69
4.17 Predicted to measured infiltration ratio plotted against wind direction for House 3. Unsheltered 356x254 mm (14x10 in.) combustion air vents on the north wall. Modelled ΔC_p. Data is binned every 22.5°, with error bars of ± one standard deviation. Wind is normal to unsheltered vents at 0°. The largest bin has 198 data points, the smallest has 32 data points. . . . 70
4.18 Predicted to measured infiltration ratio plotted against wind direction for House 4. Sheltered 356x254 mm (14x10 in.) combustion air vents on the west wall. Modelled ΔC_p. Data is binned every 22.5°, with error bars of ± one standard deviation. Wind is normal to sheltered vents at 270°. The largest bin has 184 data points, the smallest has 32 data points. . . . 71

5.1 Effective wind pressure coefficients, $C_p S_w^2$, measured on the South wall of house 2 with curve of modelled coefficients used in LOCALEAKS-2. The 1220 data points are binned in 16 wind directions with error bars of ± one standard deviation. . 76
5.2 Effective wind pressure coefficients, $C_p S_w^2$ measured on the west wall of house 2 with curve of modelled coefficients used in LOCALEAKS–2. The 1220 data points are binned in 16 wind directions with error bars of ± one standard deviation. . 77

6.1 Mechanical room with two combustion appliances. Combustion air vents and flue according to the Uniform Mechanical Code. 79
6.2 Ventilation in a mechanical room plotted against wind speed for three appliance power outputs. Wind is blowing toward unsheltered vents and indoor–outdoor temperature difference is $0°C$. 84
6.3 Ventilation in a mechanical room plotted against wind speed for three appliance power outputs. Wind is blowing toward unsheltered vents and indoor–outdoor temperature difference is $40°C$. 84
6.4 Ventilation in a mechanical room plotted against wind speed for three appliance power outputs. Vents are located on downwind side of building and indoor–outdoor temperature difference is $0°C$. 85
6.5 Ventilation in a mechanical room plotted against wind speed for three appliance power outputs. Vents are located on downwind side of building and indoor–outdoor temperature difference is $40°C$. 85
6.6 Ventilation in a mechanical room plotted against wind speed for three appliance power outputs. Vents are on an upwind wall, sheltered by an upwind building and indoor–outdoor temperature difference is $0°C$. 86
6.7 Ventilation in a mechanical room plotted against wind speed for three appliance power outputs. Vents are on an upwind wall, sheltered by an upwind building and indoor–outdoor temperature difference is $40°C$. 86
6.8 Ventilation in a mechanical room plotted against wind speed for three appliance power outputs. Wind is blowing toward unsheltered vents and indoor–outdoor temperature difference is $0°C$. The upper vent is blocked. 87

6.9 Ventilation in a mechanical room plotted against wind speed for three appliance power outputs. Wind is blowing toward unsheltered vents and indoor–outdoor temperature difference is $40°C$. The upper vent is blocked. 88

Nomenclature

A_L	Leakage area at 4 Pa. (cm^2)
A_{local}	Flow area of a local leakage site. (m^2)
A_V	Cross-sectional area of a vent. (m^2)
B_1	AIM-2 superposition factor.
ΔC_p	Difference in wind pressure coefficient between two vents.
$\Delta C_{p\ local}$	Difference in local wind pressure coefficient from the wall average.
C	Flow coefficient. ($\frac{m^3}{s \cdot Pa^n}$)
$C_{ceiling}$	Flow coefficient of distributed leakage in a ceiling. ($\frac{m^3}{s \cdot Pa^n}$)
C_{dist}	Flow coefficient of total distributed leakage. ($\frac{m^3}{s \cdot Pa^n}$)
C_d	Discharge coefficient. ($\frac{m}{s \cdot Pa^n}$)
C_{floor}	Flow coefficient of distributed leakage in a floor. ($\frac{m^3}{s \cdot Pa^n}$)
C_{local}	Flow coefficient of a local leakage site. ($\frac{m^3}{s \cdot Pa^n}$)
C_p	Wind pressure coefficient.
$C_{wall,i}$	Flow coefficient of distributed leakage in wall i. ($\frac{m^3}{s \cdot Pa^n}$)
d	Diameter of a tube. (m)
g	Accelleration due to gravity. (9.81 m/s^2)
H	Vertical displacement between two vents. (m)
K	Laminar flow coefficient of a tube. ($\frac{m^3}{s \cdot Pa}$)
L	Length of a tube. (m)

$\dot{m}$	Mass flow rate of air. (kg/s)
$\dot{m}_{total}$	Total mass ventilation rate in a structure. (kg/s)
n	Flow exponent.
n_{dist}	Flow exponent of distributed leakage.
n_{local}	Flow exponent of a local leakage site.
N	Number of data points.
ΔP	Pressure difference. (Pa)
ΔP_h	Hydrostatic pressure difference across building envelope. (Pa)
ΔP_I	Internal flow balancing pressure difference. (Pa)
ΔP_{local}	Local wind driven pressure difference across building envelope. (Pa)
ΔP_{total}	Total pressure difference across building envelope. (Pa)
ΔP_U	Wind driven pressure difference across building envelope. (Pa)
$\Delta P_{U\ local}$	Wind driven pressure difference at a local leakage site. (Pa)
P	Pressure. (Pa)
P_i	Pressure at sampling location i. (Pa)
P_{in}	Absolute indoor pressure. (Pa)
$P_{in,z}$	Absolute indoor pressure at height z. (Pa)
P_m	Measured pressure. (Pa)
P_{out}	Absolute outdoor pressure. (Pa)
$P_{out,z}$	Absolute outdoor pressure at height z. (Pa)
P_T	Pressure at a transducer. (Pa)
P_∞	Barometric pressure. (Pa)
Q	Volumetric flow–rate of air in a local or distribute leak (flow into the building is positive). (m^3/s)

Q_i	Volumetric flow-rate of air in tube i. (m^3/s)
Q_s	Infiltration rate of indoor density air due to stack effect. (m^3/s)
Q_w	Infiltration rate of indoor density air due to wind effect. (m^3/s)
Re_d	Reynolds number of tube flow.
SD	Standard deviation.
S_w	Wind shelter factor.
ΔT	Indoor–outdoor temperature difference. $(K$ or $^\circ C)$
T_{in}	Indoor air temperature. (K)
T_{out}	Outdoor air temperature. (K)
U	Average wind speed at eve's height. (m/s)
u'	Fluctuating component of wind speed parallel to U. $[m/s]$
v'	Fluctuating component of wind speed perpendicular to U. $[m/s]$
z	Height above grade level. (m)
z_{center}	Vertical height above grade of the center point between two vents. (m)
z_{local}	Vertical height above grade of a local leakage site. (m)

Greek Symbols

ρ	Density of air. (kg/m^3)
ρ_{in}	Density of indoor air. (kg/m^3)
ρ_{out}	Density of outdoor air. (kg/m^3)
μ	Viscosity of air. $(Pa \cdot s)$
θ	Wind direction. 0° = wind from the north. (degrees, clockwise from north)

Chapter 1

Introduction

Planned ventilation has been a part of our technology since the inception of constructed dwellings. Early peoples discovered that in order to benefit from the warmth of an indoor fire, it was necessary to make provisions for ventilation. For example, tightly constructed tepees of North American natives had an exhaust vent at the peak of the roof and a fresh air vent in the form of an open area at the base of the door flap. This is a form of passive ventilation. That is, ventilation is driven by natural driving forces, temperature difference between the building interior and exterior and wind pressures. The flow rate of air entering the building depends upon the prevailing weather conditions. Early peoples learned to optimize the size of the ventilation openings in their homes to maintain safe air quality and interior warmth. Over time, rules of thumb were developed and incorporated into the construction method of their traditional dwellings.

Combustion appliances in modern buildings are ventilated in essentially the same fashion. Passive vents are installed in mechanical spaces and sized according to local codes. Since the codes are based on past engineering practices and not on the physics of passive ventilation, problems can arise when installations are made in circumstances for which the original code was not intended. A particular case of this is the use of code-specified vents in cold climates. Extreme weather conditions have caused over ventilation resulting in freezing mechanical rooms and broken water lines. This study was undertaken to develop an understanding of the physics of passive ventilation in combustion air vent installations common in North America. This will aid in the development of engineered methods of providing combustion air with consideration to local climatic variation and ever changing construction methods.

1.1 Combustion Air Supply

The supply of air for combustion devices is an application of passive ventilation that is of particular importance and is the primary focus of this study. Like the simple fires used to heat our ancestors dwellings, our modern combustion appliances require a supply of fresh air. For most homes and buildings this air is supplied by passive ventilation, as specified by national building codes. In Canada these are the Natural Gas Code (Canadian Gas Association 1991a) and the Propane Code (Canadian Gas Association 1991b) and in the United States the Uniform Mechanical Code (International Conference of Building Officials 1991). These codes are similar, in that they specify passive vents for combustion air supply but they differ in application and sizing methods. Local jurisdictions frequently form individual interpretations to the codes. For simplicity, passive vent installations according to the Uniform Mechanical Code were used in this study.

Figure 1.1 is an example of a passive combustion air system typical of residences and low–rise buildings. Two combustion air ducts extend from an enclosed space containing combustion appliances to the exterior of the building, in this case an outside wall. The free area of the ducts are sized using only the maximum rated fuel input to the combustion appliances (the furnace and the water heater) in the enclosed space. The Uniform Mechanical Code specify that two ducts of equal size be used, one within 300 mm of the floor (below the draft hood of the flue) and the other within 300 mm of the ceiling (as high above the draft hood as possible to act as an exhaust hole in the case of a flue blockage).

A survey of Canadian codes dealing with combustion air was carried out by Mayo (1985). It is suggested throughout the document that the technical basis for the code provisions is unknown. It is further suggested that the sizing of vents is based on rules of thumb stemming from what worked in practice. These rules of thumb may have been acceptable when the codes were developed but given the rapid change in building technology over the past couple of decades, in particular the great increase in the tightness of building envelope construction, the validity of the sizing criteria must be questioned.

It is also clear that there is a lack of design methodology in the installation of passive combustion air vents. Passive ventilation is dependent upon natural driving forces; wind and indoor–outdoor temperature difference. Clearly a passive vent system will experience very different flow rates in Newfoundland from an identical system in the Yukon, due to the difference in average climatic conditions. The current codes give no consideration to local climate or for that matter seasonal variation in weather, which is significant in most

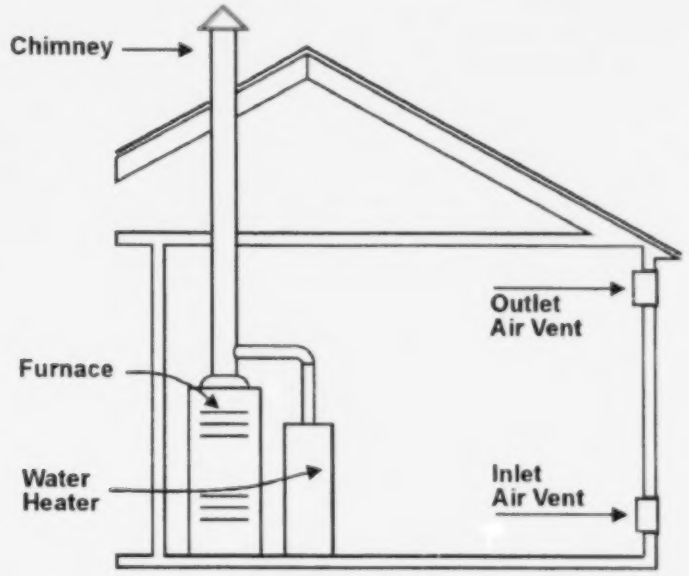

Figure 1.1: A Typical Installation of Passive Combustion Air Vents in a Mechanical Equipment Room.

parts of Canada. This means that a given combustion air system may over-ventilate a mechanical space in winter when driving forces are high, leading to freezing boiler rooms and broken water lines. In the summer the driving forces may be to low to provide adequate combustion air, leading to poor combustion and the production of carbon monoxide gas.

The variability in the flow-rate of any passive combustion air system can lead to costly over ventilation and in some cases even lethal under-ventilation. The task of improving the current codes outlining the provision of combustion air is complicated by the fact that passive ventilation is very difficult to predict given: the variation in weather conditions, variation in building envelope tightness, the presence of various mechanical ventilators, building geometry and other factors. Analytically predicting the supply of combustion air in these circumstances is impossible. The only tool available to examine the problem is to develop a computer model that may be used to develop an understanding of the problem. Once the problem is quantified and understood, new codes may be developed that can more accurately deal with supplying combustion air.

1.2 Previous Studies in Passive Ventilation

Extensive studies in ventilation have been carried out in the Department of Mechanical Engineering at the University of Alberta. Much of this work is was performed at The Alberta Home Heating Research Facility. This is a facility of unoccupied test houses maintained by the department for ventilation and other building science studies. The houses are extensively monitored using a digital data acquisition system. Measurements made on site include hourly averages of infiltration and weather conditions. A data base of thousands of hours of weather and infiltration data has been accumulated.

Recent work by I.S. Walker and D.J. Wilson in the field of passive ventilation are of particular importance to this study. The infiltration model LOCALEAKS was developed by Wilson and Walker (1992) and a refined version, LOCALEAKS–2 was developed by Walker (1993). LOCALEAKS–2 was adapted for this study to model ventilation with combustion air vents, resulting in an improved version LOCALEAKS–3.

1.3 The scope of this study

This study was undertaken to investigate the behaviour of passive combustion air vent systems and to use this information to adapt the LOCALEAKS–2 passive ventilation model into a suitable tool for predicting ventilation in passive combustion air vents. The study began with experimental work, conducted at the Alberta Home Heating Research Facility. Full scale measurements of passive ventilation in combustion air vents were taken. This data was then used to develop and validate a modified version of the LOCALEAKS–2 infiltration model. This new infiltration model LOCALEAKS–3 includes a model for estimating wind pressure on local leakage sites in order to improve ventilation estimates through such leaks.

The wind pressure coefficient models used in LOCALEAKS–2 were developed from wind tunnel tests on model buildings, due to the absence of data from full scale tests. In order to develop full scale data for the further development of LOCALEAKS–2 and other infiltration models, a wind pressure measurement program was initiated at the Alberta Home Heating Research Facility. Some of the preliminary data collected is compared with the pressure coefficient model used in LOCALEAKS–2.

Chapter 2 includes an introduction to the theory of passive ventilation. This theory of passive ventilation is applied to the two hole combustion air vent problem to demonstrate the effect of local wind pressure, and a description of the LOCALEAKS–2 model presented.

Chapter 3 presents all the experimental work that was carried out for this study. The installation of combustion air vents in the test houses and the related calibrations and measurements are described. The measurement system installed in the test house to measure wind pressure coefficients is also described.

Chapter 4 describes the development of the new local wind pressure coefficient model included in LOCALEAKS–3. The model is calibrated and validated with the measurements described in Chapter 3.

Chapter 5 is a comparison of the full scale wind pressure coefficient measurements with the model used in LOCALEAKS–2.

Chapter 6 presents some predictions of ventilation in mechanical rooms modelled with the LOCALEAKS–3 model.

Chapter 7 is a summary of conclusions and recommendations for future study.

Chapter 2

Passive Ventilation and LOCALEAKS–3

This chapter presents the basic theory of passive ventilation, with emphasis on ventilation through two combustion air vents on the same wall. The LOCALEAKS–2 infiltration model is described and the modifications for large openings in walls included in LOCALEAKS-3 are presented.

2.1 Passive Ventilation

Passive ventilation is produced by indoor–outdoor temperature differences and wind, causing air to flow through various leakage sites in building envelopes. This section provides the necessary information about driving forces and the nature of building leakage that is required to model passive ventilation.

2.1.1 Flow Characteristics of Building Leakage

Leakage sites can be split into two categories, intentional openings and unintentional leakage. Intentional openings are designed to provide ventilation for specific purposes. They include flues for venting combustion gases and combustion air vents to provide air to combustion appliances. Unintentional openings are usually small cracks and holes that form distributed leakage in the building envelope. Individually these cracks and holes may be small, but collectively they can represent a large portion of a building's leakage area.

In order to model passive ventilation an empirical power–law equation was used to describe the pressure–flow relationship for various leakage sites.

$$\dot{m} = \rho C \Delta P^n \tag{2.1}$$

Where $\dot{m}$ is the mass flow rate, ρ is the density of the air and ΔP is the change in pressure across the leakage site. Each leakage site has a flow coefficient C, and a flow exponent n, that are experimentally derived for each leakage site. The power–law equation for describing building leakage was proposed by Sherman and Grimsrud (1980), because of its usefullness in describing different leakage sites.

It can be shown that the power law equation will describe fully developed turbulent (orifice) flow with a flow exponent, n equal to 0.5. Fully developed laminar (Poiseille) flow can be described with a flow exponent equal to 1.0. Kronvall (1980) showed that for building leaks composed of a series of thin cracks, flow is never fully developed and flow exponents between 0.5 and 1.0 are appropriate. A value of 0.67 is common a building envelope's total average leakage.

The flow equations of the combustion air vents and the distributed leakage of the test houses were determined using laboratory and field testing. The combustion air vents were calibrated in a test apparatus while the house leakage was determined with a depressurization test. Both methods are described in the next chapter. Note that the sign convention for this study is that flow into the building envelope is positive.

2.1.2 Driving Forces of Passive Ventilation

In a mechanically ventilated building, ventilation can be controlled by varying the power input to the fan. With passive ventilation, pressure to move air is provided by the natural driving forces: wind and indoor–outdoor temperature difference. In this case the driving forces cannot be controlled. Furthermore the large natural variation present in hourly weather conditions complicates any effort to control natural ventilation by varying the building leakage.

Thermal Buoyancy

Thermal buoyancy or "stack effect" as it is commonly known, is driven by temperature differences between the interior and exterior of a building envelope. Energy is expended to heat or cool building interiors to maintain them at a constant temperature dictated by human comfort. The energy added or removed from the interior air to change the temperature also changes the density of the interior air. This density difference in turn causes the interior air to have different buoyancy from the exterior air, thus inducing driving pressures on the building envelope. When the building interior is cooled the interior air becomes negatively buoyant, when heated it becomes positively

buoyant. Stack effect is not purely a natural driving force because it depends on the addition of energy from internal heat sources. However, as this energy addition is dictated by interior temperature requirements and is variable with outside temperature, it causes uncontrolled ventilation forces that must be accounted for in any passive ventilation scheme.

The hydrostatic pressure gradient in still air is given by

$$\frac{\partial P}{\partial z} = -\rho g \tag{2.2}$$

where ρ is air density, g is the acceleration due to gravity and z is the height above grade level. Gradients in the horizontal directions, x and y are zero for atmospheric air under static conditions.

Equation 2.2 can be used to calculate hydrostatic pressure across the building envelope. In order to assume a linear profile for hydrostatic pressure with height, it is required that the interior and exterior air are well mixed and of constant densities. Dale and Ackerman (1993) showed that the mixing of air inside test houses is sufficient to confine the temperature gradients to a thin layer on the building envelope. This means that the density gradients will also be confined to thin layer on the interior surface of the walls making the bulk of the interior air of constant density. Andersen (1995) also showed that for atria with two large openings similar to the large openings used in this study, the air in the space is well mixed with a constant temperature. The temperatures and therefore the hydrostatic pressure gradients described by Equation 2.2 are not the same for the interior and exterior of the building. By applying Equation 2.2 to both the interior and exterior and taking the difference of these, the pressure differential across the envelope is

$$\frac{\partial \Delta P_h}{\partial z} = (\rho_{in} - \rho_{out})g \tag{2.3}$$

where ΔP_h is the hydrostatic pressure difference across the building envelope. By assuming that air is an ideal gas, the density terms may be expressed as absolute pressures and temperatures.

$$\rho_{in} - \rho_{out} = \frac{\rho_{out}\Delta T}{T_{in}}\left(1 - \frac{T_{out}\Delta P}{\Delta T P_{out}}\right) \tag{2.4}$$

Equation 2.4 is derived in Appendix A. Because the pressure change across the envelope is small compared to the atmospheric pressure, P_{out}, it can be neglected and Equation 2.3 becomes

$$\frac{\partial \Delta P_h}{\partial z} = -\rho_{out} g\left(\frac{T_{in} - T_{out}}{T_{in}}\right) \tag{2.5}$$

Equation 2.5 states that the pressure difference due to indoor–outdoor temperature difference is a linear function of vertical location on the wall and indoor–outdoor temperature difference. Equation 2.5 can be integrated to give ΔP_h as a function of height z, measured from grade level. The boundary condition of intigration is $\Delta P_h = 0$ at $z = 0$.

$$\Delta P_h = -zg\rho_{out}\left(\frac{T_{in} - T_{out}}{T_{in}}\right) \tag{2.6}$$

The constant of integration is zero because there is no pressure difference due to stack effect at grade level for the static case (no flow through the wall).

Wind Pressure

Wind pressure is the other driving force in passive ventilation. Wind action on building surfaces results in positive pressures on upwind surfaces where stagnation occurs and negative pressures in regions downstream of separation. To describe the pressure effects of wind on building surfaces, it is common industry practice for a wind pressure coefficient, C_p, to be used. The pressure coefficient is the ratio of the wind pressure on a surface of the building envelope, relative to atmospheric pressure, ΔP_U, divided by the stagnation pressure of the wind at eve's height, $\frac{\rho_{out}U^2}{2}$,where U is the wind speed at eve's height.

$$C_p = \frac{\Delta P_U}{\frac{\rho_{out}U^2}{2}} \tag{2.7}$$

Various obstacles like vegetation and other nearby structures provide wind shelter that effect the wind pressure on a given building. This is accounted for by defining a shelter factor, S_w, that modifies the wind speed in the wind pressure equation.

$$\Delta P_U = \rho_{out}C_p\frac{(S_wU)^2}{2} \tag{2.8}$$

Pressure Difference Across the Building Envelope

In order to calculate the air flow through some particular leakage site on the building envelope it is necessary to calculate the total pressure difference across the envelope, ΔP_{total}, at that location. The total pressure difference is the sum of the individual pressures acting on the internal and external surfaces of the envelope. Figure 2.1 shows a vertical profile of the various pressures acting on the internal and external surfaces of the building envelope. Stack pressure, ΔP_h, is the sum of the hydrostatic pressures on

the internal and external wall surfaces. The ΔP_h shown in Figure 2.1 has a steeper pressure gradient on the outside surface than the inside surface which is consistant with the outside air being colder and more dense than the inside air. Wind pressure, ΔP_U, is represented by an irregular profile on the external surface of the envelope and the ΔP_U shown for an upwind surface. The variation of ΔP_U in the vertical direction will be discussed in a later section. The internal mass–flow balancing pressure difference , ΔP_I, is an internal envelope pressure difference resulting from flow from various leakage sites pressurizing the interior of the building. To understand how ΔP_I arises, picture a cubical structure with two open vents. At one vent a steady driving pressure is exerted causing in–flow through that vent. In order that conservation of mass be maintained, out–flow must be induced at the other vent. In order for this flow to occur driving pressure must be transmitted to the other vent via a pressure change in the structure, ΔP_I. In a real structure every leakage site will influence ΔP_I, making it a function of the building leakage configuration as well as the wind pressure and indoor–outdoor temperature difference. Equation 2.9 shows the total pressure across the envelope, with in–flow positive.

$$\Delta P_{total} = P_{out,z} - P_{in,z} = \Delta P_U + \Delta P_h - \Delta P_I \tag{2.9}$$

The total pressure difference across the envelope, ΔP_{total}, is shown as the last profile of Figure 2.1. The pressure differences combine into a total pressure profile that is positive (inflowing) at the bottom and negative (outflowing) at the top. The negative and positive regions are separated by the neutral plane. This neutral plane can be displaced up or down the envelope by changing the wind pressure or by a change in ΔP_I (by altering the leakage for example). Normally the profile of P_{total} is assumed to be linear, implying constant ΔP_U, shown by the dashed line in Figure 2.1. The non-linear nature of wind pressure is an important aspect of this study.

2.1.3 Passive Ventilation Through Large Openings

Passive ventilation systems consisting of two vents mounted in a side wall with vertical displacement between them is a common method of providing air to combustion appliances. Figure 2.2 shows a simple model of a typical combustion air vent installation. Two passive vents of equal size are installed in an enclosed space, one near the ceiling and the other near the floor. Other leakage sites that would normally be present such as a flue and distributed leakage are neglected in order that the function of the combustion air vents may be illustrated.

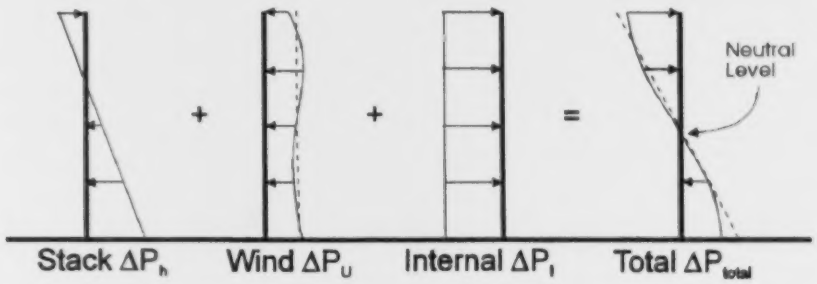

Figure 2.1: The total pressure across a building envelope is the sum of the stack pressure, ΔP_h, the wind pressure, ΔP_U and the Internal mass–flow balancing pressure difference, ΔP_I. Shown for a stagnation wall (ΔP_U positive).

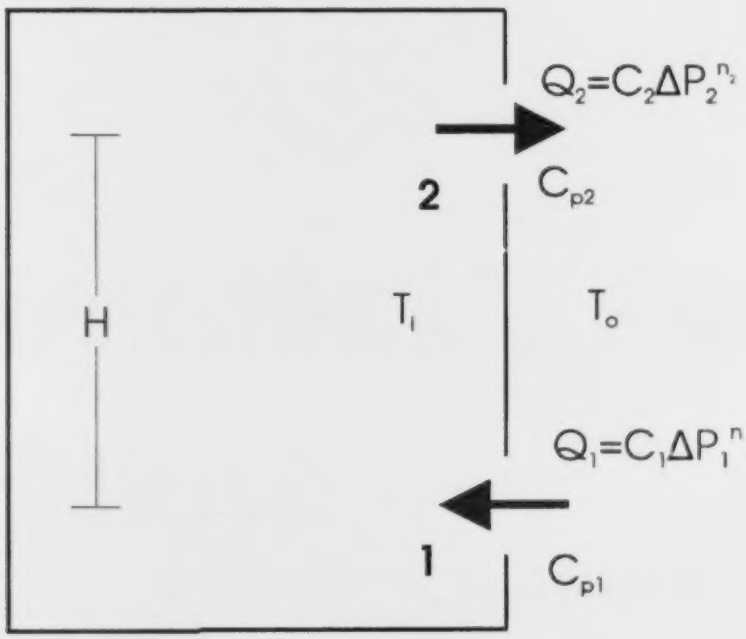

Figure 2.2: Passive ventilation in a simple structure with two large openings. Ventilation is driven by indoor–outdoor temperature difference and wind pressure. T_i and T_o are the air temperatures of the interior and exterior air, respectively. H is the vertical distance between the centre of the holes and C_{p1} and C_{p2} are the wind pressure coefficients on holes 1 and 2 respectively. Arrows indicate stack driven flow for $T_i > T_o$.

The two hole arrangement was conceived as a method of ensuring large ventilation rates through the vents. By placing one hole near the floor and the other near the ceiling, the vertical distance between the holes is maximized, ensuring the maximum possible pressure difference across the vents due to stack effect. As combustion appliances are operated at their maximum level during colder weather, combustion air supply will also be maximized during cold weather due to increased stack pressure. Under these conditions cold dense air will enter the space through the lower vent, while warm buoyant air exits through the upper vent. By placing the vents on the same wall it is believed that there will be a negligible difference in wind pressure between the two vents for any wind speed or direction, ensuring that wind pressure will have no significant effect on the ventilation rate.

By knowing the characteristic flow equation, $Q = C\Delta P^n$ for each vent and the vertical distance between them, H, the ventilation rate (kg/s) is given by Equation 2.10 for flow going in the lower vent and out the upper vent and Equation 2.11 for the reverse-flow case. Both equations are derived in Appendix A.2.

$$\dot{m}_{total} = \rho_{out} C_1 \left[\frac{\rho_{out} g H \frac{T_{in} - T_{out}}{T_{in}} - \rho_{out} \Delta C_p \frac{U^2}{2}}{1 + \left(\frac{T_{in}}{T_{out}}\right)^2 \left(\frac{C_1}{C_2}\right)^2} \right]^{0.5} \tag{2.10}$$

$$\dot{m}_{total} = \rho_{in} C_1 \left[\frac{\rho_{out} g H \frac{T_{out} - T_{in}}{T_{in}} + \rho_{out} \Delta C_p \frac{U^2}{2}}{1 + \left(\frac{T_{out}}{T_{in}}\right)^2 \left(\frac{C_1}{C_2}\right)^2} \right]^{0.5} \tag{2.11}$$

The flow exponents n_1 and n_2 are assumed to equal to 0.5, because large vents behave close to orifice flow theory and a new parameter

$$\Delta C_p = C_{p2} - C_{p1} \tag{2.12}$$

is the difference in wind pressure coefficients between the two vents. As can be seen in these equations the ΔC_p factor determines the effect wind will have on the ventilation rate in the two hole model. A ΔC_p of zero will result in no variation in ventilation rate with wind speed, while positive or negative values of ΔC_p may cause the ventilation rate to increase or decrease with U, depending on the flow direction in the vents.

To illustrate the effect of the ΔC_p factor, consider the case where $H = 2.15\ m$ and $C_1 = C_2 = 0.041$. These values are equal to those of the 356x254 mm vent configuration used in experimental work described in Chapter 3. Figures 2.3, 2.4, 2.5 and 2.6 were generated from Equations 2.10 and 2.11. Figure 2.3 shows calculated ventilation rate versus wind speed at an indoor-outdoor temperature difference of $40°C$ and several ΔC_p values. The line of

$\Delta C_p = 0.00$ has equal wind pressure on each vent, regardless of wind speed. The ventilation is purely the result of the $40°C$ indoor–outdoor temperature difference causing air to flow in the bottom hole and out the top. This line represents the generally assumed behaviour of vents on the same wall, that is, differences in wind pressure coefficients on the same wall are small and therefore can be neglected. However small differences in wind pressure coefficient (ΔC_p) can have a large effect on ventilation rates. Negative values of ΔC_p, where wind pressure is larger on the lower vent than the upper vent, increase the ventilation rate with wind speed. Positive ΔC_p places more wind pressure on the upper vent than the lower vent, resisting the stack driven flow reducing the total ventilation rate. As wind speed is increased, the flow will be reduced to a stop, at which point the flow reverses and air flows in the upper vent and out the lower vent. Figure 2.3 shows that a relatively modest ΔC_p of 0.10 causes a flow reversal at approximately 7.5 m/s wind speed, despite the very large temperature difference of $40°C$. Figures 2.4 and 2.5 show similar plots for smaller temperature differences, $20°C$ and $10°C$ respectively. In these plots the larger relative strength of the wind result in flow reversals occurring at lower wind speeds and a greater variation in ventilation rates with wind speed. Figure 2.5 shows a flow reversal at less than 4 m/s with a $\Delta C_p = 0.10$. Ventilation rates vary from 300 m^3/h to 0 m^3/h depending on wind speed and ΔC_p which is a function of wind direction. Assuming that wind has no effect on ventilation ($\Delta C_p = 0$) a constant rate of approximately 100 m^3/h is predicted. Therefore predictions of ventilation can be false if wind is not accounted for.

Along with this large variability of ventilation with wind is a large sensitivity to very small changes in wind. Referring again to Figure 2.3, note the very large change in ventilation rate with small changes in wind speed. On the $\Delta C_p = 0.10$ curve the ventilation rate can change by 100 m^3/h with a 0.5 m/s change in wind speed. Very large changes in ventilation rate can occur if the ΔC_p value changes, which would be the case with changes in wind direction. Figure 2.6 shows the case with no indoor–outdoor temperature difference where ventilation is driven by wind alone. Positive and negative values of ΔC_p result in equivalent ventilation rates, with the flow direction reversed in the vents.

2.1.4 Wind Pressure Coefficients and ΔC_p

The use of wind pressure coefficients to calculate wind pressure for load calculation and infiltration modelling is common place. In general, published data, mostly from wind tunnel studies, are used to estimate wind pressure coefficients on real structures. The complexity of wind pressure distributions

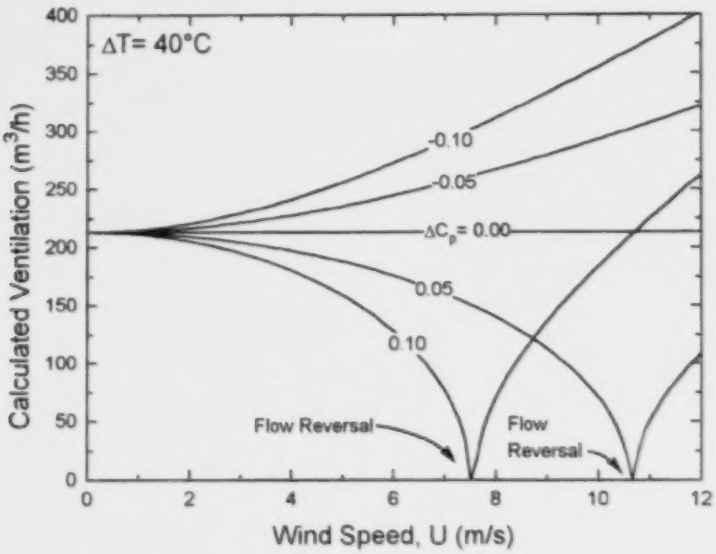

Figure 2.3: Calculated ventilation rates in a two-vent house. The indoor-outdoor temperature difference is 40°C and the flow coefficient in each vent is 0.041 $m^3/s \cdot Pa^n$. Ventilation is in m^3/h of indoor temperature air.

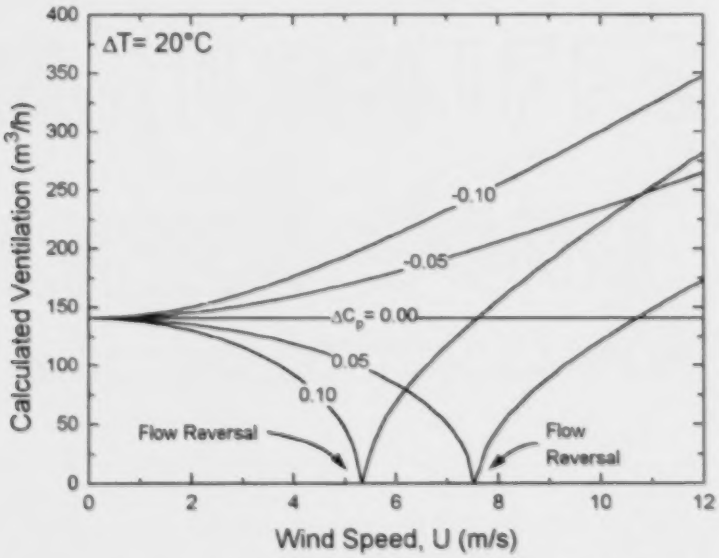

Figure 2.4: Calculated ventilation rates in a two-vent house. The indoor-outdoor temperature difference is 20°C and the flow coefficient in each vent is 0.041 $m^3/s \cdot Pa^n$. Ventilation is in m^3/h of indoor temperature air.

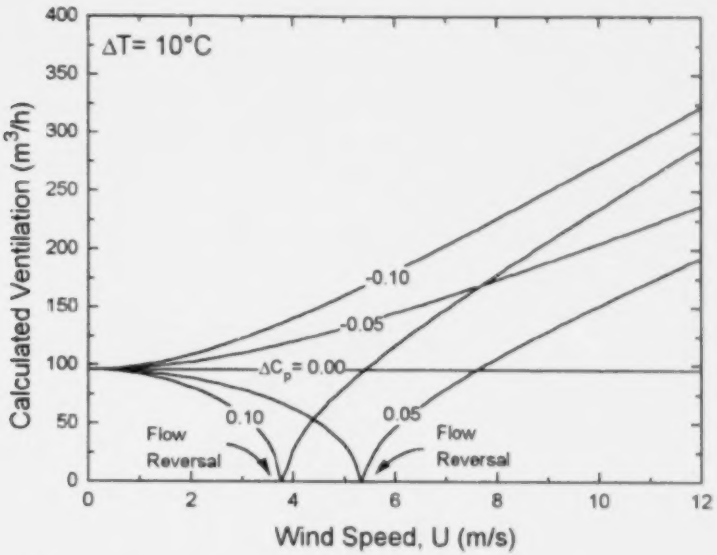

Figure 2.5: Calculated ventilation rates in a two-vent house. The indoor-outdoor temperature difference is 10°C and the flow coefficient in each vent is 0.041 $m^3/s \cdot Pa^n$. Ventilation is in m^3/h of indoor temperature air.

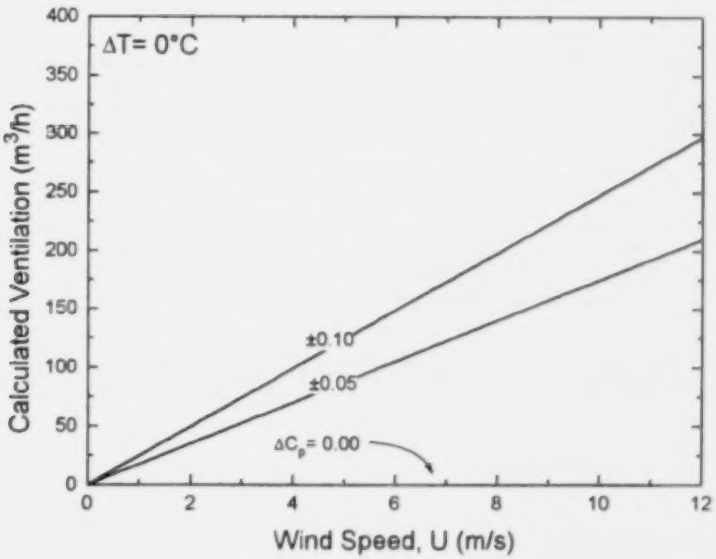

Figure 2.6: Calculated ventilation rates in a two-vent house. The indoor-outdoor temperature difference is 0°C and the flow coefficient in each vent is 0.041 $m^3/s \cdot Pa^n$. Ventilation is in m^3/h of indoor temperature air.

makes it very difficult to measure and record local pressure coefficients for an entire building surface, for every wind angle. Furthermore local pressure coefficient measurements would only be useful for the specific structure tested, making it impractical for general use in building calculations. Instead a simplified approach is taken where the pressure over entire building surfaces is measured as an average, generating wall averaged wind pressure coefficients. These wall averaged coefficients have been measured for many simple building shapes and are used to estimate wind pressure on similar buildings.

When wall averaged pressure coefficients are used, an assumption is made that wind pressure differences on that wall are small and therefore unimportant to the infiltration calculation. Walker (1993) showed that the use of wall averaged wind pressure coefficients in infiltration modelling, produces good results as long as the leakage is well distributed and large vents do not dominate the building leakage. When leakage is uniformly distributed over a surface, the error in calculating flow through particular leaks due to error in estimating local wind pressure through use of wall averaged coefficients is compensated by similar errors over that surface. On the average the errors cancel and an accurate estimate of infiltration is achieved.

However, when large vents dominate the leakage in a structure, like the combustion air vents described in the previous subsection, very small differences in wind pressure coefficient between vents can have a large effect on air flow rate. If these vents were on the same wall, the wall averaged coefficients would produce the same calculated wind pressure on each vent causing large errors in the infiltration calculation. Figure 2.7 shows wind pressure coefficient data compiled from figures in Wiren (1985), in which pressure measurements were carried out on model bungalows in a wind tunnel. Wall averaged and two local pressure coefficients are shown for a wall on an unsheltered house. Note that the wind direction convention for this study is as follows. Winds from the North are referenced as being at 0°, while winds from the East, South and West are at 90°, 180° and 270° respectively. Similarily a "north wall" is a wall with an outward normal pointing North.

The local pressure coefficients in Figure 2.7 were taken on the vertical centre line of a wall, one at approximately ceiling height and the other at floor height. These correspond very closely to the location of combustion air vents used in experimental work in Chapter 3. Figure 2.7 shows how there is large difference in pressure coefficient for most wind directions, with a difference of approximately 0.1 for half of the wind directions. Figures 2.3 through 2.6 showed how a ΔC_p of 0.1 between two vents would cause large changes in the ventilation rate with wind speed. Clearly it is necessary to develop a more accurate model of wind pressure if ventilation in large vents

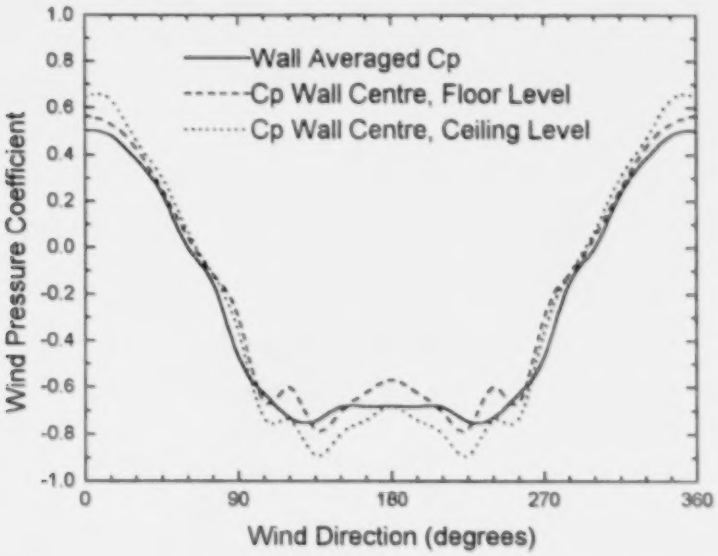

Figure 2.7: Pressure coefficients on a unsheltered bungalow taken from figures in Wiren (1985). Wiren's data was splined with data points every 15°. Wind directions are shown for a north facing wall.

is to be predicted. A model for local wind pressure will be developed later in this study for inclusion in the LOCALEAKS–3 infiltration model.

2.1.5 The LOCALEAKS–2 Passive Infiltration Model

Passive ventilation in real houses is a complex process. Cracks around windows, between walls and the foundation, in ceilings and in the vapour barrier, as well as intentional openings, like combustion air vents and flues, all contribute to a building's overall leakage. The flow through each leak depends on the pressure across it. The internal pressure of the structure is also affected by each leak. This makes the flow in any one leak a function of the building's overall leakage. The sum of the mass flows in and out of the structure must equal zero to satisfy conservation of mass. The process is further complicated by the non–linear pressure–flow relationship of building leakage that does not allow flows from different driving forces to be calculated separately and simply added.

Sherman and Grimsrud (1980) developed a passive infiltration model at Lawrence Berkeley Laboratories. The LBL model forms the basis for infiltration estimation in the Handbook of Fundamentals, ASHRAE (1993). Building leakage, including passive vents is modelled by distributing it as

uniform porosity over walls, ceiling and floor. To account for the relative importance of wind and stack effects, Sherman and Grimsrud divided the building leakage into three user defined fractions, at ceiling level, floor level and in the walls. The leakage sites were assumed to behave like orifices, with flow rates proportional to the square root of pressure difference. Flow due to stack effect and wind effect were calculated separately with the use of wind and stack effect flow factors. These factors are functions of building leakage distribution developed by solving non–linear flow equations from a wide range of leakage configurations. Wind and stack flow are then combined by squaring them, adding them together and taking the square root. These approximations allow estimation of air infiltration by simple direct calculation, eliminating the need to solve non–linear flow balance equations.

The Alberta Air Infiltration Model AIM–2 was developed by Walker and Wilson (1989). This model was developed using similar techniques to the LBL model but incorporated some advanced features. A more realistic power law flow model was included (LBL assumed orifice flow) and ventilation through a flue was modelled separately from the distributed leakage. Like LBL, AIM–2 used approximating functions to fit the numerical solutions to the infiltration flow balance equations. An alternate model for combining flow due to stack effect and wind pressure was proposed in AIM–2,

$$Q = \left(Q_s^{\frac{1}{n}} + Q_w^{\frac{1}{n}} + B_1 \left(Q_s Q_w \right)^{\frac{1}{2n}} \right)^n \tag{2.13}$$

where Q_s and Q_w are the flows due to stack effect and wind pressure respectively and n is the flow exponent of the house leakage (experimentally determined). This superposition method improves on the orifice flow assumption of the LBL model and included an extra term with an experimentally determined coefficient that accounts for interaction between the wind and stack leakage.

Both LBL and AIM–2 assume wind shelter is distributed evenly over the whole house and approximates local leakage sites by distributing their leakage over all four walls. The LOCALEAKS–2 model was developed by Wilson and Walker (1991) to more accurately account for sensitivity of wind shelter factors to wind direction and allow for modelling of local passive inlets and outlets as well as exhaust and supply fans. Unlike the LBL and AIM–2 models, LOCALEAKS–2 is based on a numerical solution of non–linear inflow–outflow balance and approximations used to develop the closed form solution to flow are not required. A summary of LOCALEAKS–2 features is as follows:

- **Distributed Leakage:** The unintentional leakage due to cracks and perforations in the building envelope is distributed by the user in six

separate locations: floor, ceiling and each of the four walls. The floor level leakage is assumed to occur along a uniform crack around the building perimeter that experiences the pressure coefficient of the wall above it. The pressure coefficient of ventilated crawl spaces and attics is approximated by a weighted mean of the four wall pressure coefficients. The weighting is based on user specified fractions of attic or crawlspace ventilator area on each wall and the roof. The pressure flow relationship of the building is given by

$$Q = C_{dist}\Delta P^{n_{dist}} \tag{2.14}$$

where C_{dist} and n_{dist} are the flow coefficient and exponent of distributed leakage, which are determined from a fan pressurization test of the structure. The flow exponent, n_{dist}, is assumed equal for all leakage sites while the flow coefficient is divided as follows

$$C_{dist} = C_{ceiling} + C_{floor} + C_{wall1} + C_{wall2} + C_{wall3} + C_{wall4} \tag{2.15}$$

where the floor, ceiling and wall coefficients are determined from user specified fractions. Estimates of these fractions used in this study are 20% ceiling, 20% floor and 15% in each wall (Walker (1993)).

- **Local Leakage Sites:** Flues and passive vents are modelled separately from the distributed leakage as local leakage sites. The default assumption for the flow in these sites is that they behave like sharp edged orifices with an $n_{local} = 0.5$ and an effective flow area of $C_d A_{local}$ where C_d is the discharge coefficient and A_{local} is flow area of the vent. Values of discharge coefficients are 0.6 for short pipes and vents and 0.56 for flues with a rain cap. Alternatively a flow coefficient C_{local} and flow exponent n_{local} in $Q = C_{local}\Delta P^{n_{local}}$ may be specified for each leak.

- **Doors and Windows:** The leakage area from an open door or window often crosses the neutral pressure level of the building, causing reversed flow directions on either side of the neutral level. LOCALEAKS-2 requires that height and width of the opening be specified. Counterflow mixing theory developed by Kiel and Wilson (1986) is used to calculate inflow and outflow separately above and below the neutral pressure plane.

- **Flues:** Flues are treated like a local leak orifice with a flow area, A_{leak} equal to the smallest restriction area of the flue. The heights

of the flue top and bottom are specified by the user. The flue is assumed to be filled with room temperature air if the flue is venting and outside temperature air if the flue is back–drafting. Alternatively the flue gas temperature can be specified to simulate hot flue gases or in LOCALEAKS–3 an energy balance can be chosen that calculates the flue gas temperature based on power input and gas flow–rate in the flue. This gives a more realistic estimation of an actual flue gas temperature given the steady combustion nature of most combustion appliances and variable flow dilution of flow hoods.

- **Supply and Exhaust Fans:** High pressure supply and exhaust fans can be specified that supply constant flow rates regardless of envelope pressures. Alternatively user specified fan performance curves can be included and fan location can be input for fans which vary flow–rate with external pressure differences.

- **Wind Shelter and Pressure Coefficients:** Two sets of pressure coefficients are used in LOCALEAKS–2 to calculate wall wind pressures. For an isolated house, pressure coefficients derived from Akins, Peterka, and Cermak (1979) are used. Air flow over an isolated house causes large regions of separation on walls parallel to the wind, resulting in negative pressure coefficients on these side walls. However when another house is located upwind, these regions of separation will be smaller and the resulting sidewall pressure coefficient will be less negative. A house in a closely spaced row of houses will experience this effect on the walls parallel to the row. For this reason these walls use a modified pressure coefficient. Figure 2.8 shows the two sets of pressure coefficients used in LOCALEAKS–2. The dashed curve is pressure coefficient on the wall of an isolated house. The solid curve is the pressure coefficient for an unsheltered wall on a house in a closely spaced row.

  Recalling Equation 2.8, the wind pressure on a wall is modelled by the use of the wind shelter coefficient, S_w, as well as the wind pressure coefficient. The wind shelter factor modifies the wind speed in Equation 2.8 to model the effect of nearby obstacles effecting the speed of the on-coming wind. The wind shelter coefficients used in LOCALEAKS–2 were developed by Walker (1993). The model accounts for the distance of obstacles from the house and for the natural variability of atmospheric turbulence over time. Values of S_w were calculated for every one degree of wind direction for each wall and roof surface of the test houses to be discussed in Chapter 3. Equation 2.8 can be re–arranged slightly to combine pressure coefficient and the wind shelter coefficient

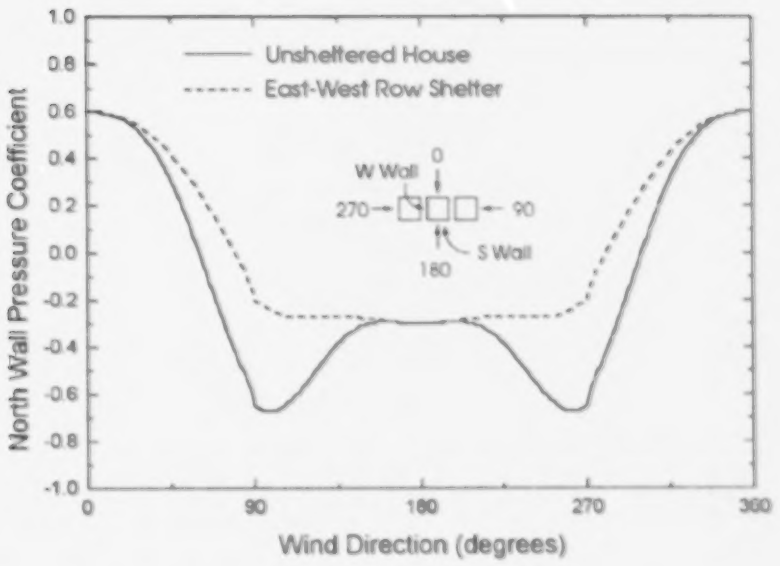

Figure 2.8: Pressure coefficients used in LOCALEAKS-2 for a north (0°) facing wall on an isolated house and a house in an east–west row. The east–west row C_p is less negative when wind is blowing along the row (90° or 270°) because separation is reduced by the upwind houses.

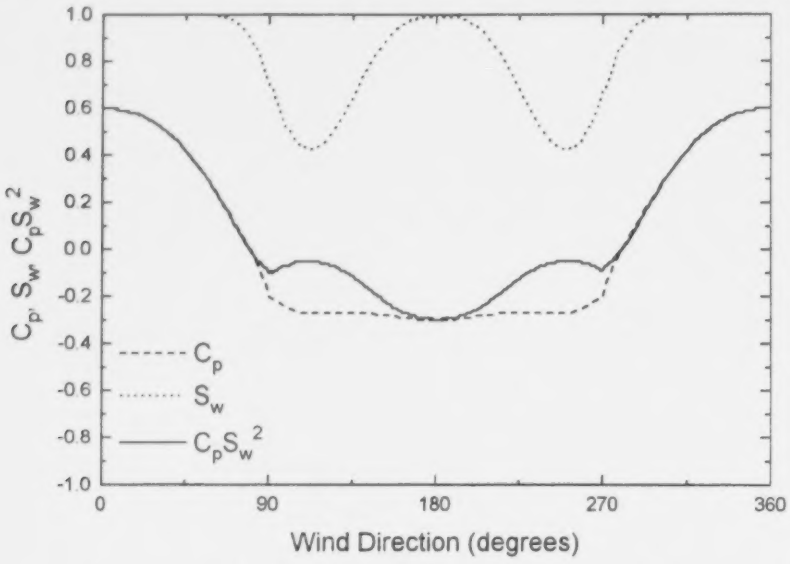

Figure 2.9: Pressure and shelter coefficients used for modelling wind on the north (0^o) wall of the test houses. As the test houses are in an east–west row, the north wall uses the row sheltered C_p. South wall is similar with 180^o shift.

into a single factor, the effective wind pressure coefficient.

$$\Delta P_U = (C_p S_w^2)\frac{U^2}{2} \tag{2.16}$$

Figures 2.9 and 2.10 are plots of the wall averaged wind pressure coefficient, C_p, wall averaged wind shelter coefficient, S_w and the combined coefficient $C_p S_w^2$ for walls on the test houses used by LOCALEAKS–2.

- **Method of Solution:** As the internal pressure ΔP_I of the structure is dependant upon the flow through all the leakage sites and flow through any one leakage site is in part dependant upon P_I, a closed form solution to the total building ventilation is not possible. Instead a numerical solution is achieved by calculating the inflow and outflow through all local and distributed leaks which must total zero to satisfy the conservation of mass in a control volume defined by the building envelope. The numerical method is to iterate values of P_I and calculate the flow balance. The first estimation of P_I is $P_I - P_\infty = 0$. The next guess is P_I is $P_I - P_\infty = 1000Pa$ if total inflow exceeds total outflow or $-1000Pa$ if outflow exceeds inflow. Successive iterations use a method

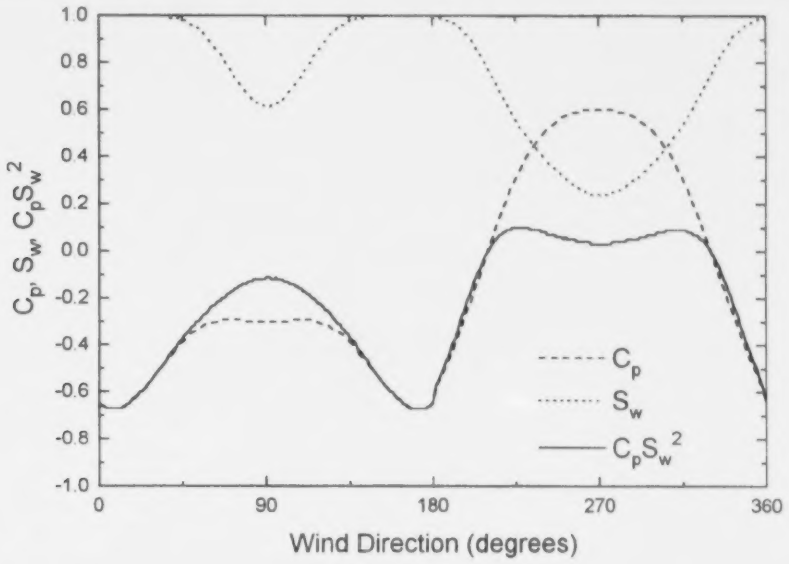

Figure 2.10: Pressure and shelter coefficients used for modelling the west (270°) wall of the test houses. The west wall does not experience reduced sidewall flow separation from the east-west row of houses, so the C_p is same as an unsheltered house. The effect of the row of houses is accounted for in S_w. The east wall is similar with 180° shift.

of bisection to estimate P_I. The P_I for the next iteration is reduced by half the difference between the previous two iterations. The iteration continues until the sign of the mass balance changes, at which point the iteration steps in the opposite direction. This continues until the mass balance converges to zero.

2.1.6 LOCALEAKS–3

Two major improvements to the LOCALEAKS–2 model were developed for this study. First, the development of a wind pressure coefficient correction for local leakage sites based on vertical placement of the leak. Second, the inclusion of a routine to estimate flue temperature based on power input to the flue. These improvements along with other minor changes form the LOCALEAKS–3 model.

The local leak pressure correction was developed to improve model predictions when large local leakage sites are present in the building envelope. A ΔC_p factor was developed as a function of wind direction and distance of the leak from the horizontal center line of the wall. The full development of

this factor is described in Chapter 4.

Heated flues have large driving pressures across them due to the stack effect caused by the hot flue gases. LOCALEAKS–2 allowed the user to specify the flue temperature. This temperature is then used to calculate the stack pressure in the flue which is added to the other envelope pressures. The total pressure is then used to calculate the flow–rate of air in the flue.

In reality, the flue temperature changes with the flue flow–rate. Combustion appliances generally have a fixed fuel consumption rate and a constant portion of the generated heat is exhausted with the flue gases. Because the flue flow–rate is variable with the total pressure across the flow, the temperature in the flue can vary. Assuming constant flue temperature can therefore lead to errors.

A more realistic model was developed in the present study by assuming constant heat input into the flue, not a constant temperature. In LOCALEAKS–3 a first law energy balance is performed on the flue. The flue temperature and the resulting flow–rate is iterated until the energy balance flowing in and out of the flue is equal. This iteration to find the correct flue–flow rate is carried out within every iteration of total envelope pressure carried out by LOCALEAKS–3.

Chapter 3

Infiltration Model Validation

The LOCALEAKS–3 infiltration model introduced in Chapter 2 is an improvement to an existing model. In particular this new model is designed to give a better estimate of infiltration through passive openings in exterior walls by improving the estimation of wind pressures on these openings. This chapter discusses the experimental work that was carried out to provide confirmation of these improvements. The work took place in two parts at the Alberta Home Heating Research Facility, a facility of test houses dedicated to ventilation and building energy studies. The first part was to install passive vents in the test houses and measure the resultant ventilation rates for comparison with model predictions. Details of these experiments along with samples of the data will be presented. The second part of this research was to collect full scale wall averaged pressure data for comparison with those used in LOCALEAKS–2.

3.1 Test Facility

All the field testing for this study took place at the Alberta Home Heating Research Facility, located south of Edmonton Alberta. The facility consists of six unoccupied test houses situated in a close row, in open farm country (Figure 3.1).

The houses were built specifically for ventilation and heating studies. They are single room bungalows with full basements and gable ended attics. There are no closed partitions in the buildings, so they may be treated as a single zone for air infiltration studies. The houses are electrically heated and the interior air is circulated with a centrifugal fan. Construction details are provided in Table 3.1.

The houses are located on rural farm land, placed in a close east–west

Table 3.1: Relevant construction Dimensions of Alberta Home Heating Research Facility Test Houses.

Component	Value	Remarks
Basement floor thickness	100 mm	Poured concrete slab on 0.152 mm polyethylene sheet.
Basement wall height above basement floor	2300 mm	Poured concrete wall, 200 mm thick. extends 500 mm above grade.
Floor joist depth	190 mm	Wood floor joists rest on basement walls and support exterior walls
Room wall height	2440 mm	Wood framed walls (except masonry unit 1) 41x92 mm studs on 406 mm centres with 13 mm drywall inside, 11 mm plywood exterior.
Flue top height above room floor	4400 mm	Flue top located at same height as roof ridge
Outside building dimensions	6700x7300 mm	Long dimension on north and south walls. Conservation house 3 is 7100x7700 mm.
Inside floor dimensions	6500x7120 mm	Plywood floor covered with rubber backed carpet.
Inside floor area	46.3 m^2	About $\frac{1}{2}$ to $\frac{1}{3}$ the floor area of a typical one story house.
Total volume inside envelope	228 m^3	Neglecting volume of equipment, floor joists and partition walls
Net active air exchange volume	220 m^3	varies by up to 2% depending on equipment and furnishings
Envelope area above grade	126 m^2	Inside air–vapour barrier includes basement wall above grade (0.5 m)

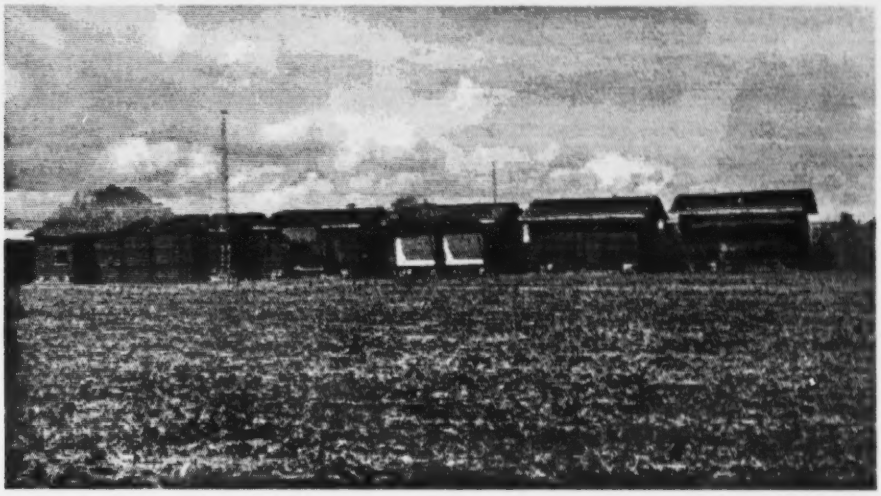

Figure 3.1: The Alberta Home Heating Research Facility viewed from the south. The houses are numbered one through six, from left to right.

row with approximately 3 m of separation between each house. Wind shelter is dominated by the close proximity of the houses to each other. Winds from the north and south are not sheltered and impact the houses directly. Winds from the east and west are influenced by the houses upstream before they affect the houses within the row, where all of the houses in this study are situated. Some shelter may be provided by two farm buildings located about 50 m to the north–west of the test houses. Figure 3.2 is a site plan of the Alberta Home Heating Research Facility and the neighbouring farmyard, showing the potential for wind shelter from nearby buildings to the north–west of the facility while winds from the north, south and east are free from large obstructions. Note that the houses used for this study are numbered 2, 3 and 4 in Figure 3.2.

The houses are continuously monitored by a digital data–acquisition system that records numerous conditions regarding ventilation, energy use and ambient conditions. This includes a tracer–gas injection infiltration rate measuring system. This system monitors the concentration of sulphur hexafluoride (SF_6) gas in the interior air of each house with a Miran gas analyzer, while known quantities of the gas are injected into the house air circulation. From this information a computer then calculates the hourly average infiltration rate for each house. Weather information is also monitored by the system. A 10 m meterological tower is located 20 m north of the houses and is equipped with a vane anemometer. Wind direction and speed as well as

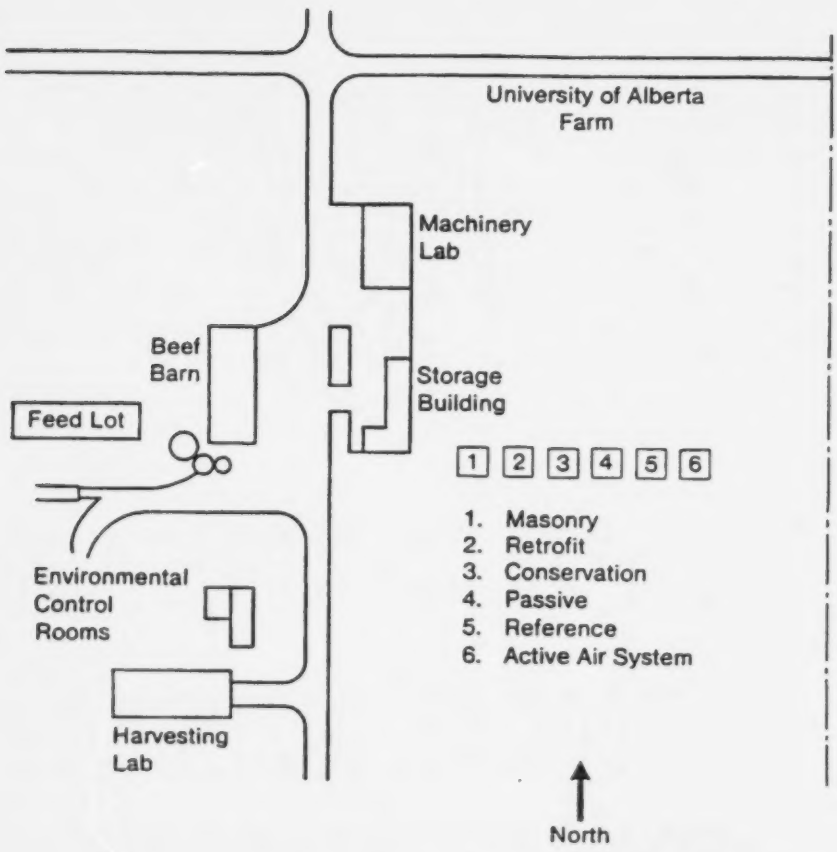

Figure 3.2: Plan view of the Alberta Home Heating Research Facility, showing the row of test houses and adjacent farm buildings.

temperature are continuously monitored and stored as hourly averages.

3.2 Combustion Air Vents

To test the performance of the LOCALEAKS–2 infiltration model with the presence of large openings in the building envelope, two test houses were equipped with passive vents. These vents were designed and installed using the standards of the Uniform Mechanical Code (International Conference of Building Officials 1991) for passive combustion air vents which are common installations on low–rise buildings in North America and therefore a meaningful test of the LOCALEAKS–2 model. Weather conditions, infiltration rates and pressures across the passive vents were all sampled continuously for the two heating seasons 1992–1993 and 1993–1994.

3.2.1 Detail and Calibration of the Passive Combustion Air Vents

It is common for the code to specify passive vents which are sized in proportion to the combustion capacity of the appliances they are ventilating. A common configuration consisting of two passive vents fixed on an exterior wall; one near the ceiling of the ventilated space and the other near the floor was chosen for this study. Two rectangular vents of 356x254 mm (14x10 in.) cross section were chosen to be installed on each of the two test houses. This size was chosen based on the maximum air flow that could be accurately measured by the tracer gas injection system used to measure the infiltration rate in the test houses and represent those required for a $120kW$ furnace. For comparison purposes, tests were also conducted with the area of the vents reduced by 50% to 356x178 mm (14x5 in.). The vents were equipped with motorized dampers so that data without large leakage sites could be collected consecutively by cycling the vents open and closed. A drawing of a passive vent and the area reduction method is shown in Figure 3.3.

In order to model these vents in LOCALEAKS–3 it was first necessary to determine their flow characteristics. This was done in the laboratory prior to installation. Both the 356x254 mm (14x10 in.) and the reduced area 356x178 mm (14x5 in.) ducts complete with damper assembly and 1/4 in. mesh screens were tested in the apparatus shown in Figure 3.4. The vent to be calibrated was installed in an air tight box. Air was drawn through the vent using an axial flow fan. By varying the flow rate and recording the corresponding pressure drop across the vent, the head–flow characteristics of the vent could be determined. This was done for both flow directions

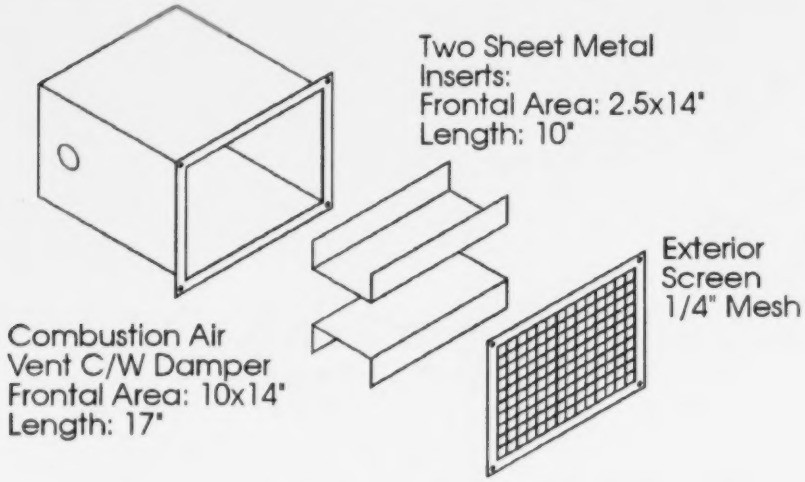

Figure 3.3: Passive vent installed in Houses 3 and 4. NTS

through the vent. Typical results are given in Figures 3.5 and 3.6. These figures show calibration curves determined by this method. They also include curves derived from house depressurization tests of test houses equipped with the combustion air vents. The house depressurization tests are described in Section 3.2.3. Comparison of the lab calibrations with the depressurization tests conducted on the installed vents show a maximum difference of 8% between the two curves. The difference between the two curves is probably due to inaccuracy in the house depressurization test. The house depressurization test pressure is not measured across the vent, but across the building envelope and is assumed to be constant (pressure differences will be similar over the entire envelope as the test were conducted during summer days with wind speeds less that 2 m/s). Small differences in pressure differential between the two vent locations may cause the error. However, the results were close

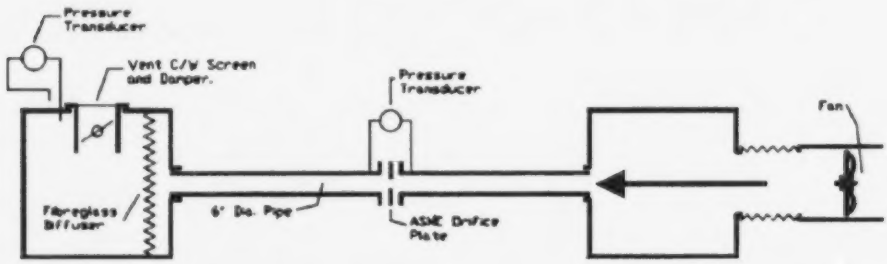

Figure 3.4: Calibration apparatus for air vent flow characteristics.

to those recorded in the laboratory tests.

Comparing theses two figures shows that while the cross sectional area of the vent is reduced by 50 % the flow at $4Pa$ pressure difference, was reduced by 4%. At first it was believed that this apparent contradiction of orifice flow theory was caused by the wire screen dominating the flow characteristics, but further testing revealed that the screens had a negligible effect on the flow characteristics of the vents. The flow exponents for both the vents are very near 0.5, indicating that the flow for both vents is of a turbulent nature and is by no means laminar. This indicates that the geometric differences in the vents are producing very different flow characteristics for the two vents. Any specifics of the flow characteristics of the vents would be speculation but in terms of orifice flow it can be said that the two vents have different discharge coefficients.

Because the flow equations for the vents do not follow ideal orifice theory (the flow exponents are slightly larger than 0.5), discharge coefficients can not be calculated. However a similar parameter, the ratio of the equivalent orifice leakage area at 4 Pa over the real vent area can serve similarly. In the case of the 356x254 mm duct, the equivalent orifice leakage area at 4 Pa, A_L, is 314 cm^2, giving a ratio of A_L to the actual vent area, A_V, equal to 0.35. For the case of the 356x127 mm vent the leakage area is 300 cm^2 and the ratio of leakage area to actual area is 0.66. The smaller vent discharges nearly twice as much air per unit area at 4 Pa as the large duct making the vents nearly equivalent as far as building ventilation is concerned.

3.2.2 Installation of the Passive Combustion Air Vents

In order to examine the effects of wind shelter the passive combustion air vents were installed on two test houses; House 3, with the vents installed on a north–facing unsheltered wall (Figure 3.7) and on House 4, with the vents on a west–facing sheltered wall (Figure 3.8). Figure 3.9 shows the interior view of the vent installation. One vent was installed near the ceiling of the ventilated space and the other near the floor. Figure 3.9 also shows the motorized damper actuator and linkage that opens and closes both the dampers under control of the digital data–acquisition system.

Flow in each vent was calculated using a Setra pressure transducer to measure the change in pressure across building envelope at the vent location. The transducer measures pressure differential between a line extending to the building exterior and an interior line. The line that extends to the exterior of the building is connected to two taps that are flush mounted on the surface of the wall. The taps are located at the same height as the centre line of the vent, 356 mm (14 in.) from either side of the vent. Splitting the

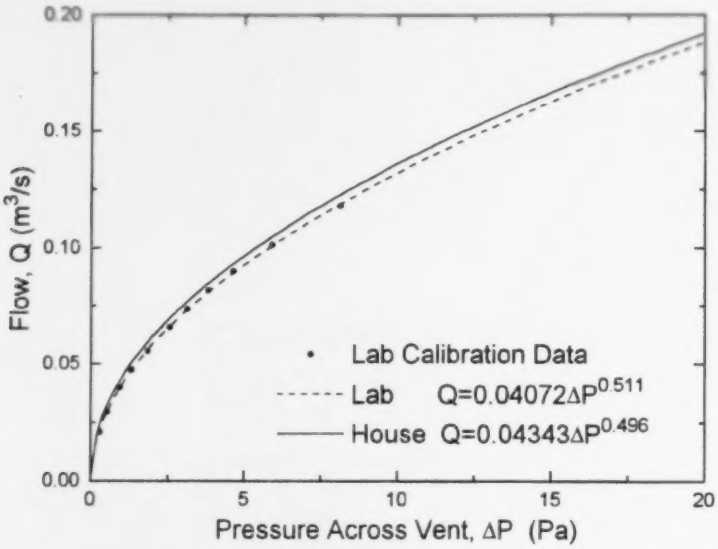

Figure 3.5: Calibration of a 356x254 *mm* (14x10 in.) combustion air vent as fitted to Houses 3 and 4. Solid line is the curve derived from house depressurization tests conducted by M.Y. Ackerman (private communication).

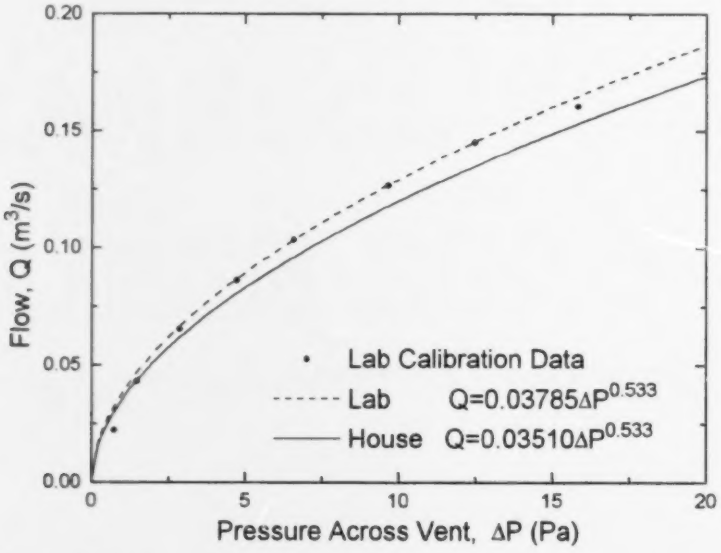

Figure 3.6: Calibration of a reduced area 356x127 *mm* (14x5 in.) combustion air vent as fitted to Houses 3 and 4. Solid line is the curve derived from house depressurization tests conducted by M.Y. Ackerman (private communication).

pressure line in two results in the average pressure of the two tap locations being sensed at the transducer (This is the same as for the wind pressure measurement mannifolds discussed in Section 3.3.1). Another line mounted on the interior wall, near the vent, at the same height as the external lines provides the reference to internal pressure. The transducer output is damped by means of a capacitor in parallel with the signal output. The time constant is approximately 60 seconds. Eight readings are taken every hour. The mean square root of the readings is recorded for each hour for conversion to average flow which is a function of the average root of the pressure.

3.2.3 Fan Depressurization Testing

Fan depressurization was used to determine the flow characteristics of the test houses. The test is performed by using a large fan to depressurize the structure. By measuring several flow rates through the fan and measuring the corresponding pressure drops across the building envelope, a flow–pressure relationship of the form $Q = C\Delta P^n$ can be determined.

A schematic of the test procedure is shown in Figure 3.10. An axial fan depressurizes the structure to a maximum pressure difference of approximately 50 Pa. This depressurization process is carried out for 15 seconds while flow through the fan and corresponding pressure drops are measured. In order to reduce the effect of wind and stack pressures on the test results, tests were carried out on summer days when the wind speed was less than 2 m/s. For a more complete description of the test apparatus see Walker (1989). The test was performed on Houses 3 and 4 with the combustion air vents open and closed. The flow–pressure relationships derived from tests with the vents closed were used in the infiltration model to describe the distributed house leakage, while the tests with the vents open were used as confirmation of the vent calibrations described earlier. The difference between the characteristic flow equation with the vents open and the equation with the vents closed, divided by 2 (two vents) represents the flow equation for a single vent. The results are summarized in Table 3.2.

3.2.4 Infiltration and Vent Pressure Data

Infiltration and vent pressure measurements were taken over two heating seasons in Houses 3 and 4, one season with the large 356x254 *mm* (14x10 in.) vents installed and another season with the reduced area 356x127 *mm* 14x5 in. vents. The vent dampers were cycled open or closed every twenty four hours so that data without large leakage sites could be used for comparison. The major differences in configuration between Houses 3 and 4 were the

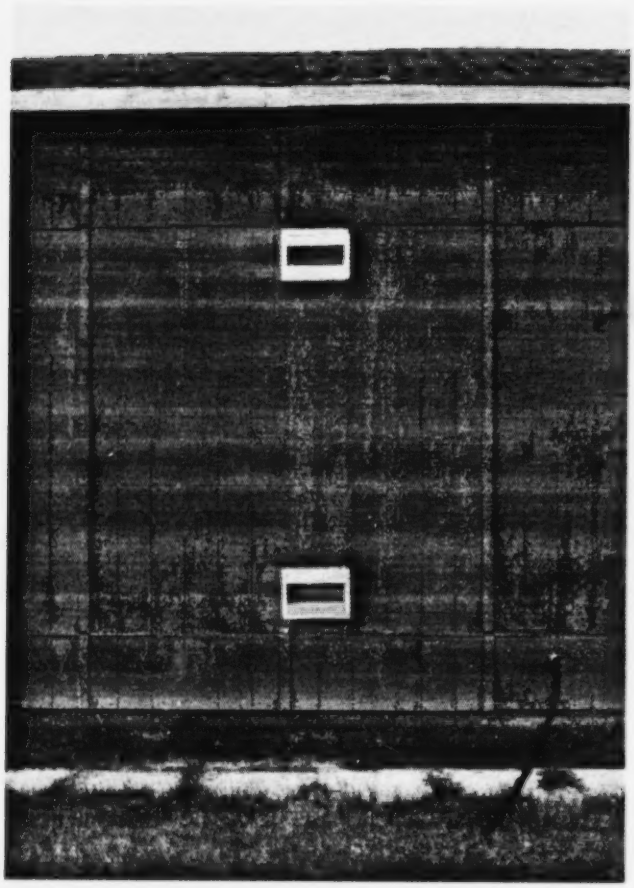

Figure 3.7: Unsheltered combustion air vents on north wall of House 3

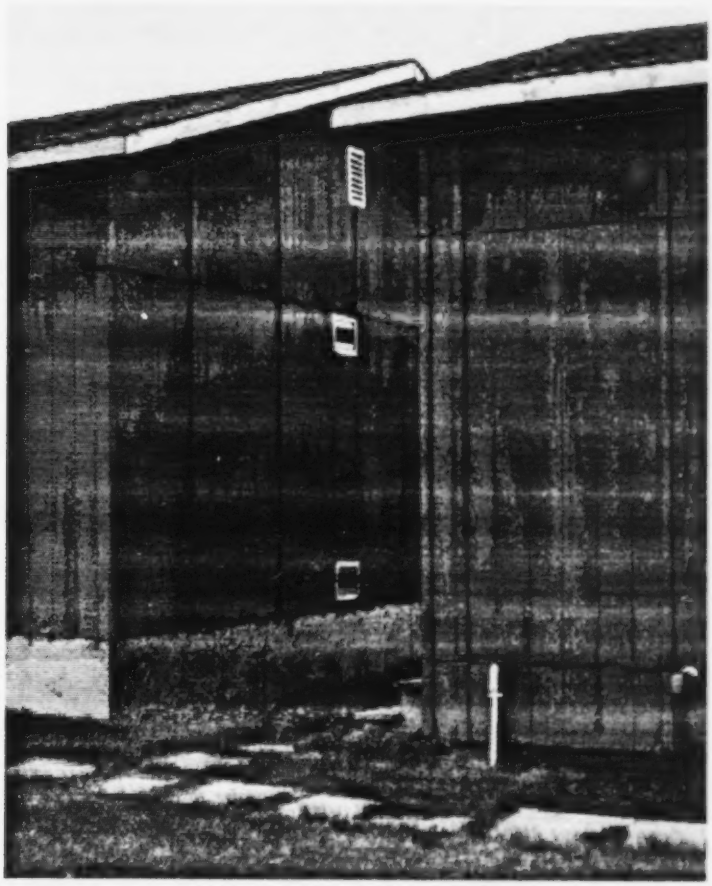

Figure 3.8: Sheltered combustion air vents on west wall of House 4

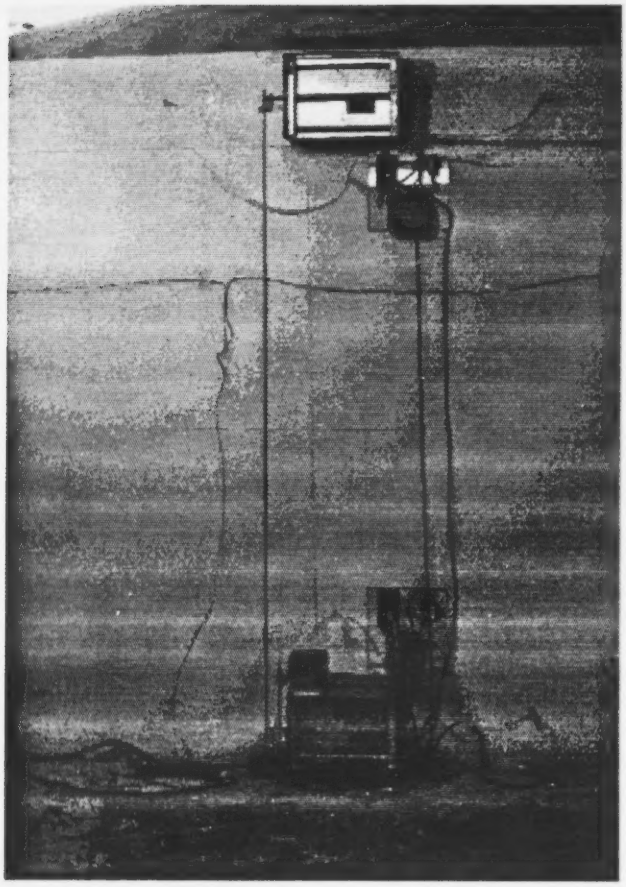

Figure 3.9: Indoor view of combustion air vents in House 4 showing the motorized damper control and pressure transducers.

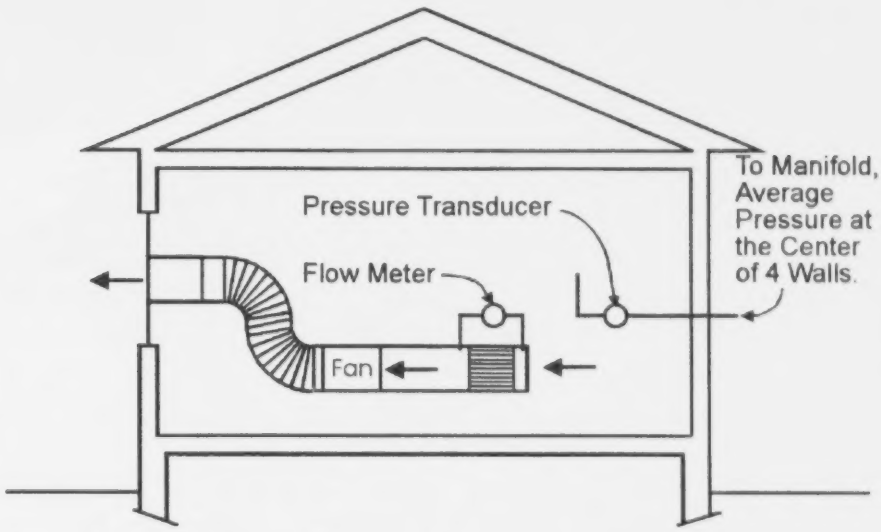

Figure 3.10: Schematic diagram of house depressurization equipment.

Table 3.2: Depressurization Test Results for Houses 3 and 4.

Test House	Configuration	Flow Coefficient C $\frac{m^3}{s \cdot Pa^n}$	Flow Exponent n	Leakage Area A_L at 4 Pa (cm^2)
House 3	Unsheltered Vents Closed	0.0087	0.669	85
House 3	Unsheltered Vents Open (Large)	0.0954	0.515	755
House 3	Unsheltered Vents Open (Small)	0.0788	0.550	654
House 4	Sheltered Vents Closed	0.0124	0.659	120
House 4	Sheltered Vents Open (Large)	0.0850	0.555	711
House 4	Sheltered Vents Open (Small)	0.07830	0.552	651

presence of an unheated flue in House 4 and that the passive vents installed on House 3 were on a north–facing unsheltered wall while the vents on House 4 were installed on a west–facing sheltered wall. The house configurations are summarized in Table 3.3. In total, 8410 hours of average infiltration data were collected in House 3 and 5713 hours in House 4. A similar amount of average vent pressure data was collected for each of the four passive vents (two on each house).

Figures 3.11 and 3.12 show infiltration data in House 4 plotted against wind direction, for the vents open and closed respectively. While these plots use wind direction as the independent variable they do not show the other major driving forces of passive ventilation, wind speed and indoor–outdoor temperature difference. This makes it very difficult to compare data sets directly unless they were taken concurrently. This is one very useful aspect of infiltration modelling, many driving forces and building configurations can be used to generate an infiltration rate prediction that can be compared directly with measured infiltration data.

Figures 3.13 and 3.14 show samples of the vent pressure in House 4 for the upper and lower vents respectively. Again, because of the many driving forces and building configurations, it is difficult to interpret this data directly, however it can be compared directly with pressure and flow predictions generated by LOCALEAKS–3.

3.3 Measurement of Wall Averaged Wind Pressure Coefficients

Wind pressure is one of the two important driving forces of passive ventilation. While this driving force accounts for a large portion of passive ventilation, it is difficult to predict and model. For this reason wall averaged wind pressure coefficients are used in LOCALEAKS–3. This mean value is then assumed to represent the pressure coefficient for that particular surface in the infiltration model. The wall averaged wind pressure coefficients used in LOCALEAKS–2 was derived from pressure coefficients taken from the wind tunnel data in Akins, Peterka, and Cermak (1979). In order to confirm this data, an experiment was undertaken to measure the wall averaged pressure coefficients on the test house walls. This section describes the experimental measures that were taken and presents the pressure coefficient data that was collected.

Table 3.3: Infiltration and Ventilation Characteristics of Test Houses.

Test House	Polyethylene Air Vapour Barrier Thickness	Double Glazed Windows (% floor area)	South Facing Windows (% floor area)	Flue	Dampered Combustion Air Vents
House 3	0.152 mm	14%	11%	none	2 on unsheltered north wall 24 hour open/closed cycle
House 4	0.152 mm	25%	23%	152 mm with 76 mm metered orifice	2 on sheltered west wall 24 hour open/closed cycle

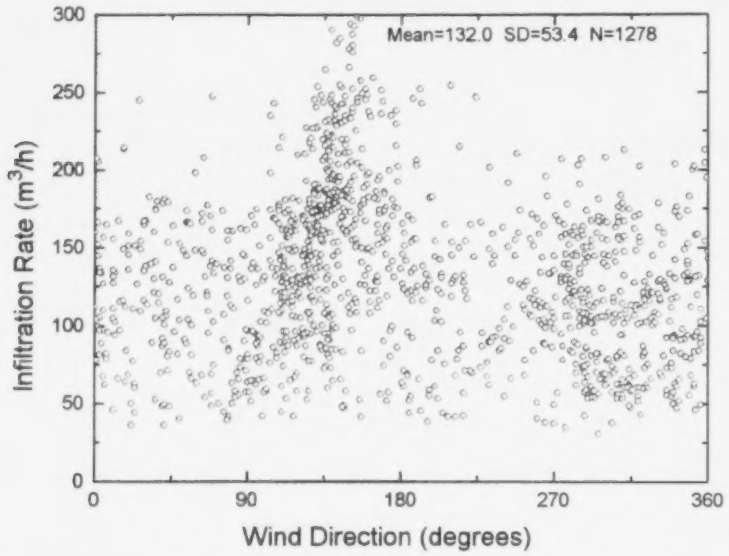

Figure 3.11: Indoor air infiltration rate in House 4 with large 356x254 *mm* (14x10 in), sheltered combustion air vents, vents open.

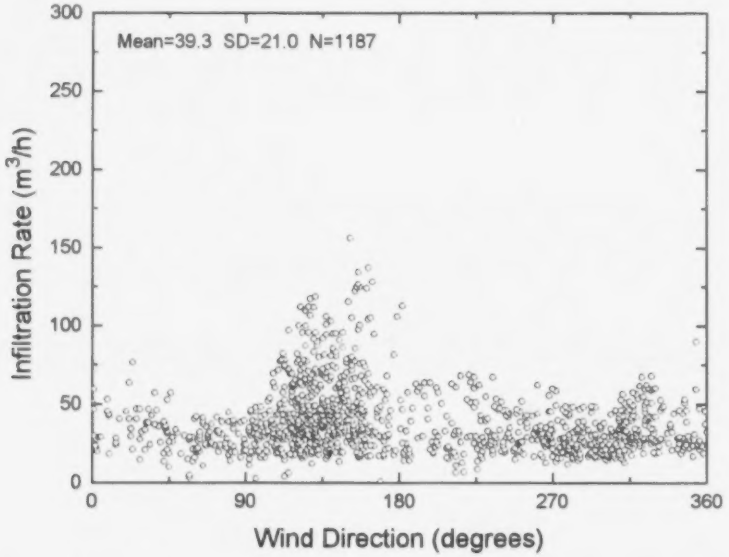

Figure 3.12: Indoor air infiltration rate in House 4 with large 356x254 *mm* (14x10 in), sheltered combustion air vents, vents closed

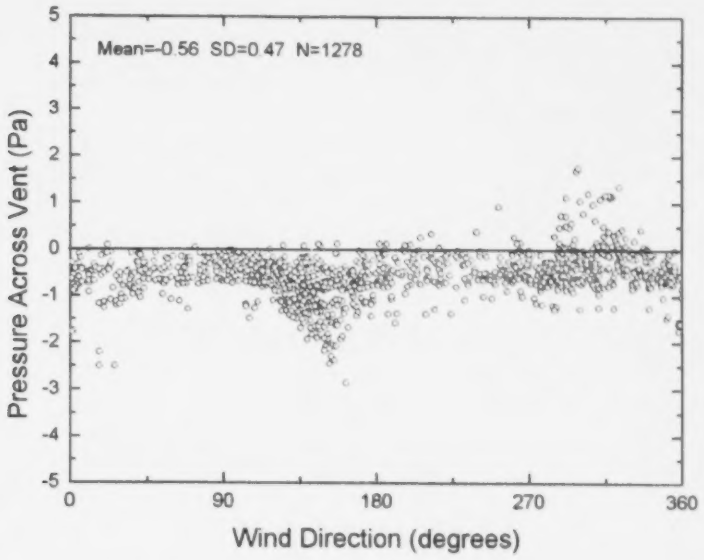

Figure 3.13: Pressure across upper vent of House 4 (sheltered vents). Vents are large, 356x254 *mm* (14x10 in). Positive pressure is inflow.

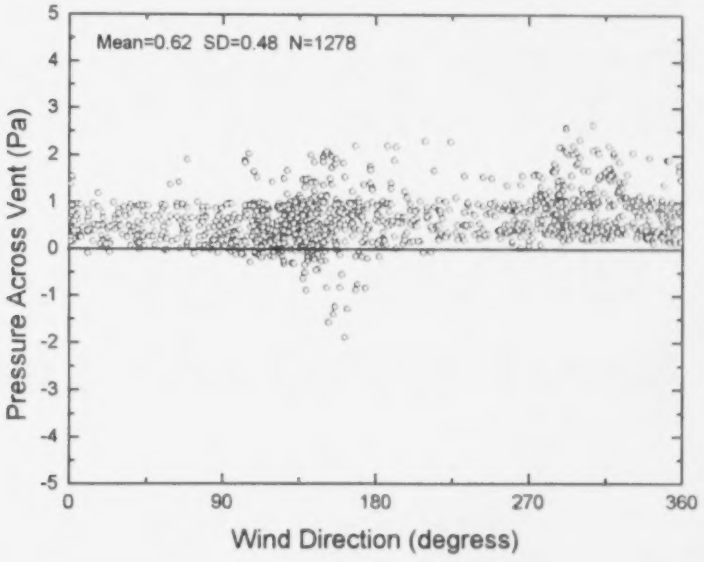

Figure 3.14: Pressure across lower vent of House 4 (sheltered vents). Vents are large, 356x254 *mm* (14x10 in). Positive pressure is inflow.

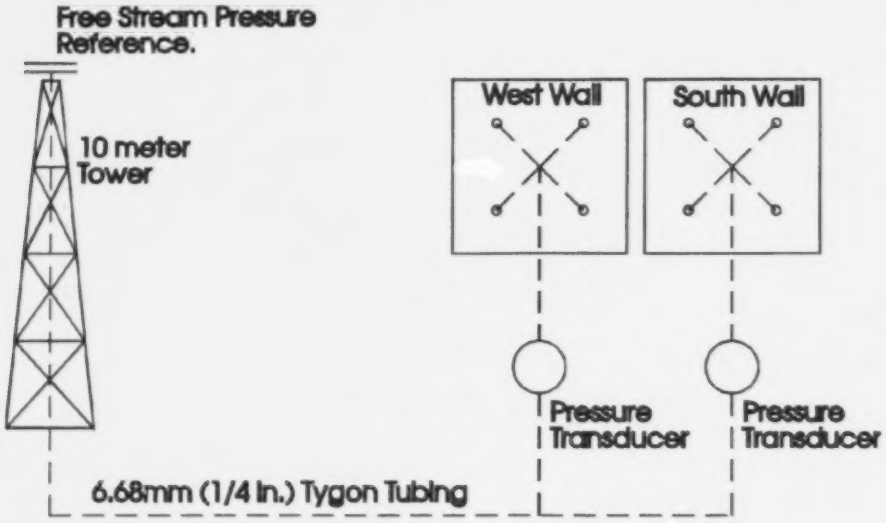

Figure 3.15: Schematic diagram of the pressure measurements made on the exterior walls of House 2 for the measurement of wall averaged wind pressure coefficients.

3.3.1 Experimental Method for Pressure Coefficient Measurements

The estimation of wall averaged wind pressure coefficients was carried out by equipping test house 2 with pressure transducers and averaging manifolds that would measure the difference in pressure between two wall surfaces (south and west side–walls) and free-stream atmospheric pressure. Simultaneous weather data was collected from the meterological tower on site. The data was continuously sampled (640 readings per hour) and stored as hourly averages, generating a data base of wind pressure coefficients for each wall and their corresponding wind directions.

A schematic of the pressure measurement is shown in Figure 3.15. The two exterior walls of the test house are each equipped with a pressure transducer that measures the difference in pressure between a free–stream location and a pressure averaging manifold fitted to the exterior of the wall.

The pressure averaging manifold consists of four flexible lines connected to a central hub, another line leads from this hub to pressurize the transducer. Because the pressure at the four sampling locations are not equal, a flow will be induced in the four sample lines extending from the hub (not the line extending to the transducer). If this flow is laminar, viscous pipe flow theory can be used. The Reynolds number for fully developed laminar flow in a tube

as a function of the pressure drop, ΔP across the tube is (White (1986))

$$Re_d = \frac{\rho d^3 \Delta P}{32 \mu^2 L} \tag{3.1}$$

Where d is the diameter of the tube, L is the length of the tube and μ and ρ are the viscosity and density of air, respectively. For the air in the 6.68mm tubing extending from the taps to the transducer inlet to remain laminar a maximum Reynolds number of 2400 is allowable. This gives a maximum allowable pressure difference of approximately 190 Pa, larger than any wind pressure. Therefore laminar flow theory is valid and flow in the tubes is given by (White (1986))

$$Q = \frac{\pi d^4}{16 \mu L} \Delta P \tag{3.2}$$

where d, L, and μ can all be assumed constant, reducing Equation 3.2 to a linear function of ΔP with a flow coefficient K.

$$Q = K \Delta P \tag{3.3}$$

Equation 3.3 can be expressed for the flows in each of the pressure lines as follows

$$Q_1 = K_1 (P_1 - P_T) \tag{3.4}$$

$$Q_2 = K_2 (P_2 - P_T) \tag{3.5}$$

$$Q_3 = K_3 (P_3 - P_T) \tag{3.6}$$

$$Q_4 = K_4 (P_4 - P_T) \tag{3.7}$$

Where Q_1, Q_2, Q_3 and Q_4 are the flows in each line (positive flow is to the centre hub of the manifold). The variables P_1, P_2, P_3 and P_4 are the pressures at the sampling locations on the wall and P_T is the pressure at the hub measured by the transducer. The lines are of equal length and diameter therefore the K's are equal. These equations are solved for P_T with the conservation of mass (ρ constant) equation at the hub

$$Q_1 + Q_2 + Q_3 + Q_4 = 0 \tag{3.8}$$

the result is

$$P_T = \frac{P_1 + P_2 + P_3 + P_4}{4} \tag{3.9}$$

which is the true mean of the pressure at the four sampling locations. Therefore, the pressure transducer reads the average pressure of the four sampling locations as long as the length and diameter of the four lines are equal and the flow in the lines is laminar.

In order to avoid over–weighting any part of the wall in this average it was necessary to arrange the sampling locations in a symmetric fashion on each wall. Each wall was divided into four imaginary quarters, the centres of which are the sampling locations. The pressure measurement is the average of the pressure of four equal areas, ensuring that no single area is over–weighted by the averaging manifold. Four sampling locations is the maximum number possible while maintaining symmetry in the vertical and horizontal directions, without using a more complicated and costly measurement system.

Referring again to Figure 3.15, each wall is equipped with a pressure transducer pressurized by wind pressure on the wall. In order to isolate this pressure an accurate reference to atmospheric pressure must be provided. This is supplied by a static pressure probe located atop a 10 m tower approximately 20 m south of the test houses. The probe consists of a pair of thin horizontal disks, 12.5 mm apart. A pressure tap is located on the inside centre of the upper disk. The probe was calibrated by I.S. Walker (unpublished) in a wind tunnel to remove wind speed effects from the static pressure measurement. The resultant calibration is

$$P_\infty = P_m + C_p \frac{\rho U^2}{2} \tag{3.10}$$

Where P_∞ is the true static pressure and P_m is the pressure seen inside the probe and referenced to the transducer. U is the wind speed measured on site and C_p is a wind pressure coefficient determined to be 0.0195. Note that this calibration is independent of wind direction as the circular disks are radially symmetric for all wind directions. Using this static pressure probe with the correction factor allows the true wind pressure to be seen by the pressure transducers.

The wind pressure measurements were sampled by computer at a rate of 640 measurements per hour. This data was then stored as one hour averages for each wall, along with average wind speed and direction and outdoor temperature. This data was then to be used to generate wall averaged wind pressure coefficients as a function of wind direction.

3.3.2 The Wall Averaged Pressure Coefficient Data

The pressure measurements were carried out over two heating seasons, collecting over 6000 one hour averages of wind direction, wind speed and the four point mean wind pressure on the south and west exterior walls of House 2. The data collected was converted to pressure coefficient form

$$C_p = \frac{P_T - P_\infty}{\frac{1}{2}\rho U^2} \tag{3.11}$$

where $P_T - P_\infty$ is the average pressure measured by the transducer, U is the average wind speed and ρ is the outside air density calculated from the average outdoor temperature and pressure using the ideal gas law. Figures 3.16 and 3.17 show the wall averaged wind pressure coefficients as a function of wind direction (0° is north).

The large degree of scatter present in Figures 3.16 and 3.17 is due to the turbulent nature of atmospheric motion. Wind direction fluctuations are caused by heating and cooling processes near the ground. As the wind speed, U decreases the turbulent velocity components u' and v' do not decrease proportionally. Therefore at low wind speeds turbulent fluctuations become relatively large.

The one hour averages of wind conditions and wall pressures become invalid due to the significant fluctuations and the result is scattered wind pressure coefficient data as seen in Figures 3.16 and 3.17. In order to reduce this scatter it is necessary to filter out the low wind speed data where fluctuations are relatively large compared to the mean conditions. Figures 3.18 and 3.19 show the same wall average wind pressure coefficients but only for wind speeds greater than 4 m/s. This results is pressure coefficient data with greatly reduced scatter, while preserving enough data for a complete data set. Figures 3.20 and 3.21 show the same data binned for every 22.5° of wind direction with error bars representing plus or minus one standard deviation.

It is important to note that the natural variability in wind conditions and it's resulting effect on passive ventilation are not eliminated by averaging the pressure and wind data. Averages merely serve as a method of seeing the effect of steady wind.

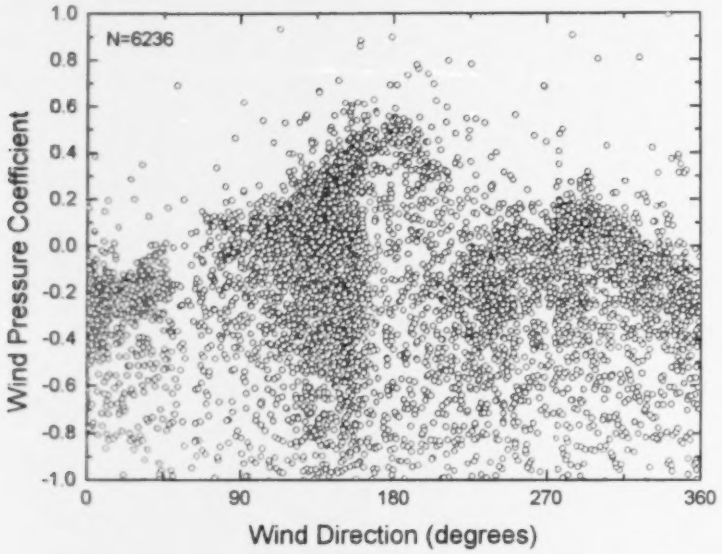

Figure 3.16: Wall averaged pressure coefficients, measured on the unsheltered south wall ($\theta = 180°$) of House 2. The 6236 data points have wind speeds greater than 1 m/s.

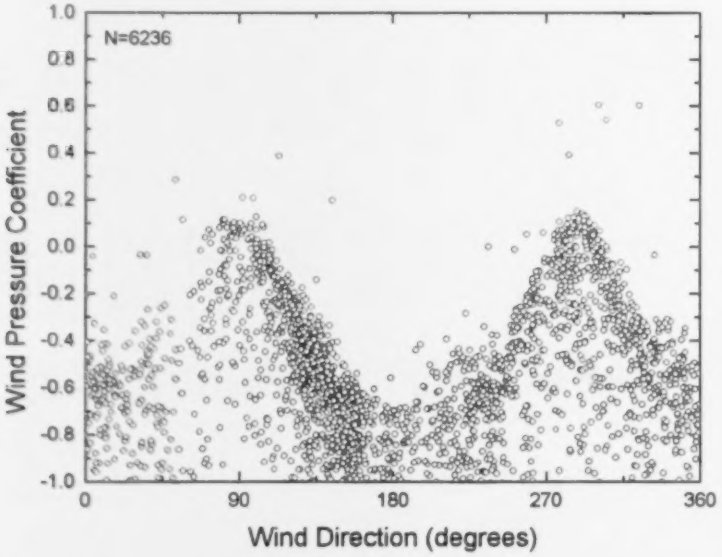

Figure 3.17: Wall averaged pressure coefficients measured on the sheltered west wall ($\theta = 270°$) of House 2. The 6236 data points have wind speeds greater than 1 m/s.

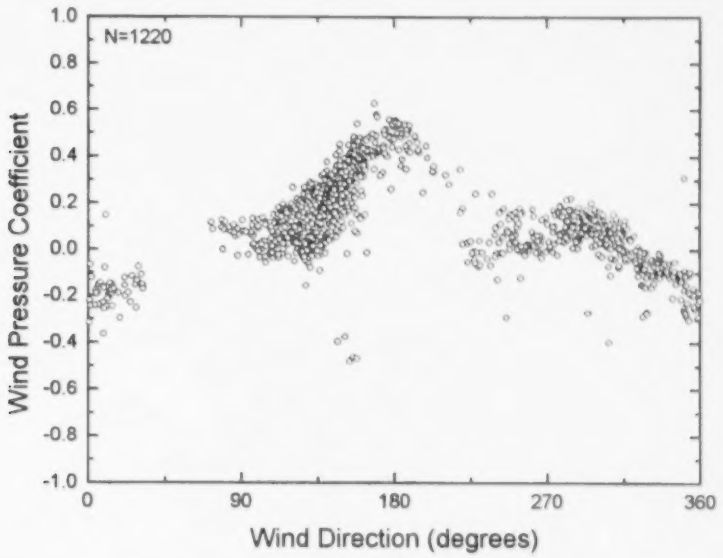

Figure 3.18: Wall averaged pressure coefficients measured on the unsheltered south wall ($\theta = 180°$) of House 2. The 1220 data points have wind speeds greater than 4 m/s.

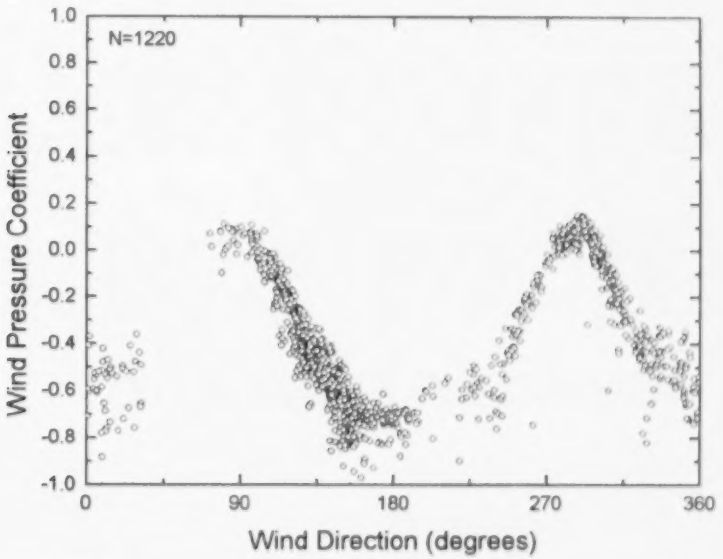

Figure 3.19: Wall averaged pressure coefficients measured on the sheltered west wall ($\theta = 270°$) of House 2. The 1220 data points have wind speeds greater than 4 m/s.

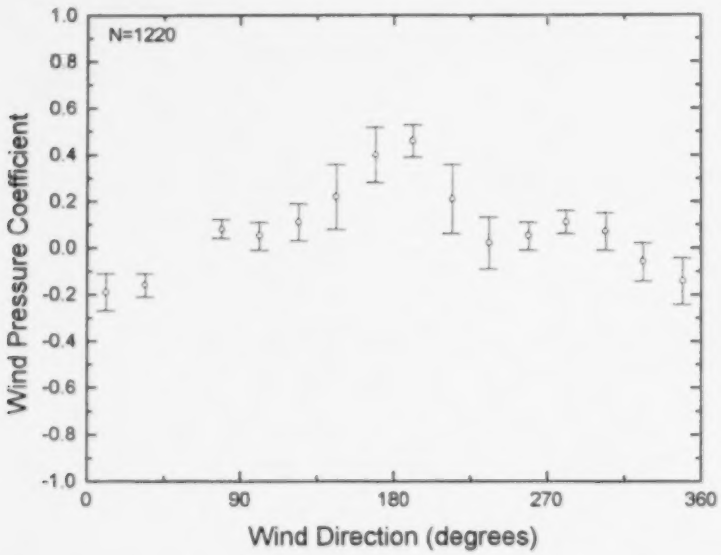

Figure 3.20: Binned wall averaged pressure coefficients measured on the unsheltered south wall ($\theta = 180°$) of House 2. The 1220 data points have wind speeds greater than 4 m/s. Bars show plus or minus one standard deviation.

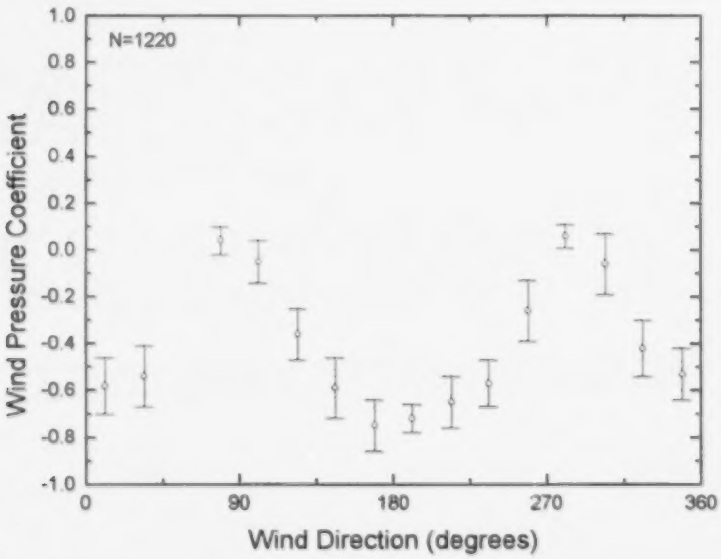

Figure 3.21: Binned wall averaged pressure coefficients measured on the sheltered west wall ($\theta = 270°$) of House 2. The 1220 points have wind speeds greater than 4 m/s. Bars show plus or minus one standard deviation.

Chapter 4

The Local Wind Pressure Model

As described in the previous chapter, two test houses were equipped with combustion air vents of the type prescribed by various regulating agencies in the United States and Canada. Total ventilation rates were measured in the houses with a tracer gas injection system and pressure (flow) measurements were made in each vent. This data was stored as hourly averages along with wind and temperature data. In this chapter the data will be compared with LOCALEAKS–2 predictions and a model for applying a ΔCp correction for local leakage sites will be developed for an improved model, LOCALEAKS–3.

4.1 Flow Measurements in Combustion Air Vents

Pressure differences were measured across each combustion air vent in houses 3 and 4, as described in Chapter 3. Average pressure difference and the average square-root of pressure difference were recorded hourly. Noting that the average flow–rate through a vent is

$$\overline{Q} = C\overline{\Delta P_{local}^{n}} \tag{4.1}$$

where ΔP is the pressure difference across the vent, C is the flow coefficient and n is the flow exponent which can be assumed to equal 0.5, giving

$$\overline{Q} = C\overline{\Delta P_{local}^{0.5}} \tag{4.2}$$

where $\overline{\Delta P_{local}^{0.5}}$ is the average of the square–root of pressure difference across the vent. Average pressure difference across the vent, $\overline{\Delta P}_{local}$ cannot be used

to calculate average flow across the vent because

$$\overline{Q} \neq C\overline{\Delta P}^{0.5}_{local} \tag{4.3}$$

Average flows in the vents were calculated using equation 4.2.

House 3 was equipped with two combustion air vents on a north facing, unsheltered wall. House 3 was not equipped with a flue, making the combustion air vents the only local leakage sites. Figures 4.1 and 4.2 show the average mass flow-rate of air versus wind direction, in the upper and lower combustion air vents of House 3, respectively. The flow rates have been normalized by dividing them by the total building mass infiltration rate for the same hour. Note that air flow into the building is positive and that the wind blows at the vents at 0°. Figure 4.1 shows that for most wind directions the normalized mass flow rate of air is approximately -1.0, that is, almost all of the air that enters House 3 exits out the top vent. However, when the wind blows toward the vents, the flow can be reduced or even reversed by wind pressure on the wall. This shows that wind does have a strong effect on the ventilation in the two vent system, in contrast to the generally held belief that wind pressure has little or no effect on the ventilation rate because the difference in wind pressure coefficient between the vents is small, and is generally assumed to be the same.

Figure 4.2 shows that when the vents are on the downwind side of the house, the lower vent flow-rate is almost always equal to 1, all the air that enters the building does so through the lower vent. When the wind blows toward the vents flow reversals corresponding to those of the upper vent were expected and indeed some were present. However, an unusual situation seems to develop. Scatter in the mean flow rates increases as the wind blows toward the holes, developing a bias in mean flow-rate that approaches 1.5 when the wind is blowing directly at the vents. This indicates that 150% of the air entering the building is flowing in the lower vent, which is impossible! This was attributed to a problem in either the tracer gas injection system that measures the infiltration rate or in the flow measurement system in the vents.

If the problem is with the infiltration system, then it is under-measuring. That is, air is entering through the lower vent and escaping through the upper vent before it can be thoroughly mixed with the tracer gas. Because the air in the house is constantly circulated by a central fan, it is unlikely that the infiltration system would fail when the infiltration rates are low. The air velocity of the inside air would be more than adequate to mix the small amounts of air entering the lower vent before they exited the upper vent. When the infiltration rate is large, which normally occurs during periods of

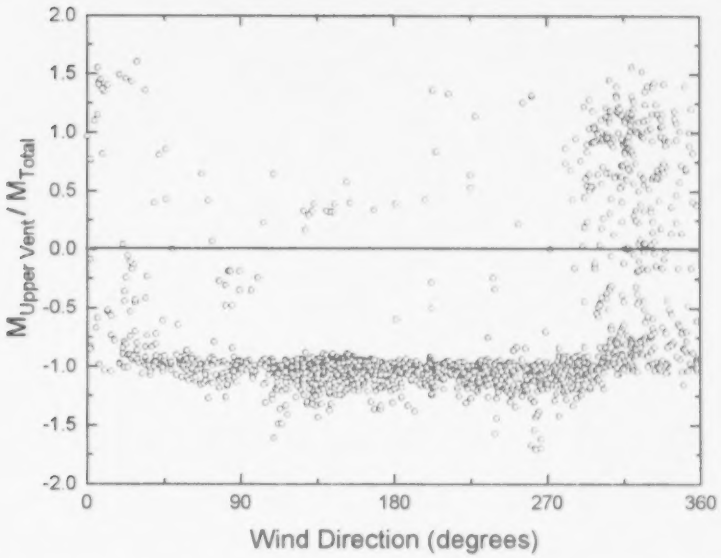

Figure 4.1: Unsheltered combustion air vents on north wall of House 3 (no flue). Measured mass flow rate of air through the upper vent, normalized with total infiltration rate versus wind direction. All wind speeds. The wind is normal to unsheltered vents at 0°. In-flow is positive

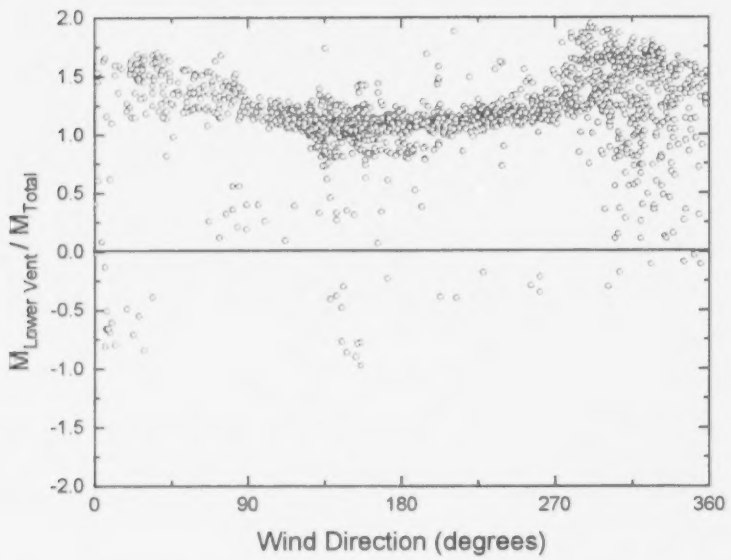

Figure 4.2: Unsheltered combustion air vents on north wall of House 3 (no flue). Measured mass flow rate of air through the lower vent, normalized with total infiltration rate versus wind direction. All wind speeds. The wind is normal to unsheltered vents at 0°. In-flow is positive.

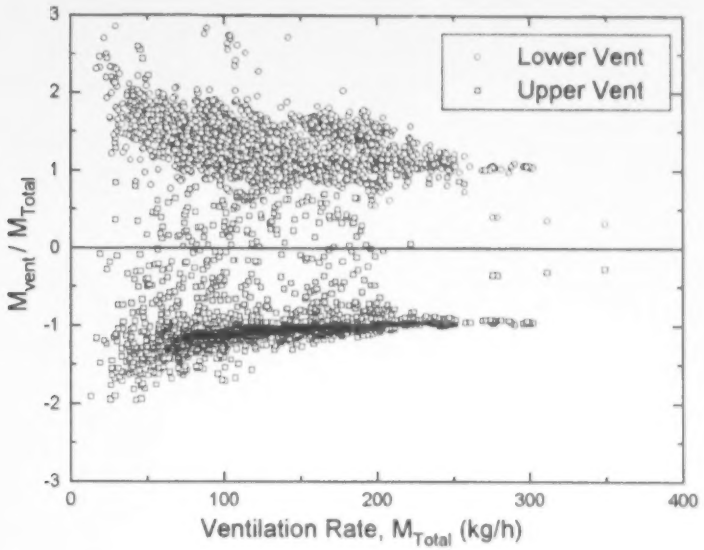

Figure 4.3: Unsheltered combustion air vents on north wall of House 3 (no flue). Measured mass flow rate of air through the upper and lower vents, normalized with total building infiltration rate versus total infiltration rate. In–flow is positive.

low outdoor temperature, the cold air that enters the lower vent would be negatively buoyant, requiring that it mix with the warm indoor air before it can rise and exit the upper vent. This would require that the infiltration system fail because it was unable to inject enough tracer gas into the house, which was not indicated by the system log.

Figure 4.3 shows the normalized flow rates for the upper and lower vents plotted against the total infiltration rate of the house. The biased scatter occurs more strongly at low infiltration rates and asymptotically goes to zero as the infiltration rate increases. Also the scatter for the lower inflowing vent is greater than that for the out flowing upper vent. Recalling Figure 4.2, the bias is dependant upon the wind direction.

The flow was measured by recording the total change in pressure across the vent as described in Section 3.2.2. The pressure measurement was recorded as an hourly average of the square–root of pressure across the vent (8 readings per hour). The pressure–flow calibration was then used to calculate the average flow in the vent. A possible source of error was that because the vent was calibrated in quiescent air, no wind blowing at the vent, the dynamic pressure of the wind was not being measured by the transducer. However, in the case of the lower vent inflowing, the flow bias is high, indicating that the

pressure transducer sees more pressure difference than that which drives flow through the vent. This contradicts the idea that the measurement somehow misses the dynamic pressure. The bias is amplified by wind blowing toward the inflowing vent, when increased fluctuations are present in the vent flow and the bias is higher for low infiltration rates when the pressure across the vent is low, a fraction of a pascal. The possibility exists that the bias is due to inadequacies in the measurement system. The vents were calibrated over a range of pressures as high as 10 Pa and the pressure transducers have a range of ±25 Pa. An investigation into the very low pressure–flow characteristics of the vents was not carried out for this study but it is necessary in order to obtain accurate flow measurements through the vents.

Because of this biased measurement in vent flow, the flow measurements were only used as a qualitative tool and none of the modelling was based on them. Despite the flaw in the flow measurements they can still be used to see the nature of ventilation in the test house when the vents are open. Figure 4.4 is a plot of the normalized flow in the upper vent over the normalized flow in the lower vent. The vast majority of the points on the graph have upper vent flows of approximately -1 and lower vent flows of approximately 1 (ignoring the positive bias in much of the data). This indicates that for most of the time almost all of the air that enters the building does so through the lower vent, and exits via the upper vent, as stack flow theory would indicate.

The plot also shows some points where high wind pressure can drive flow in both vents, and out the distributed leakage (high wind, low temperature difference conditions) and a few points where the flow in the vents is reversed by high outdoor temperatures. Flow reversals due to wind are rare because of the rarity of a strong north wind at the test location, which must occur on a day with a small indoor–outdoor temperature difference. Consequently a good data base of flow reversal due to wind was not obtained. Had the vents been mounted on a southerly wall this may have been different.

4.2 LOCALEAKS–2 Predictions of Measured Infiltration

The LOCALEAKS–2 model was described in Chapter 2. The model is a useful tool for predicting passive ventilation. For comparison with hourly averages of measured infiltration, the leakage configuration of a house along with hourly averages of driving forces (temperature difference, wind speed and direction) can be input into the model and an infiltration prediction generated for direct comparison with the measured value for that hour. Figure

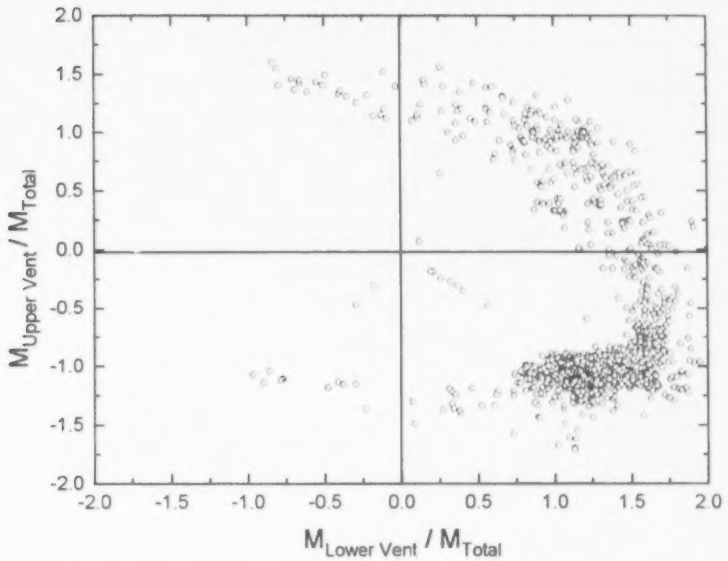

Figure 4.4: Unsheltered combustion air vents on north wall of House 3 (no flue). Measured mass flow rate of air through the upper vent versus that of the lower vent. Both flow rates are normalized with the total infiltration rate of the house. In–flow is positive

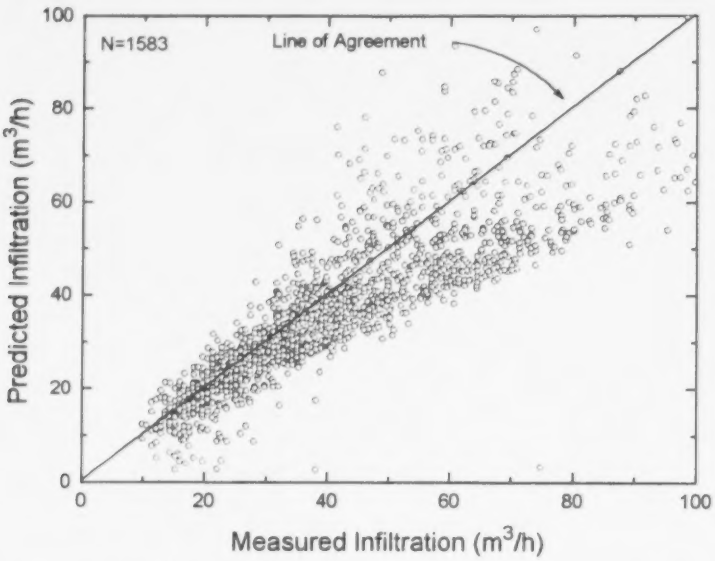

Figure 4.5: Predicted Infiltration versus measured infiltration for House 4, with an open, unheated flue and combustion air vents closed.

4.5 is a plot of the ratio of predicted to measured infiltration for test house 4. The house is equipped with an unheated flue. There is no other leakage other than distributed leakage. The data set is from February 1993 to August 1993. Figure 4.5 shows that predictions scatter ± 30% around the line of agreement (1:1). More points are under predicted rather than over predicted giving a small under prediction bias to the model of about 9%.

Figure 4.6 shows the same data set as Figure 4.5. Here the ratio of predicted infiltration to measured infiltration is plotted against wind direction. The data is processed by dividing it into 22.5° wind direction bins and averaging the data in the bins. The error bars are ± one standard deviation. Plotting the data in this fashion reveals a wind direction bias in predicting infiltration. In this house the largest single leakage site is the unheated flue. The wind pressure coefficient at the top of the flue used by LOCALEAKS–2 is taken as -0.5 for all wind directions. However, the flue on House 4 was installed with the top of the flue at the height of the roof peak. This means that the flue top to be in the roofs wake for some wind directions, causing the actual pressure coefficient on the flue top to vary with wind direction. This is likely the source of the relatively modest bias in predicted infiltration rate (9%), shown in Figure 4.6. Information on the true nature of the wind pressure coefficient on the top of the flue was unknown at the time of this study, so a correction could not be applied to the model. Despite this

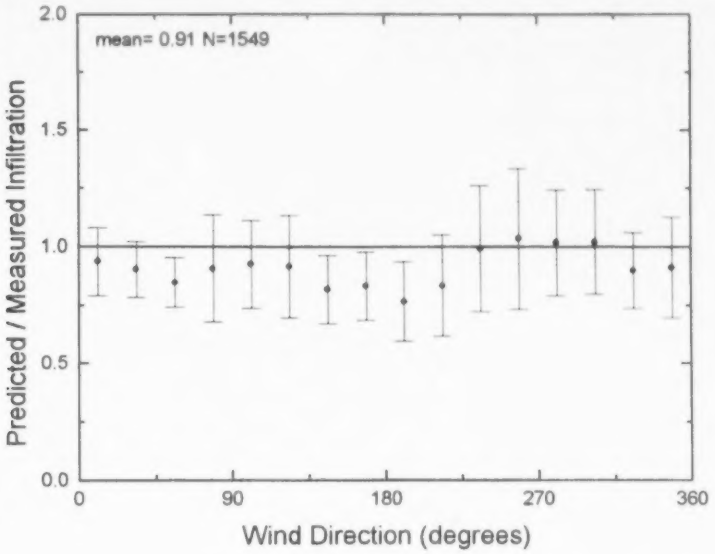

Figure 4.6: Predicted infiltration divided by measured infiltration versus wind direction for House 4 with an unheated, open flue and no combustion air vents. The largest wind direction bin has 170 data points, the smallest has 24.

error, Figures 4.6 and 4.5 show the capability of LOCALEAKS–2 at predicting infiltration through distributed leakage and we may move on to applying LOCALEAKS–2 to configurations with combustion air vents.

Figure 4.7 shows the predicted to measured infiltration ratio, plotted against wind direction for House 3. House 3 is equipped with two unsheltered 356x127 *mm* combustion air vents on the North facing wall. The same binning method as used in Figure 4.6 was used here. Keep in mind that flow through the open combustion air vents dominates the total building infiltration and that wind blows directly into the vents at 0° (wind from the North) and the vents are in the building wake at 180°. At 180° the predictions are on average equal to the measured values with only a small amount of scatter, less than ± 10%. As the angle between wind direction and the normal to the vent decreases from 180°, scatter in the predictions increases and bias in average prediction grows to a maximum of approximately 30% at 0°. Flow through the vents is much lower than predicted when wind is blowing toward the vents (at 0° and 360°). LOCALEAKS–2 uses the same wall averaged wind pressure coefficient for both vents. This causes the model to predict identical wind pressure on both the vents resulting in no net wind pressure between the two modelled vents and little wind effect on the total modelled

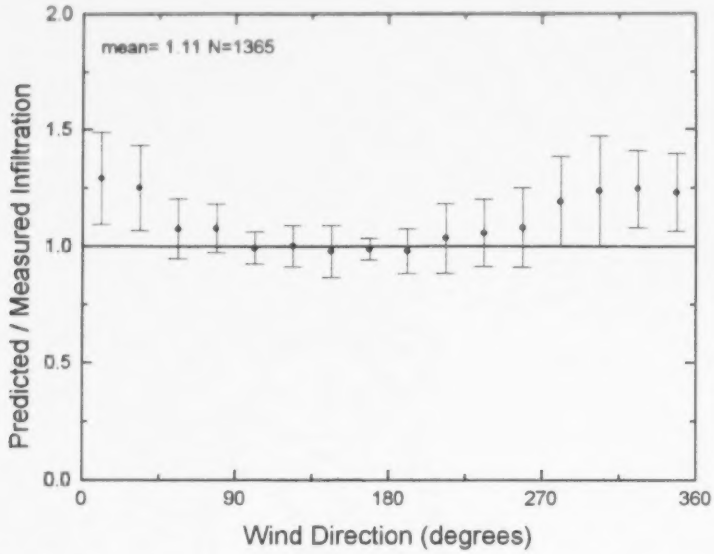

Figure 4.7: Predicted divided by measured infiltration for House 3 with sheltered 356x127 mm (14x5 in.) combustion air vents open. Data is binned every 22.5° and error bars are ± one standard deviation. Wind is normal to unsheltered vents at 0°. The largest bin has 178 data points, the smallest has 23 data points.

ventilation. However, as the measurements indicate the wind does effect the vent flow, resisting stack flow when wind blows toward the vents. The small wind pressure difference between the real vents has a significant effect on the real ventilation rate. This LOCALEAKS–2 prediction shows that using wall averaged pressure coefficients to model local leakage sites can result in large errors in model predictions.

Figure 4.8 is a plot similar to Figure 4.7 except that it is for House 4, which is equipped with the 356x127 mm vents on a west facing (270°), sheltered wall. Unlike House 3, House 4 is equipped with a flue, which was unheated for these measurements. A similar effect can be observed here for the sheltered vents as discussed previously for the unsheltered vents on House 3. Over predictions in ventilation rate grow as the wind blows toward the sheltered vents at 270°. In this case the over–predictions do not peak when the wind is blowing directly toward the vents, rather they grow as the wind approaches 270° but dip around 270° due to the effect of wind shelter from the adjacent house.

From Figures 4.7 and 4.8 it is clear that wind pressures do have a strong effect on coupled vents in the same wall. There is some difference in wind

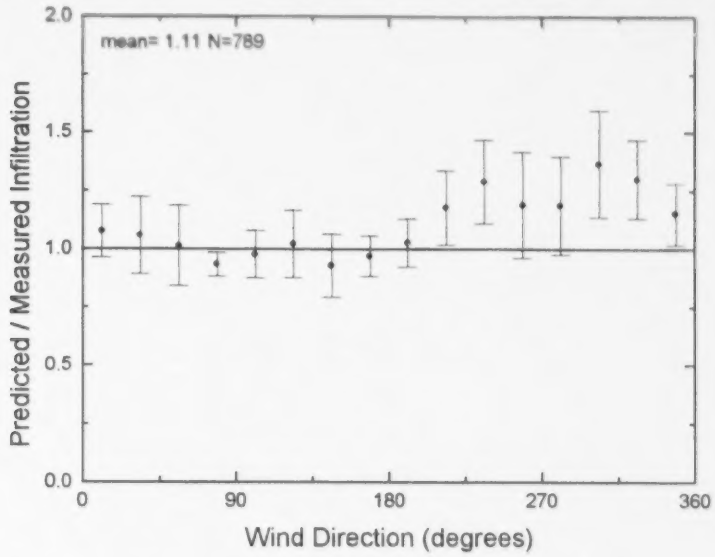

Figure 4.8: Predicted divided by measured infiltration for house 4 with sheltered 356x127 mm (14x5 in.) combustion air vents open and an unheated flue. Data is binned every 22.5° and error bars are ± one standard deviation. Wind is normal to sheltered vents at 270°. The largest bin has 169 data points, the smallest has 25 data points.

pressure coefficient that affects the flow in the vents, reducing flow due to stack effect when the wind is blowing directly at the vents. There is also evidence that this difference in wind pressure coefficient (ΔC_p) is affected by wind shelter.

4.3 Development of the Local ΔCp Model

In the previous section it was shown that wind pressure has a significant effect on combustion air vents that are mounted on the same wall. Flow in the coupled vent system is not only dependant upon temperature difference causing stack flow but also on the difference in wind pressure between the vents. While the standard practice of assuming wall averaged pressure coefficients for local leakage sites may be adequate for predicting infiltration through distributed leakage, using the same method for local leakage sites will result in large errors in passive ventilation predictions. Wall averaged pressure coefficients were originally applied to the calculation of infiltration because of the availability of data and the ease with which data could be

applied to buildings of varying design, configuration and situation with reasonable accuracy. Now that wall averaged coefficients have been shown to be inadequate for predicting ventilation in large local leaks, ideally, one would prefer to apply local pressure coefficient data for predicting infiltration. This is not a practical solution because of the complex nature of wind pressure distributions over buildings and the great variability that minor changes in architectural features have on wind shelter. Very small changes such as the addition of an awning or the planting of a tree would make previous wind pressure coefficient data inaccurate. One approach to developing better ventilation predictions is to continue to use wall averaged wind pressure coefficients in LOCALEAKS–3 for predicting infiltration in distributed leakage while developing a model for estimating the difference in local pressure coefficient from the wall average.

The new model for estimating wind pressure coefficients on local leakage sites was developed using the infiltration data from the two test houses and comparing the data with LOCALEAKS–2 predictions. A model for the wind pressure difference was developed that reduced the average bias in predictions to zero. Several assumptions were made:

- All bias in the LOCALEAKS–2 predictions was attributed to error in flow prediction through the combustion air vents. This is a good assumption because as shown in Section 4.1, the flow through the vents accounts for most of the ventilation in the test houses (at least 90%) for the vast majority of data points.

- All the bias in infiltration predictions is due to error in the wind pressure estimate on the vents. This is a good assumption because as shown in Figure 4.7, bias occurs when wind is blowing at the vents, while bias reduces to near zero when the vents are in the building wake, where air velocities are small and pressure differences between the vents are also small.

- The pressure difference between the two vents was assumed to be equal and opposite. This is the best assumption that could be made in the absence of any full scale wind pressure profile measurements on houses. This will have very little effect on two vent systems in the same wall (combustion air vents) because it is the difference in wind pressure between the vents and not the absolute pressure that has the largest effect on infiltration.

The LOCALEAKS–2 predictions in Figures 4.7 and 4.8 were recalculated with the introduction of a ΔC_p factor between the vents. The difference in

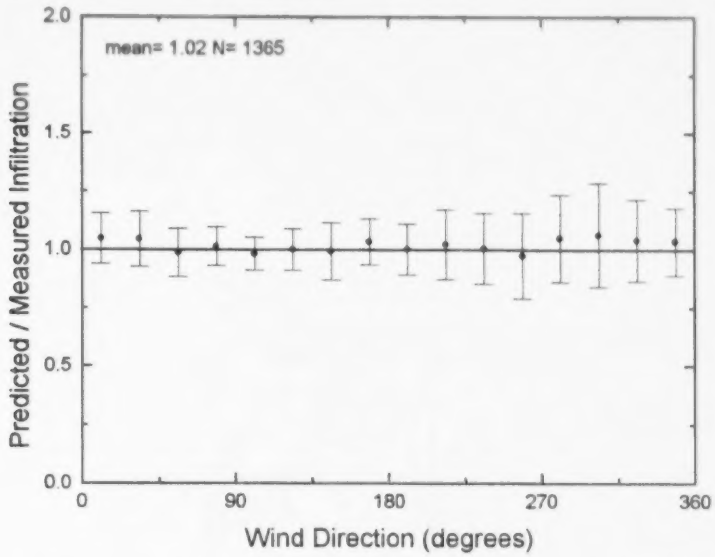

Figure 4.9: Predicted divided by measured infiltration for house 3 with unsheltered 356x127 mm (14x5 in.) combustion air vents open. Binned ΔC_p correction. Data is binned every 22.5° and error bars are ± one standard deviation. Wind is normal to unsheltered vents at 0°. The largest bin has 178 data points, the smallest has 23 data points.

wind pressure between the two vents, ΔC_p was assumed to act equally and in opposite direction to each other ($\Delta C_p/2$ on the upper vent and $-\Delta C_p/2$ on the lower vent). Values of ΔC_p were found for each binned wind direction that reduced the average prediction bias to it's lowest possible value. Figure 4.9 is a plot of the same data as Figure 4.7 with the binned ΔC_p LOCALEAKS–2 predictions. With the unsheltered vents the bias can be reduced to nearly zero. Figure 4.10 is the same data as Figure 4.8 with the binned ΔC_p LOCALEAKS–2 predictions. Bias was not entirely reduced for House 4 with the unsheltered vents. This is in part due to the inaccurate flue wind pressure coefficients used in LOCALEAKS–2 to model House 4's unheated flue. The flue flow prediction becomes a source of error that cannot be eliminated without studying the wind pressure coefficients on the flue top.

The ΔC_p values developed from the averaged data in sixteen 22.5° bins, demonstrated that accounting for the wind pressure difference between the two vents does produce more accurate ventilation predictions. A model of local wind pressure coefficient difference from the wall averaged coefficient was developed from the binned ΔC_p values. The model is now included in LOCALEAKS–3. Some of the key features of the model are as follows:

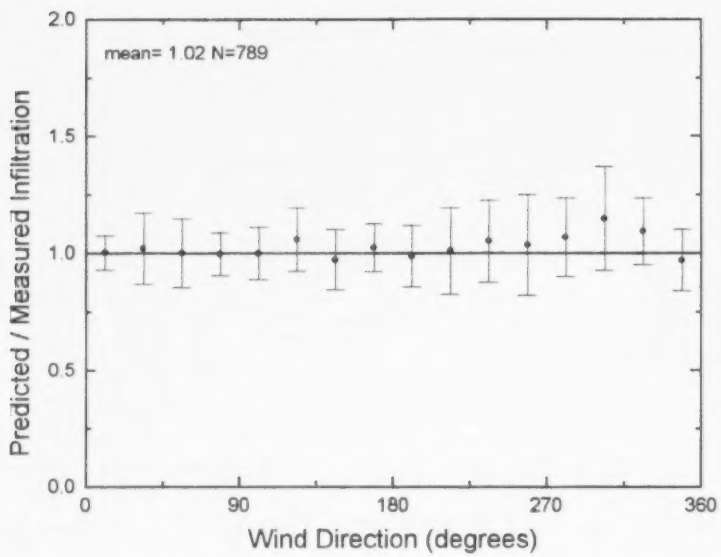

Figure 4.10: Predicted divided by measured infiltration for house 4 with sheltered 356x127 mm (14x5 in.) combustion air vents open. Binned ΔC_p correction. Data is binned every 22.5° and error bars are ± one standard deviation. Wind is normal to sheltered vents at 270°. The largest bin has 169 data points, the smallest has 25 data points.

- The local wind pressure coefficient model is used to improve estimates of wind pressure on local leakage sites. Infiltration through distributed leakage is modelled with the original wall averaged pressure coefficients.

- The model assumes a linear profile of wind pressure coefficient in the vertical direction. The profile is based on the assumption that the ΔC_p factor acts in equal and opposite halves on the upper and lower vents in the field tests. Using this and the vertical distance between the vents, a linear wind pressure coefficient was developed. Note that no correction for horizontal vent position was developed, thus this correction is useful for modelling coupled vents with vertical displacement and caution should be exercised in applying it to vents with large horizontal displacements. As this model was developed with pressure data along the wall centre line, caution should be exercised in modelling vents placed near corners.

- A harmonic function approximating the behaviour of ΔC_p with wind direction was used in the model. The harmonic function is identical in form to the function developed by Wilson and Walker (1992) for LOCALEAKS–2 wall averaged wind pressure coefficients. This harmonic function was fitted to the binned ΔC_p developed from the infiltration data in House 3, with the unsheltered vents. The same function is used to model all walls regardless of shelter which is accounted for separately. House 3 was used because it has only a small wind shelter component and House 4 is equipped with a flue that is a source of prediction error.

- The ΔC_p factor is modified by a wind shelter factor. The wind shelter factors are the same wall averaged wind shelter factors developed by Wilson and Walker (1992) and used for the wall averaged pressure coefficients. This is not a local wind shelter factor at the vent location but is the best estimate of wind shelter at the time of this writing.

Figure 4.11 shows a plot of the ΔC_p function, wind shelter, S_w, and the effective wind pressure coefficient difference, $\Delta C_p S_w^2$, that are used to calculate the difference in wind pressure between the vents on the north wall of House 3. Note that North is 0° on this plot and that the wind shelter factor is for a row of houses in an east–west line.

Figure 4.12 compares the $\Delta C_p S_w^2$ modelled in LOCALEAKS–3 of the north wall of House 3, with the binned $\Delta C_p S_w^2$ values on which the LOCALEAKS–3 model is based. Note that in LOCALEAKS–3 the $\Delta C_p S_w^2$ factor shown in Figure 4.12 would act as $\frac{1}{2}\Delta C_p S_w^2$ on the upper vent and $-\frac{1}{2}\Delta C_p S_w^2$ on the

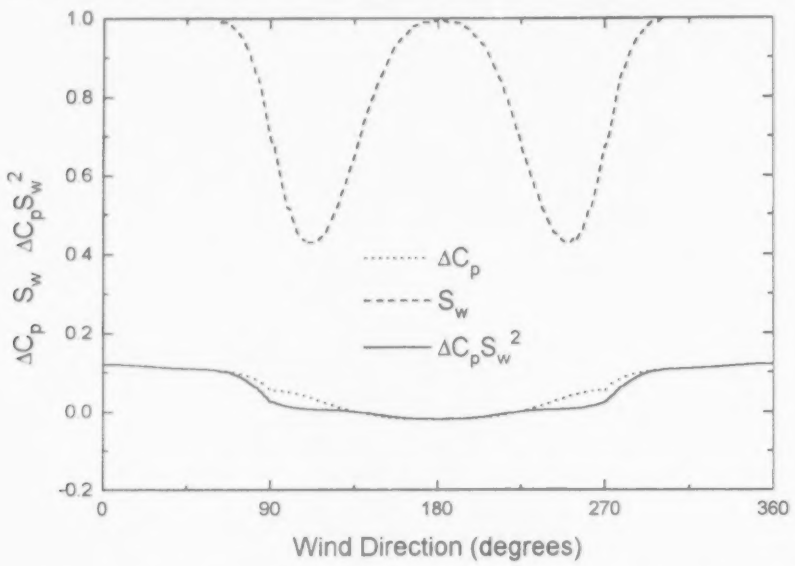

Figure 4.11: Modelled ΔC_p and wind shelter factor, S_w, used in LOCALEAKS-3 for the north (0°) wall.

lower vent. In LOCALEAKS-3 each vent wind pressure is calculated independently.

$$\Delta P_{U\ local} = \frac{\rho_o U^2}{2}\left(C_p S_w^2 + \Delta C_{p\ local} S_w^2\right) \tag{4.4}$$

where $\Delta C_{p\ local}$ is the local difference in pressure coefficient from the wall average, calculated from the linear function of vertical wall location

$$\Delta C_{p\ local} = \left(\frac{\Delta C_p}{H}\right)(z_{local} - z_{center}) \tag{4.5}$$

where ΔC_p is the difference in pressure coefficient between the test house vents, which is calculated from the harmonic function of wind direction described earlier. H is the vertical distance between the test house vents ($2.14m$), x_{local} is the vertical height above grade of the local leak and x_{center} is the vertical height above grade of the mid point between the two vents ($1.83m$).

Figure 4.13 shows the ΔC_p, S_w and combined $\Delta C_p S_w^2$ factors for the vents on the sheltered west facing wall of House 4. The ΔC_p factor is identical to the factor used on the north wall, except that it is 90° out of phase. LOCALEAKS-3 uses the same ΔC_p function for all the walls regardless of the direction the wall is facing or the particular shelter situation for that wall. The wind shelter is accounted for in the wall averaged wind shelter

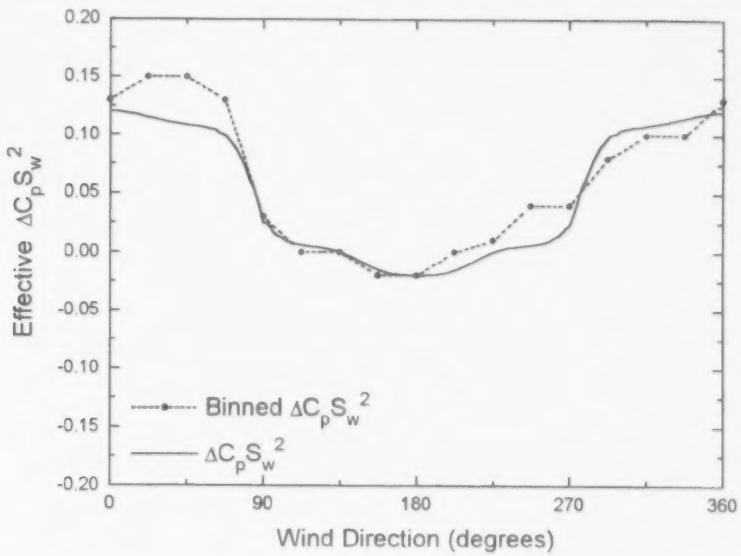

Figure 4.12: Modelled $\Delta C_p S_w^2$ factor used in LOCALEAKS–3 for the north (0°) wall, with binned $\Delta C_p S_w$ values, that produce minimum bias in the model.

factor, S_w. Figure 4.13 shows the wind shelter factor used on the west facing wall with it's particular row shelter.

Figure 4.14 shows the net modelled $\Delta C_p S_w^2$ function with the binned ΔC_p values developed earlier for the combustion air vents on House 4. Clearly there is considerable difference between the theoretical model and the actual values of difference in pressure coefficient between the vents. Differences of ± 0.05 are common and a maximum difference of -0.10 does occur. The difference can be attributed to three sources.

- The binned ΔC_p values were developed in the presence of House 4's flue which is incorrectly modelled in LOCALEAKS–2 due to the variation in the flue top wind pressure coefficient with wind direction. This results in minor errors in the binned values as they were generated assuming all the prediction error was due to error in pressure difference between the combustion air vents.

- The wind shelter function applied to the theoretical model was developed as a wall averaged value and is only used here because no true estimate of local wind shelter exists at the time of this writing.

- The ΔC_p function, that was developed using the unsheltered vents on the north wall of House 3, does not account for the difference in upwind

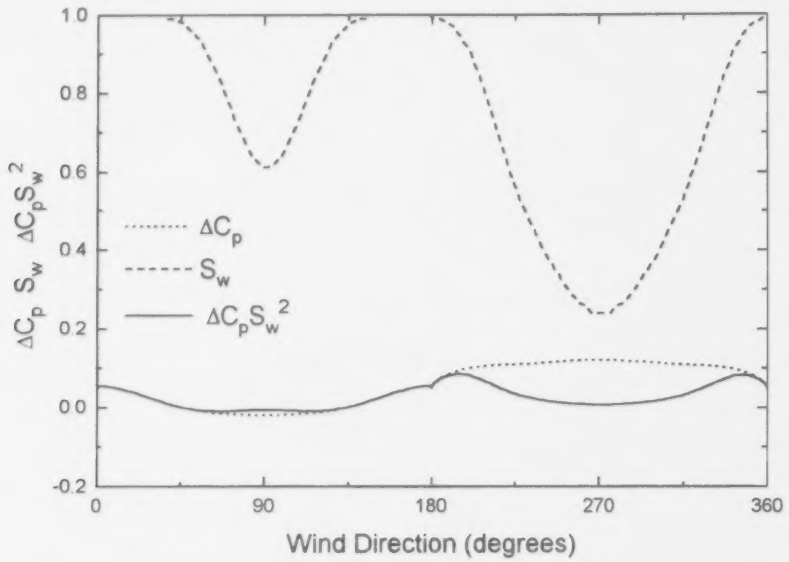

Figure 4.13: Modelled ΔC_p and wind shelter factor, S_w, used in LOCALEAKS–3 for the west (270°) wall.

effects of separation between a row sheltered and unsheltered wall. This could have large effects around 0° and 180° on Figure 4.14.

Figures 4.15 and 4.16 are LOCALEAKS–3 predictions of infiltration in Houses 3 and 4 with 356x127 mm combustion air vents. The data sets are the same as the previous examples in this chapter. The ΔC_p model in LOCALEAKS–3 performs well at predictions with unsheltered vents as shown in Figure 4.15 where the average bias in predictions is +3%. The model is not as well suited to sheltered combustion air vents, as shown in Figure 4.16, where bias can be as high as +20% for some wind directions. Separating the error in the ΔC_p model from the error in the flue flow predictions of House 4 are impossible without further experimentation.

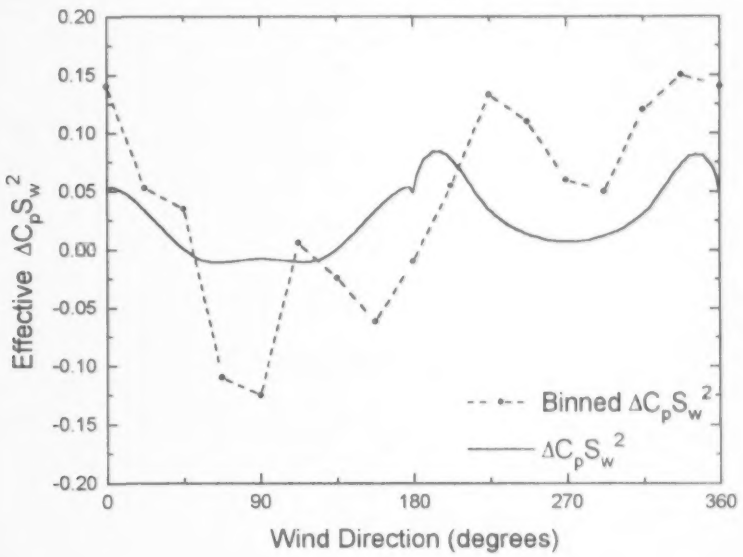

Figure 4.14: Modelled $\Delta C_p S_w^2$ factor used in LOCALEAKS–3 for the west (270°) wall, binned $\Delta C_p S_w$ values, that produce minimum bias in the model.

LOCALEAKS–3 was tested further by applying it to infiltration data taken in Houses 3 and 4 equipped with larger 356x254 mm combustion air vents. The data set also differed in being taken from early spring to late summer. Figure 4.17 shows the predictions for House 3 equipped with two 356x254 mm, unsheltered combustion air vents. LOCALEAKS–3 predictions have an average bias of -1% compared to measured values. Prediction scatter is larger for this data set which is partly due to the increased ratio of natural variation of driving forces to driving forces, common to spring. Figure 4.18 shows LOCALEAKS–3 predictions for House 4 with two 356x254 mm, sheltered combustion air vents. LOCALEAKS–3 problems with sheltered vent predictions combined with the greater seasonal variation in weather cause a large average bias of +12%. Indicating further experimentation is required to develop the level of accuracy developed for unsheltered vents, for sheltered vents.

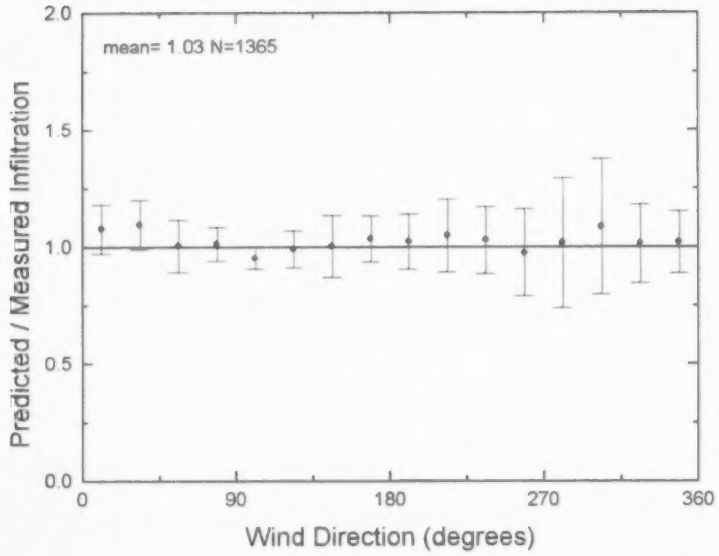

Figure 4.15: Predicted to measured infiltration ratio plotted against wind direction for House 3. Unsheltered 356x127 mm (14x5 in.) combustion air vents on the north wall. Modelled ΔC_p. Data is binned every 22.5°, with error bars of ± one standard deviation. Wind is normal to unsheltered vents at 0°. The largest bin has 178 data points, the smallest has 23 data points.

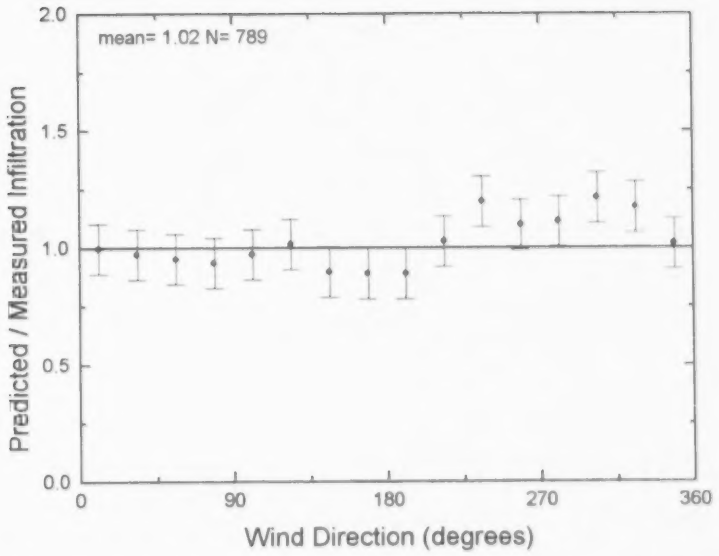

Figure 4.16: Predicted to measured infiltration ratio plotted against wind direction for House 4. Sheltered 356x127 mm (14x5 in.) combustion air vents on west wall. Modelled ΔC_p. Data is binned every 22.5°, with error bars of ± one standard deviation. Wind is normal to sheltered vents at 270°. The largest bin has 169 data points, the smallest has 25 data points.

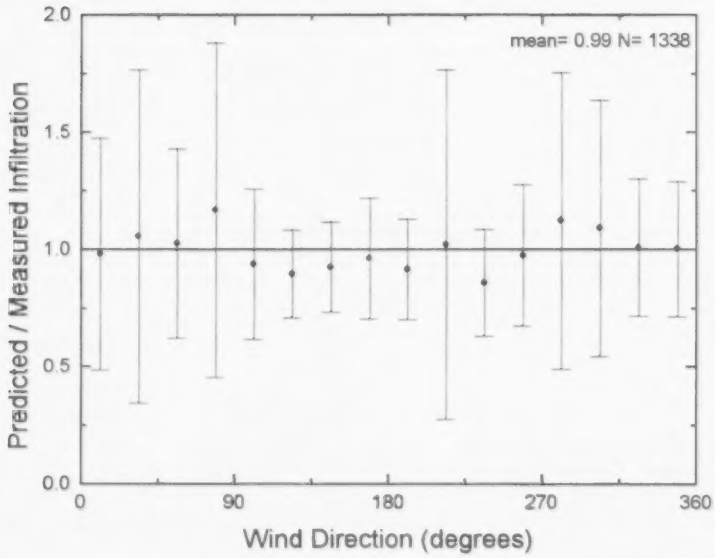

Figure 4.17: Predicted to measured infiltration ratio plotted against wind direction for House 3. Unsheltered 356x254 mm (14x10 in.) combustion air vents on the north wall. Modelled ΔC_p. Data is binned every 22.5°, with error bars of ± one standard deviation. Wind is normal to unsheltered vents at 0°. The largest bin has 198 data points, the smallest has 32 data points.

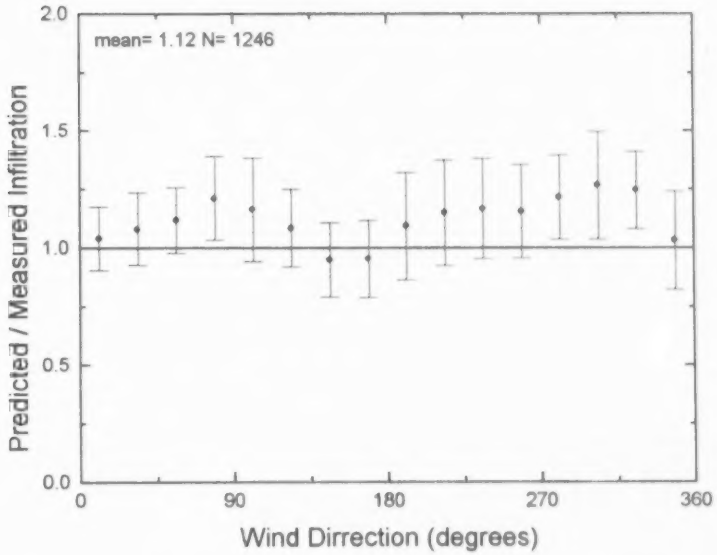

Figure 4.18: Predicted to measured infiltration ratio plotted against wind direction for House 4. Sheltered 356x254 mm (14x10 in.) combustion air vents on the west wall. Modelled ΔC_p. Data is binned every 22.5°, with error bars of ± one standard deviation. Wind is normal to sheltered vents at 270°. The largest bin has 184 data points, the smallest has 32 data points.

Chapter 5

Pressure Coefficient Measurements

Wall averaged wind pressure coefficients were measured on House 2 of the Alberta Home Heating Research Facility. These measurements were compared with the wind pressure coefficients and wind shelter theory used in the LOCALEAKS–2 model. This investigation was carried out to benefit future experimental work that will be used to improve the wind shelter model used in LOCALEAKS–2. The current wind–shadow model used in LOCALEAKS–2 was developed from data collected on scale models in wind tunnels, without the aid of any full scale tests. This preliminary study marks the beginning of future investigations into full scale wind shelter.

5.1 Comparison of Effective Wind Pressure Coefficients of LOCALEAKS–2 with Measured Coefficients

Figures 5.1 and 5.2 are plots of measured wind pressure coefficients versus wind direction for the south and west walls of House 2, respectively. The data are one hour averages of wind pressure divided by one hour averages of wind speed. The data has been further processed by creating sixteen bins of wind direction and averaging the data within. Figures 5.1 and 5.2 show the binned data points plotted at the centre of their wind direction bins (data in each bin is from the data point's wind direction $\pm 11.25°$). The error bars represent plus or minus one standard deviation of the pressure coefficient. Also plotted on these graphs is a line of the effective wall averaged wind pressure coefficient ($C_p S_w^2$) used in the LOCALEAKS–2 model for the test

houses.

Figure 5.1 shows the measured wall averaged effective wind pressure coefficient compared with the values of effective wind pressure coefficient ($C_p S_w^2$) modelled in LOCALEAKS–2. Comparison of the measured values and the model show some important differences and similarities. The magnitude of the measured coefficients is smaller than the modelled values. When the south wall is experiencing unsheltered stagnation at 180° the modelled value is 0.6 while the measured magnitude is approximately 0.5. When the south wall is in the building wake at 0°, the theoretical value is -0.3 while the measured value is approximately -0.2. When the wind is blowing parallel to the wall surface, the model predicts negative coefficients due to separation on the leading edge of the wall, while measured values are small positive values. However the profile of both the measured and modelled pressure coefficients are similar and show no sign of large difference between the two (the largest difference is 0.2).

The smaller magnitude of the measured pressure coefficients compared with the modelled coefficients derived from wind tunnel studies is not easy to explain. The behaviour when the wind is blowing parallel to the wall can be attributed to the tightness of the spacing between the test houses (3 m). Houses placed in a row will not only affect wind shelter, but the wind pressure coefficient on the walls parallel to the row. Wind blowing along the row will reduce the negative pressure on the parallel walls from the unsheltered case (from -0.65 to -0.20 in bungalows). This is accounted for in the LOCALEAKS–2 model. However, the very tight spacing of the test houses may reduce the sidewall separation to such an extent that the wall averaged pressure becomes positive. The LOCALEAKS–2 model was derived from wind tunnel tests where the tightest spacing was a house–width apart.

Figure 5.2 shows the measured effective wind pressure coefficients for the sheltered west wall of the test house. Comparison of the measured and modelled values for effective wind pressure coefficient show significant differences. The wind–shadow model (Walker (1993)) estimates wall averaged wind shelter factors by projecting linear wind shadows of up–wind obstacles on the building wall and applying a Gaussian flapping function to the wind direction to calculate an hourly average for wall averaged wind shelter factor. This model assumes that sheltered walls are still experiencing stagnation, which is clearly not the case. This is particularity clear when the measured values of pressure coefficient on the sheltered west wall are compared with the model values. The model shows different effects for wind blowing toward the wall (270°) and wind blowing in the opposite direction (90°). However, there is little difference in the measured values from these two wind directions. It

appears that with the very close row shelter that air is similarly channelled down the space between the instrumented wall and the wall on the opposite house. Clearly, the wind–shadow shelter model is not realistic when dealing with closely spaced shelter where air may be channelled or modified in such a way as to cause non–stagnation flow on a wall surface.

The test houses are near to some other farm structures to the North–West. Figure 3.2 showed a plan view of the test houses and their proximity to some farm buildings labelled "Storage Building" and "Machinery Lab". A fenced in equipment yard is located between these buildings. To determine if these buildings have an effect on the wind pressure on the test house Figure 5.2 can be examined. Wind from the North–West is 315° on Figure 5.2. By symmetry the wind pressure measured from the South–West (225°) should be equal if distant wind shelter is neglected. Comparing the measured values of wind pressure at 315° and 225° are approximately −0.25 and −0.6 respectively. Thus the magnitude of the pressure coefficient is reduced by the presence of the farm buildings. This should be accounted for in any further studies carried out at the site.

5.2 Discussion

This preliminary study has revealed several aspects of wind pressure coefficient measurement and modelling that can be used for future work to be carried out in this field.

- The current wind shelter model used in the LOCALEAKS–2 infiltration model does not realistically model wind pressure on the sheltered walls of the test houses. Walker (1993) was aware of the lack of realism in the wind shelter model but tolerated it because it kept the model simple and generated reasonably accurate infiltration predictions for distributed leakage. However, a maximum difference between measured and modelled effective wind pressure coefficient, $C_p S_w^2$, of approximately 0.7 was observed on the west wall of the test house. This has not led to large errors in predicted infiltration through distributed leakage. Predictions of ventilation through large local leakage sites in this study were not effected significantly by this unrealism. This is because the predicted ventilation is determined largely by the difference in wind pressure between the vents, ΔC_p and is not very sensitive to the wall averaged pressure coefficient. However, situations could arise where this lack of realism in wall averaged wind pressure coefficients could cause larger errors in predicted ventilation. For instance, large local leakage sites located on two or more different walls, where

the predicted difference in wind pressure between the vents could be flawed due to unrealistic wall averaged coefficients. Therefore, it is desirable to improve the wind shelter model used in LOCALEAKS-2 and LOCALEAKS–3.

- Wind shelter from other farm buildings effect the wind pressure measurements on the test houses. This must be recognised in any future experimental plan.

- Magnitude differences between pressure coefficients derived from wind tunnel tests and the full scale data taken here, do exist. In order to properly measure wall pressure coefficients, measurements should be made in more detail than the simple four point measurements made here. Given the importance of local wind pressure coefficients to large local leakage sites, it would be useful for a future measurement program to include local wind pressure measurements.

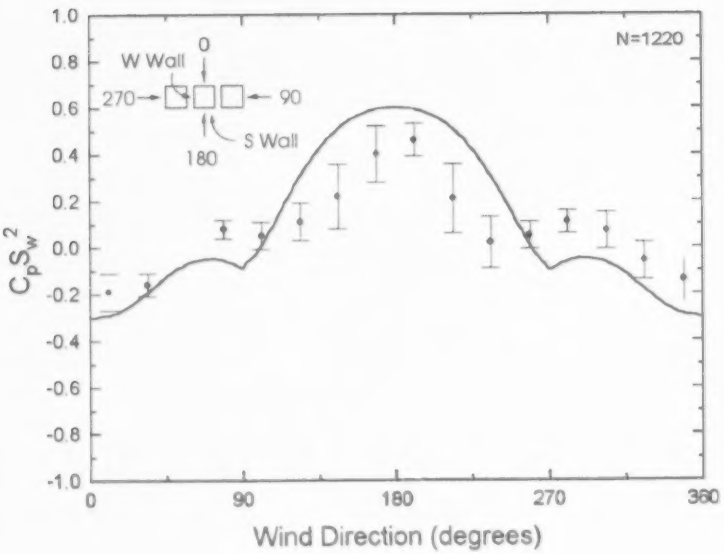

Figure 5.1: Effective wind pressure coefficients, $C_p S_w^2$, measured on the South wall of house 2 with curve of modelled coefficients used in LOCALEAKS-2. The 1220 data points are binned in 16 wind directions with error bars of $\pm$ one standard deviation.

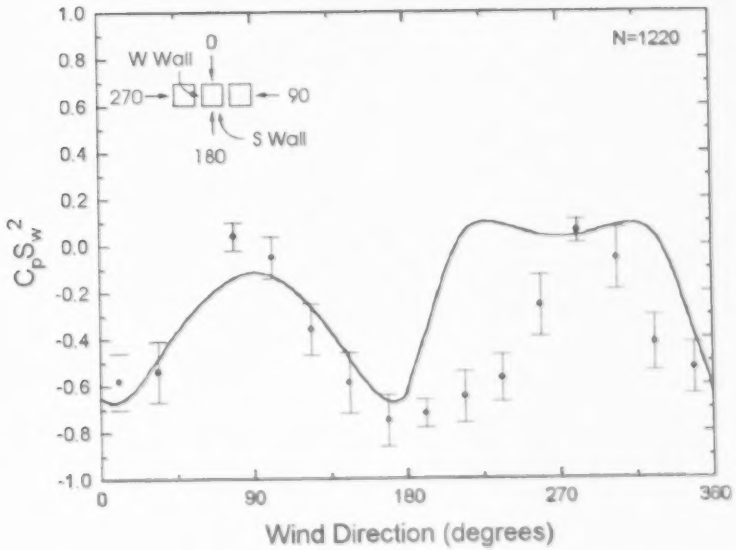

Figure 5.2: Effective wind pressure coefficients, $C_pS_w^2$ measured on the west wall of house 2 with curve of modelled coefficients used in LOCALEAKS–2. The 1220 data points are binned in 16 wind directions with error bars of $\pm$ one standard deviation.

Chapter 6

Parametric Study of Mechanical Room Ventilation

In order to gain further understanding of air flow in combustion vents a realistic installation was modelled with LOCALEAKS–3. A mechanical room with two combustion appliances, one of 60 kW (200 000 Btu/h) capacity and another of 15 kW (50 000 Btu/h) was used. The flue and combustion air vents were sized according to the Uniform Mechanical Code by the International Conference of Building Officials (1991). This reference specifies a flue (B–vent) of 200 mm (8 in.) diameter for the total 75 kW load as well as two combustion air vents communicating to the outdoors each of 413 cm^2 (64 in^2) cross sectional area. Figure 6.1 is a drawing of the mechanical room that was modelled.

The mechanical room was assumed to be of very tight construction, therefore no distributed leakage was included in the LOCALEAKS–3 model. There are three local leakage sites, the flue and two combustion air vents. The combustion air vent flow was assumed to behave like orifice flow ($n = 0.5$), with a discharge coefficient of 0.6. The flue flow was also assumed to be orifice flow with a discharge coefficient of 0.56. The temperature of the hot flue gases was modelled by a first–law energy balance on the flue, where 20% of the combustion appliances power input was assumed to exit via the flue gases. A simple iteration was performed in the flue model to balance flue temperature and flow rate.

A rule of thumb for air required for safe combustion is 150% of the stoichiometric air for an appliances fuel consumption rate. This includes the air necessary for flue gas dilution. For the maximum combustion rate in the mechanical room (75 kW) the air requirement is 105 m^3/h (corrected to indoor air density). At 15 kW the requirement is 21 m^3/h. The model was solved for eight different ambient conditions to compare predicted ventilation rates

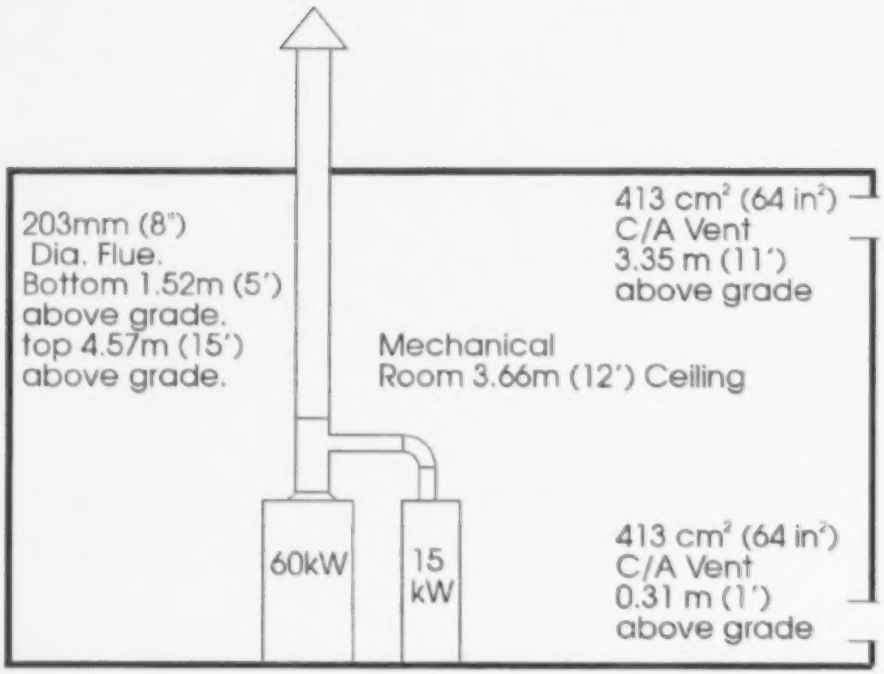

Figure 6.1: Mechanical room with two combustion appliances. Combustion air vents and flue according to the Uniform Mechanical Code.

with that required for safe combustion.

1. **Wind blowing toward wall with combustion air vents (0°) and an indoor–outdoor temperature difference of** $0°C$. Figure 6.2 is the LOCALEAKS–3 ventilation prediction plotted against wind speed for three conditions: an unheated flue, the 15 kW appliance running and both appliances (75 kW) running. When both appliances are running the flue experiences a very large differential pressure, causing the flue to constantly exhaust, while drawing air in both combustion air vents. The ΔP across the flue is large enough to place the flue flow in a regime with little sensitivity to pressure (recall $Q = C\Delta P^{\frac{1}{2}}$ becomes less sensitive to ΔP as it increases.). This is evident from the very small change in total ventilation rate as the increasing wind speed pressurizes the mechanical room, and increases the negative pressure on the flue cap. Thus at large heat inputs the total space ventilation rate is most sensitive to the diameter of the flue (or its smallest constriction). Under the influence of the strong flue exhaust, both vents inflow until the wind speed reaches approximately $12m/s$. The wind pressurizes the building sufficiently to cause the lower vent to exhaust (Its wind pressure coefficient is less than the upper vent). When only the 15 kW appliance is running the flue pressure still sufficient to keep the flue exhausting and draw air in both combustion air vents. However, the lower flue pressure allows the wind to reverse the flow in the lower vent at a lower wind speed, $7m/s$. With no heat input and no indoor–outdoor temperature difference, the room ventilation is driven entirely by wind pressure differences between the flue and combustion air vents giving a linear profile of ventilation with wind speed. Air is drawn out the flue and upper vent, while the lower vent in–flows.

2. **Wind blowing toward wall with combustion air vents (0°) and an indoor–outdoor temperature difference of** $40°C$. Figure 6.3 is the LOCALEAKS–3 ventilation prediction plotted against wind speed for three conditions: an unheated flue, the 15 kW appliance running and both appliances (75 kW) running. The addition of the strong indoor–outdoor temperature difference has little effect on the 75 kW case. The flue continues to exhaust nearly 400 m^3/h, while both vents in–flow. In the 15 kW case the lower flue pressure allows more interaction between the temperature and wind effects. The flue continues to out–flow but the large indoor–outdoor temperature difference causes the upper vent to out–flow while the lower vent in–flows. As the wind speed increases it causes the upper vent to reverse and become in–flow

at approximately 2 m/s. The jagged curve occurs due to fluctuations in the predicted neutral pressure level crossing the vent height. As the wind pressure increases it becomes sufficiently strong to cause the lower vent to reverse and become outflow at 11 m/s. In the case of the unheated flue, ventilation is driven by the interaction of stack effect and wind pressure. Initially stack pressure causes air to flow in the lower vent and out the flue and the upper vent. As the wind pressure increases the upper vent reverses to in–flow at 7 m/s. When the wind reaches 10 m/s the lower vent reverses to out–flow. The wind has reversed the stack flow in both vents.

3. **Wind blowing away from the wall with combustion air vents (180°) and an indoor–outdoor temperature difference of** $0°C$. Figure 6.4 is the LOCALEAKS–3 ventilation prediction plotted against wind speed for three conditions: an unheated flue, the 15 kW appliance running and both appliances (75 kW) running. With the vents on the leeward side of the building, wind effects are reduced. The heated flues exhaust, drawing air through both vents with very little variation in rate. In the case with the unheated flue, the small wind pressure difference between the vents causes air to flow in the lower vent and out the upper vent.

4. **Wind blowing away from the wall with combustion air vents (180°) and an indoor–outdoor temperature difference of** $40°C$. Figure 6.5 is the LOCALEAKS–3 ventilation prediction plotted against wind speed for three conditions: an unheated flue, the 15 kW appliance running and both appliances (75 kW) running. In the 75 kW case the flue draws air in both vents at a constant rate. The 15 kW case draws air in the lower vent but stack effect drives air out the upper vent at a low rate (note the jagged nature of the line, as the neutral level fluctuates across the upper vent). In the case with the unheated flue, stack effect draws air in the lower vent and out the upper vent. This is enhanced by a less negative pressure coefficient on the lower vent than the upper vent.

5. **Wind blowing toward the wall with combustion air vents (0°) and an indoor–outdoor temperature difference of** $0°C$. The vent bearing wall is sheltered by another building approximately 3 m distant (Shelter factor, $S_w = 0.25$). Figure 6.6 is the LOCALEAKS–3 ventilation prediction plotted against wind speed for three conditions: an unheated flue, the 15 kW appliance running and both appliances (75 kW) running. Again, under hot flue conditions, wind has only a small effect

on ventilation rates. Flow reversals would require a very large wind speed due to the adjacent building sheltering oncoming wind. For the unheated flue case, ventilation is driven by wind alone, and is very small due to the wind shelter.

6. **Wind blowing toward the wall with combustion air vents (0°) and an indoor–outdoor temperature difference of** $40°C$. The vent bearing wall is sheltered by another building approximately 3 m distant (Shelter factor, $S_w = 0.25$). Figure 6.7 is the LOCALEAKS–3 ventilation prediction plotted against wind speed for three conditions: an unheated flue, the 15 kW appliance running and both appliances (75 kW) running. Again wind has virtually no effect on ventilation rate with appliances running, because of wind sheltering. Under unheated flue conditions ventilation is the result of stack effect with little wind effects.

7. **Wind blowing toward the wall with combustion air vents (0°) and an indoor–outdoor temperature difference of** $0°C$. The upper vent has been blocked. Figure 6.8 is the LOCALEAKS–3 ventilation prediction plotted against wind speed for three conditions: an unheated flue, the 15 kW appliance running and both appliances (75 kW) running. In the previous cases when the appliances were running at 75 kW, the flue and C/A vents sized to that load according to International Conference of Building Officials (1991), ventilation rates varied very little from nearly 400 m^3/h, approximately four times the requirement for safe combustion. When the small 15 kW appliance is running with the flue and vents sized for 75 kW, ventilation is approximately twelve times what is necessary. As one method of reducing the over ventilation a system was envisioned in which the upper vent would be fitted with a one way flap that allowed outflow only. This would allow the upper vent to fulfill it's intended safety function of venting combustion gases in the case of a flue blockage, while reducing over ventilation during periods when the flue is hot. This does reduce the ventilation rate in the 75 kW mode but the overall rate is still over 300% of the requirement. Wind has more of an effect on the ventilation rate in this case.

8. **Wind blowing toward the wall with combustion air vents (0°) and an indoor–outdoor temperature difference of** $40°C$. The upper vent has been blocked. Figure 6.9 is the LOCALEAKS–3 ventilation prediction plotted against wind speed for three conditions: an unheated flue, the 15 kW appliance running and both appliances (75 kW)

running. Similar to the previous case, a small reduction in ventilation rate due to the blocked upper vent.

From this parametric study it is clear that a heated flue produces the dominant force in the simulated mechanical room ventilation with natural processes. Indoor–outdoor temperature difference and wind had very little effect on the ventilation rate when both appliances were running with the flue and combustion air vents sized to the 75 kW load. It was also found that the ventilation rate was 300% of that required for safe combustion.

This steady over–ventilation, regardless of ambient conditions, is good from a combustion safety standpoint but ensures over–ventilation during cold conditions which can lead to freezing boiler rooms and resulting in ruptured water lines or worse, non–engineered solutions to the over ventilation (occupants blocking the combustion air vents). Placing a one–way damper on the upper combustion vent reduces over–ventilation slightly during appliance–on conditions but does not solve the over–ventilation problems.

It is evident from this study that the size of the flue is the most significant controlling factor in the ventilation rate. Under full load conditions the flue is operating in the pressure insensitive region of its pressure–flow relationship. This is observable by the small effect of wind and stack pressure on the flue flow rate. By reducing the diameter of the flue, ventilation rates could be reduced significantly. This would also have the less desirable effect of making the flue flow–rate variable with ambient weather conditions. Any plan to reduce the size of flues to reduce mechanical room ventilation would require extensive experimentation and study before a safe method could be determined. For this reason no modelling of reduced area flue was done here. Other factors such as over–heating of the flue and the possibility of back–drafting must be thoroughly investigated beforehand.

The problem of over–ventilation during unheated flue conditions is due to wind and stack pressures driving air through combustion air vents and the flue. The ventilation rates under these conditions can also be significant. This becomes more problematic during cold weather when stack effect can cause very large ventilation rates of cold air, giving rise to the freezing problem discussed earlier. This is most easily solved with the addition of dampers on the combustion air vents that close when the appliances are not being fired.

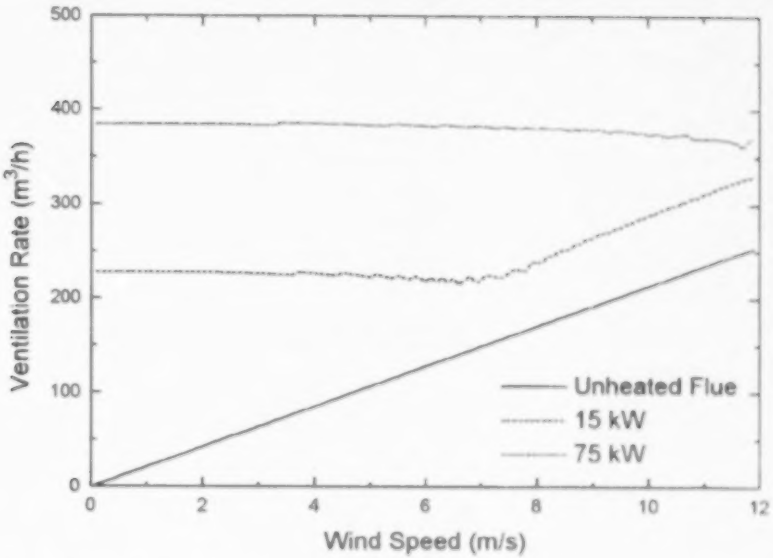

Figure 6.2: Ventilation in a mechanical room plotted against wind speed for three appliance power outputs. Wind is blowing toward unsheltered vents and indoor–outdoor temperature difference is $0°C$.

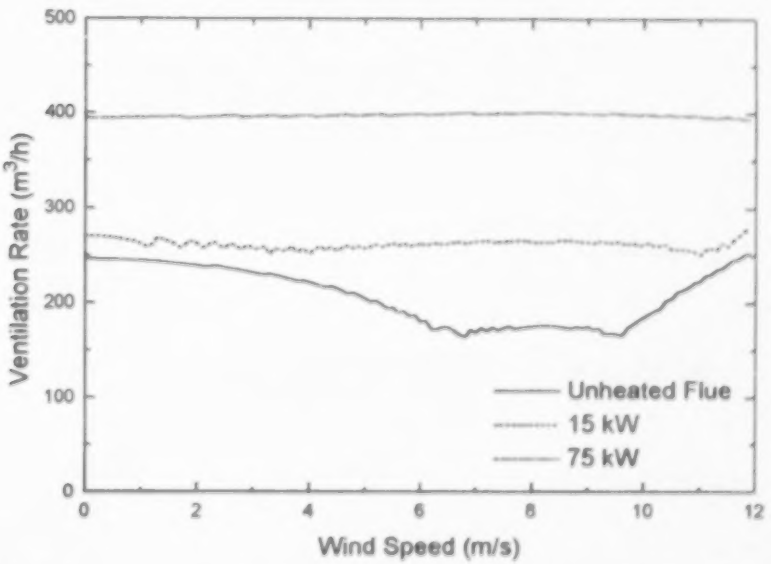

Figure 6.3: Ventilation in a mechanical room plotted against wind speed for three appliance power outputs. Wind is blowing toward unsheltered vents and indoor–outdoor temperature difference is $40°C$.

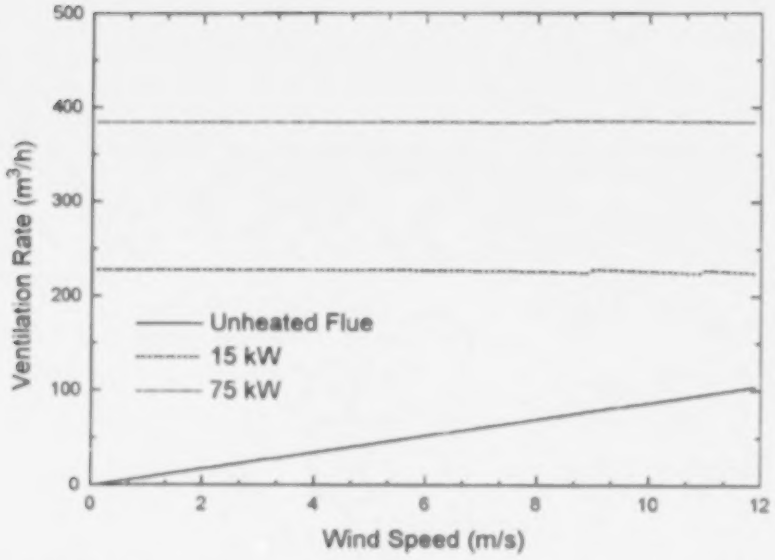

Figure 6.4: Ventilation in a mechanical room plotted against wind speed for three appliance power outputs. Vents are located on downwind side of building and indoor–outdoor temperature difference is $0°C$.

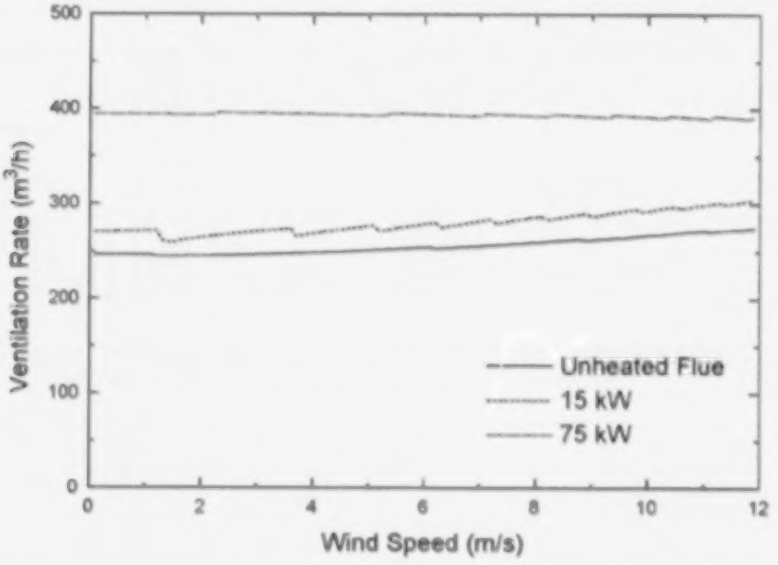

Figure 6.5: Ventilation in a mechanical room plotted against wind speed for three appliance power outputs. Vents are located on downwind side of building and indoor–outdoor temperature difference is $40°C$.

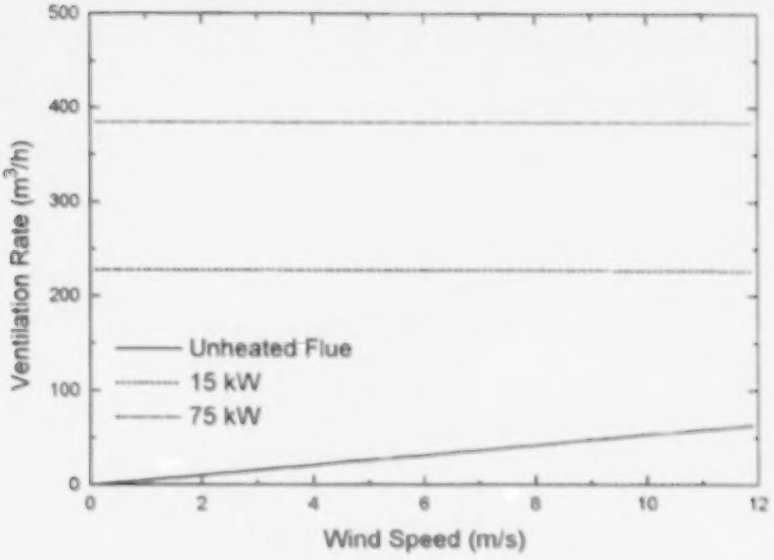

Figure 6.6: Ventilation in a mechanical room plotted against wind speed for three appliance power outputs. Vents are on an upwind wall, sheltered by an upwind building and indoor–outdoor temperature difference is $0°C$.

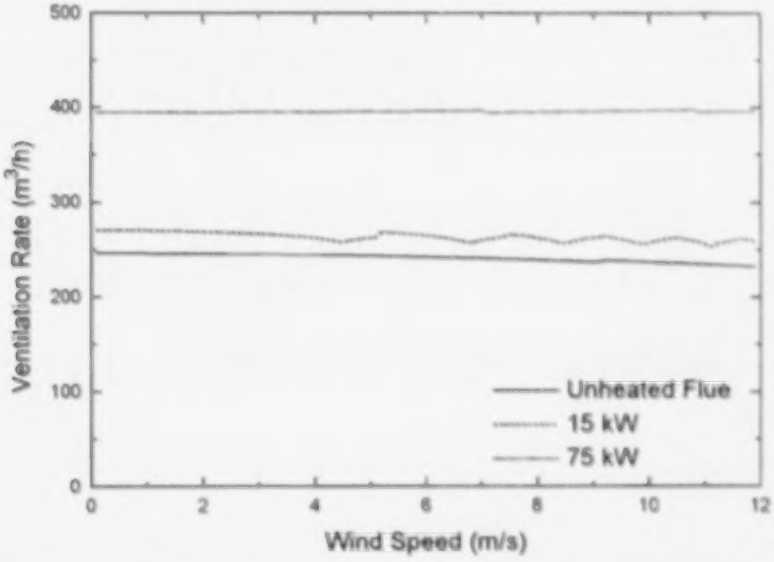

Figure 6.7: Ventilation in a mechanical room plotted against wind speed for three appliance power outputs. Vents are on an upwind wall, sheltered by an upwind building and indoor–outdoor temperature difference is $40°C$.

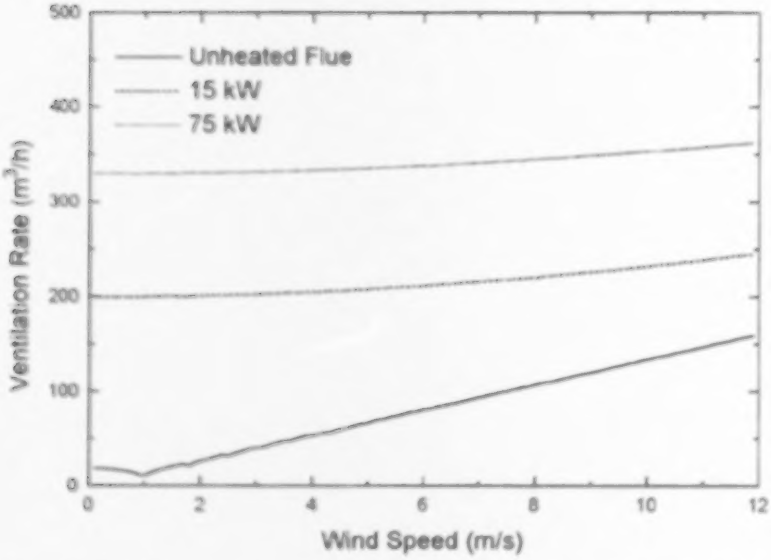

Figure 6.8: Ventilation in a mechanical room plotted against wind speed for three appliance power outputs. Wind is blowing toward unsheltered vents and indoor–outdoor temperature difference is $0°C$. The upper vent is blocked.

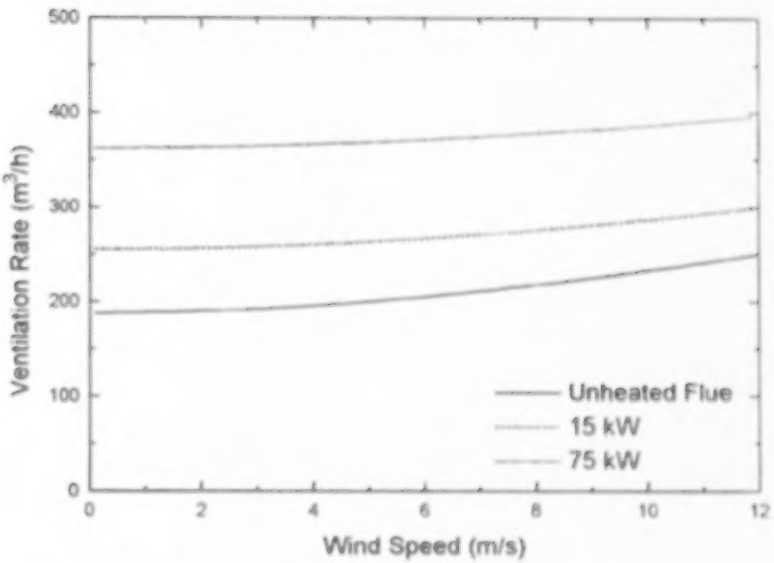

Figure 6.9: Ventilation in a mechanical room plotted against wind speed for three appliance power outputs. Wind is blowing toward unsheltered vents and indoor–outdoor temperature difference is $40°C$. The upper vent is blocked.

Chapter 7

Conclusions and Recommendations

7.1 Conclusions and Summary of Results

1. Small changes in wind pressure coefficients at local leakage sites can have a very large effect on the total passive ventilation rate for a building. Accurate estimation of the local wind pressure coefficient on passive vents is critical for accurate calculation of passive ventilation rates. The practice of applying wall averaged wind pressure coefficient values to large passive vents will lead to significant errors in modelling passive ventilation. The bias in LOCALEAKS–2 predictions were removed successfully by inputting a difference in wind pressure between passive vents.

2. A model was developed to estimate local wind pressure coefficients on walls based on vertical location. This model was incorporated into the LOCALEAKS–3 infiltration model to estimate wind pressure on passive vents. In comparison studies, LOCALEAKS–3 predictions compared favourably with measured values of ventilation in a test house with unsheltered combustion air vents. LOCALEAKS–3 was successful in improving ventilation predictions with combustion air vents, by using the local pressure coefficient model to predict the difference in wind pressure between the two passive combustion air vents. Average bias of all the in predicted to measured ventilation ratios for all wind directions was less than 3% (note that this is an average of all the data, not the binned sets and the maximum $\pm$ 25% scatter in predicted to measured data is due to the natural variability of ambient conditions in all averaged field measurements). Predictions with sheltered com-

bustion air vents were less successful due primarily to the models flaws in predicting local wind shelter effects on sheltered walls.

3. Parametric studies of predicted ventilation rates in a mechanical room with passive combustion air vents were carried out. During hot flue conditions, the flue flow dominates the passive ventilation of the mechanical room. The flue becomes a very large source of outflow. The large pressures across the flue cause the flue to be insensitive to change in pressure across the flue. This makes the total ventilation rate of the flue insensitive to ambient temperature or wind conditions. This insensitivity to ambient conditions comes at the price of over–ventilation, approximately 300% the safe requirement. During periods when the flue is not heated, wind and temperature differences drive passive ventilation in the space. This causes ventilation rates to vary widely depending on indoor–outdoor temperature difference, wind speed, wind direction and wind shelter. Ventilation rates as high as 125% of combustion air requirements were calculated during cold flue conditions. Because of the large seasonal variation in ventilation rates due to seasonal shift in temperatures, combined with the fluctuation in wind direction and speed, it is impossible to size passive combustion air vents to provide acceptable ventilation rates for all weather conditions. While over–ventilation could be reduced with the introduction of dampers that close the vents for appliance–off conditions, a better solution is to abandon passive vents for combustion air supply. A fan with high static pressure and flow control in the form of an orifice plate would supply a constant supply of air regardless of passive driving forces. Such a fan could also be equipped with an interlocking switch that would ensure air flow before the appliances were allowed to fire.

7.2 Recommendations for Future Study

1. In order to develop an improved version of the LOCALEAKS–3 passive ventilation model, in particular the estimation of local wind pressure, and the calculation of the effects of wind shelter, further full scale experimentation must be continued. The wind–shadow shelter model used in LOCALEAKS–2 was found to be unrealistic for sheltered walls on the Alberta Home Heating Research Facility test houses, where it is likely that the close proximity of the test houses causes channelling of air flow through the space between adjacent houses. An improved wind shelter model that incorporates channelling as well as wind shadowing

may be helpful. Further experimentation should include measurement of wind pressure profiles on exterior walls to improve the local wind pressure coefficient model developed in this study.

2. The calibrations and flow measurements in the passive combustion air vents raised serious questions about how they function. Calibrations of the combustion air vents found that flow coefficients in the vents were not proportional to the cross sectional area of the vent, and that other geometric factors probably have a very large effect on the flow coefficients of these vents. The cross sectional area of passive combustion air vents are sized proportionally to the combustion air requirement, which could result in large variations in combustion air supply depending on the details of the particular installation. During measurement of flow through passive vents installed on the test houses, it was found that the pressure measurement across the vent inferred larger flows than were actually occurring. This was accentuated when wind was blowing directly at an inflowing vent. It is not known if this is a problem with how the pressure across the vent is measured or if some unknown flow condition in the vent is occurring. A detailed study to investigate flow in these passive vents would aid further experimental work carried out in this field and may result in an improved design methodology for combustion air vents.

3. The flue cap on House 4 has unknown wind pressure coefficients. This is due to the fact that the flue cap is at the same height as the roof peak, making the flue cap sensitive to wind effects on the roof surface. To improve passive ventilation studies the flue caps on all the test houses should be altered to make their wind pressure coefficients less sensitive to wind direction. Alternatively a measurement program could be initiated to gain more understanding of the general effects that roof structures have on flue–top pressure coefficients.

Appendix A

Derivations

A.1 Derivation of Equation 2.4

$$\rho_{in} - \rho_{out} = \rho_{out}\left(\frac{\rho_{in}}{\rho_{out}} - 1\right) \tag{A.1}$$

Introduce ideal gas law to express densities as temperaures and pressures.

$$\rho_{in} - \rho_{out} = \rho_{out}\left(\frac{P_{in}T_{out}}{T_{in}P_{out}} - 1\right) \tag{A.2}$$

$$\rho_{in} - \rho_{out} = \rho_{out}\left(\frac{P_{in}T_{out} - T_{in}P_{out}}{T_{in}P_{out}}\right) \tag{A.3}$$

$$\rho_{in} - \rho_{out} = \rho_{out}\left(\frac{P_{out}\left(T_{out} - T_{in}\right) - T_{out}\left(P_{out} - P_{in}\right)}{T_{in}P_{out}}\right) \tag{A.4}$$

$$\rho_{in} - \rho_{out} = \frac{\rho_{out}\left(T_{out} - T_{in}\right)}{T_{in}}\left(1 - \frac{T_{out}\left(P_{out} - P_{in}\right)}{\left(T_{out} - T_{in}\right)P_{out}}\right) \tag{A.5}$$

Pressure differences can be introduced to get Equation 2.4.

$$\rho_{in} - \rho_{out} = \frac{\rho_{out}\Delta T}{T_{in}}\left(1 - \frac{T_{out}\Delta P}{\Delta T P_{out}}\right) \tag{A.6}$$

Absolute pressure changes are small across the building envelope, therefore ΔP can be assumed to go to zero reducing Equation 2.4 to

$$\rho_{in} - \rho_{out} = \frac{\rho_{out}\Delta T}{T_{in}} \tag{A.7}$$

A.2 Derivation of Equations 2.10 and 2.11

Refering to Figure 2.2 the ventilation rate equation in the direction shown, 2.10 is as follows. The pressure differences across the vents can be expressed as absolute pressures.

$$\Delta P_1 = P_{out,1} - P_{in,1} \tag{A.8}$$

$$\Delta P_2 = P_{in,2} - P_{out,2} \tag{A.9}$$

Where the P_{in} values are the absolute pressures on the interior side of the vents and the P_{out} values are the asolute pressures on the exterior side of the vents. Note that the pressure differences are positive when the flow matches the direction represented by the arrows in Figure 2.2. Pressures on the vent interiors can be equated with the interior hydrostatic pressure difference between them.

$$P_{in,1} = P_{in,2} + \rho_{in} g H \tag{A.10}$$

Similarily the exterior pressures can be equated with the exterior hydrostatic pressure and the wind pressure difference on the exterior surfaces.

$$P_{out,1} = P_{out,2} + \rho_{out} g H - \Delta C_p \frac{\rho_{out} U^2}{2} \tag{A.11}$$

Where $\Delta C_p = C_{p,2} - C_{p,1}$, the difference in wind pressure coefficients between the vents. Taking the difference, Equation A.11 minus Equation A.10 gives

$$(P_{out,1} - P_{in,1}) + (P_{in,2} - P_{out,2}) = gH\,(\rho_{out} - \rho_{in}) - \Delta C_p \frac{\rho_{out} U^2}{2} \tag{A.12}$$

Which can be expressed as pressure differences.

$$\Delta P_1 + \Delta P_2 = gH\,(\rho_{out} - \rho_{in}) - \Delta C_p \frac{\rho_{out} U^2}{2} \tag{A.13}$$

Equation A.13 states that the sum of the pressure drops across the two vents is equal to the total driving pressure across the vents. The pressure differences may now be equated, because the the vents must have equal mass flow rates to satisfy consevation of mass in the structure.

$$\dot{m}_1 = \dot{m}_2 \tag{A.14}$$

By assuming orifice flow with n_1 and n_2 equal to $\frac{1}{2}$ the following may be derived

$$\frac{\Delta P_2}{\Delta P_1} = \left(\frac{C_1}{C_2}\right)^2 \left(\frac{\rho_{out}}{\rho_{in}}\right)^2 \tag{A.15}$$

By combining Equations A.13 and A.15 and expressing densities as temperatures an expression of one of the vent pressure differences as a function of the driving forces can be derived.

$$\Delta P_1 = \frac{gH\rho_{out}\left(\frac{T_{in}-T_{out}}{T_{in}}\right) - \Delta C_p \frac{\rho_{out}U^2}{2}}{1+\left(\frac{C_1}{C_2}\right)^2\left(\frac{T_{in}}{T_{out}}\right)^2} \tag{A.16}$$

The pressure difference across vent 1 may now be used to calculate the flow across the vent by assuming $n_1 = \frac{1}{2}$. As the flow in the vents are equal and opposite the mass flow rate in one vent is equal to the total ventilation rate of the structure.

$$\dot{m}_{total} = \rho_{out} C_1 \left(\frac{gH\rho_{out}\left(\frac{T_{in}-T_{out}}{T_{in}}\right) - \Delta C_p \frac{\rho_{out}U^2}{2}}{1+\left(\frac{C_1}{C_2}\right)^2\left(\frac{T_{in}}{T_{out}}\right)^2} \right)^{\frac{1}{2}} \tag{A.17}$$

This is Equation 2.10 which is the ventilation rate due to wind pressure and temperature difference in the two vent structure shown in Figure 2.2. For cases when the driving forces reverse the flow direction from the arrows in Figure 2.2 a new equation must be derived. Equation 2.11 is derived as above with the flow directions reversed.

$$\dot{m}_{total} = \rho_{in} C_1 \left(\frac{gH\rho_{out}\left(\frac{T_{out}-T_{in}}{T_{in}}\right) + \Delta C_p \frac{\rho_{out}U^2}{2}}{1+\left(\frac{C_1}{C_2}\right)^2\left(\frac{T_{out}}{T_{in}}\right)^2} \right)^{\frac{1}{2}} \tag{A.18}$$

References

Akins, R., J. Peterka, and J. Cermak (1979, July). Averaged pressure coefficients for rectangular buildings. In *Proceedings of the Fifth International Wind Engineering Conference*, Fort Collins, USA., pp. 369–380.

Andersen, K. T. (1995). Theoretical considerations on natural ventilation by thermal buoyancy. Submitted for publication in ASHRAE Transactions 1995, V. 101, PT. 2.

ASHRAE (1993). *Handbook of Fundimentals*, Chapter 23, pp. 23.1–23.23. 1791 Tullie Circle, N.E., Atlanta, GA 30329: ASHRAE.

Canadian Gas Association (1991a, January). *CAN/CGA-B149.1M91 Natural Gas Installation Code*. 55 Scarsdale Road, Don Mills, Ontario, Canada, M3B 2R3: Canadian Gas Association.

Canadian Gas Association (1991b, April). *CAN/CGA-B149.2M91 Propane Installation Code*. 55 Scarsdale Road, Don Mills, Ontario, Canada, M3B 2R3: Canadian Gas Association.

Dale, J. D. and M. Y. Ackerman (1993). The thermal performance of a radiant panel floor–heating system. *ASHRAE Transactions 99*(1), 28–32.

International Conference of Building Officials (1991, December). *Uniform Mechanical Code*. 5360 South Workman Mill Road, Whittier, California 90601: International Conference of Building Officials.

Kiel, D. and D. Wilson (1986). Gravity driven flows through open doors. In *Proceedings of the Seventh Air Infiltration and Ventilation Centre Conference*, Coventry, pp. 15.1–15.16.

Kronvall, J. (1980). Air flow in building components. Technical Report TVBH-1002, Lund Institute of Technology, Building Technology Division, Lund, Sweden.

Mayo, T. (1985). Combustion air supply codes in housing. Technical Report 85.01, Buildings Energy Technology Transfer Program, Energy, Mines and Resourses Canada.

Sherman, M. and D. Grimsrud (1980). The measurement of infiltration using fan pressurization and weather data. Technical Report LBL-10852, Lawrence Berkely Laboritories, University of California.

Walker, I. (1989). Single zone air infiltration modelling. Master's thesis, University of Alberta Department of Mechanical Engineering.

Walker, I. (1993). *Prediction of Ventilation, Heat Transfer and Moisture Transport in Attics.* Ph. D. thesis, University of Alberta Department of Mechanical Engineering.

Walker, I. and D. Wilson (1989). The alberta air infiltration model aim–2. Technical Report 71, Department of Mechanical Engineering, University of Alberta.

White, F. M. (1986). *Fluid Mechanics* (second ed.). McGraw–Hill.

Wilson, D. and I. Walker (1991). Passive ventilation to maintain indoor air quality. Technical Report 81, Department of Mechanical Engineering, University of Alberta.

Wilson, D. and I. Walker (1992, October). Feasibility of passive ventilation by constant area vents to maintain indoor air quality in houses. In *IAQ 92: Environments for People*, San Francisco, CA, USA, pp. 272–290.

Wiren, B. G. (1985). Effects of surrounding buildings on wind pressure distributions and ventilation losses for single-family houses. Technical Report M85:19, The National Swedish Institute for Building Research.